Analysis of the regulation and function of the diguanylate cyclase

DgcZ from *Escherichia coli*

Dissertation

Zur Erlangung des Doktorgrades

der Naturwissenschaften

(Dr. rer. nat.)

dem Fachbereich Biologie

der Philipps-Universität Marburg

Vorgelegt von

Egidio Lacanna

aus Stigliano (Italien)

Marburg an der Lahn, 2016

Vom Fachbereich Biologie der Philipps-Universität Marburg

als Dissertation angenommen am: 22.06.16

1. Gutachterin: Prof. Dr. Anke Becker

2. Gutachter: Prof. Dr. Erhard Bremer

Tag der mündlichen Prüfung: 27.09.16

Dedicated to

my supervisor and mentor Prof. Dr. Alex Böhm

List of publications stemming from this study

1. **Lacanna E, Bigosch C, Kaever V, Boehm A, Becker A.** (submitted, 2016). Evidence for Escherichia coli diguanylate cyclase DgcZ interlinking surface sensing and adhesion via multiple regulatory routes. J Bacteriology

2. **Zähringer F, Lacanna E, Jenal U, Schirmer T, Boehm A.** 2013. Structure and signaling mechanism of a zinc-sensory diguanylate cyclase. Structure **21:**1149-1157.

Table of Contents

I. Summary

Cyclic dimeric GMP (c-di-GMP) is a widespread second messenger regulating several processes including bacterial motility, biofilm formation, and virulence. The enzymes responsible for c-di-GMP production and degradation, diguanylate cyclases (DGCs) and phosphodiesterases (PDEs), respectively, are abundant and often present in multiple copies within bacterial genomes. DGCs possess a characteristic GGDEF domain, whereas PDEs have either an EAL or an HD-GYP domain. In the *Escherichia coli* K-12 strain MG1655, 29 proteins containing GGDEF and/or EAL domains have been identified.

In *E. coli*, the diguanylate cyclase DgcZ (formerly YdeH) is the major DGC controlling the production of the exopolysaccharide poly-N-Acetylglucosamine (poly-GlcNAc, PGA), which is involved in biofilm formation.

DgcZ contains a GGDEF domain, responsible for c-di-GMP production, and a sensory domain. First identified in the chemoreceptor TlpD of *Helicobacter pylori*, this domain was named chemoreceptor zinc-binding (CZB) domain after its capability to bind zinc. Researchers from the University of Basel's Biozentrum solved the three-dimensional structure of the DgcZ protein and indeed found a zinc ion bound to the 3His/1Cys motif of the CZB domain. Additionally, zinc was shown to inhibit the activity of DgcZ *in vitro* with a subfemtomolar constant K_i.

This study investigates the regulation and function of the diguanylate cyclase DgcZ in *E. coli*. To ascertain the role of zinc in the function of DgcZ activity *in vivo*, site-directed mutagenesis was employed to construct *dgcZ* alleles encoding protein variants with amino acid exchanges in the CZB domain involved in zinc coordination, thus reducing or abolishing binding. The activity of these DgcZ variants was derived by measuring the levels of PgaD, an enzyme involved in exopolysaccharide production, and of the exopolysaccharide poly-GlcNAc (PGA) produced, both proportional to DgcZ-derived c-di-GMP. Although single exchanges of zinc binding amino acids did not strongly affect the protein activity, a DgcZ variant carrying two such exchanges (H79L and H83L) displayed a significant increase of protein activity.

The influence of zinc ions on DgcZ activity was further tested by applying increasing concentrations of $ZnSO_4$ and measuring the ability of bacteria to form a PGA biofilm. Externally applied zinc inhibited PGA biofilm formation in a DgcZ- and c-di-GMP-dependent fashion. The evidence obtained *in vivo* therefore confirms the results from the *in vitro*

experiments showing that the diguanylate cyclase DgcZ is allosterically regulated by zinc. The relevance of this regulatory mechanism is still unsettled, but potential explanations are that it might help the bacteria discriminate among different niches, characterized by high or low levels of zinc, or that it could "signal" the cell´s own physiological condition.

Following these studies on allosteric regulation, the physiological role of DgcZ was examined, as its primary function and the conditions in which the protein is active are still not well defined. Analyses of DgcZ protein localization performed in this study revealed that a combination of carbon starvation and alkaline pH (8.7) induces localization at one bacterial cell pole. Polar localization occurred in non-dividing bacteria and disappeared after restoring nutrient-sufficient conditions. The role of this localization phenotype until now remains elusive.

Further, Co-Immunoprecipitation analyses were performed and 11 proteins identified with a significant score. Among these, FrdB, a subunit of the fumarate reductase complex (FRD), interacted with DgcZ within a bacterial two-hybrid system. The FRD complex proved essential in the superoxide-stimulated increase of DgcZ-dependent biofilm, suggesting new roles of this complex and oxidative stress in DgcZ-mediated biofilm formation.

Finally, the role of DgcZ in CpxAR-mediated surface adhesion was investigated, as it had already been established that *dgcZ* is transcriptionally regulated by this two-component system. The Cpx complex in turn had been shown to be responsible for surface sensing and to stimulate bacterial adhesion through an up to now unknown mechanism. This work reveals an involvement of DgcZ in Cpx-mediated surface adhesion, providing evidence for a physiological function of this diguanylate cyclase in connecting the processes of surface sensing and surface attachment.

II. Zusammenfassung

Zyklisches-dimeres-GMP (c-di-GMP) ist ein weit verbreiteter sekundärer Botenstoff, der verschiedenste zelluläre Prozesse reguliert, einschließlich bakterieller Motilität, Biofilmbildung und Virulenz. Die c-di-GMP-Menge in der Zelle wird von zwei Enzym-Typen reguliert: sogenannten Diguanylat-Zyklasen (DGCs), die c-di-GMP synthetisieren, und Phosphodiesterasen (PDEs), die es abbauen. Beide Enzymklassen sind weit verbreitet und liegen in bakteriellen Genomen oft in mehreren Kopien vor. DGCs besitzen eine charakteristische GGDEF-Domäne, während PDEs entweder eine EAL- oder eine HD-GYP Domäne aufweisen. In *Escherichia coli* K-12 MG1655 wurden 29 Proteine identifiziert, die eine GGDEF- und/oder eine EAL-Domäne aufweisen.

In *E. coli* hat die Diguanylat-Zyklase DgcZ (früher YdeH) den größten Einfluss auf die c-di-GMP-abhängige Produktion des Exopolysaccharids Poly-N-Acetylglucosamine (Poly-GlcNAc, PGA), das wiederum bei der Biofilmbildung eine Rolle spielt.

DgcZ verfügt über eine GGDEF-Domäne, welche verantwortlich für die c-di-GMP-Produktion ist, sowie über eine sensorische Domäne. Diese wurde erstmals im Chemorezeptor TlpD von *Helicobacter pylori* identifiziert und aufgrund ihrer Fähigkeit, Zink zu binden, Chemorezeptor-Zink-Binde-Domäne (CZB-Domäne) genannt. Forscher vom Biozentrum der Universität Basel haben die dreidimensionale Struktur des DgcZ-Proteins gelöst und dabei tatsächlich ein Zink-Ion im 3His/1Cys-Motiv der CZB-Domäne entdeckt. Zusätzlich wurde gezeigt, dass die Aktivität von DgcZ *in vitro* durch Zink mit einer Konstante K_i im subfemtomolaren Bereich gehemmt wird.

Die vorliegende Studie untersucht die Regulation und Funktion der Diguanylat-Zyklase DgcZ in *E. coli*. Um den Einfluss von Zink auf die Aktivität von DgcZ *in vivo* zu analysieren, wurden mittels ortsgerichteter Mutagenese *dgcZ*-Allele konstruiert, in deren Proteinprodukten die für die Zink-Koordination verantwortlichen Aminosäuren ausgetauscht waren, wodurch die Affinität von Zink reduziert oder vollständig aufgehoben wurde. Die Aktivität dieser DgcZ-Varianten wurde durch Messung der Menge an PgaD bestimmt, eines Enzyms im Exopolysaccharid-Syntheseweg, und der Menge des Exopolysaccharids Poly-GlcNAc (PGA); beides ist proportional zur c-di-GMP-Produktion durch DgcZ. Während einzelne Mutationen in der CZB-Domäne die Proteinaktivität geringfügig beeinflussten, zeigte eine DgcZ-Variante mit zwei Aminosäureaustäuschen (H79L und H83L) eine deutliche Steigerung der Proteinaktivität. Der Einfluss von Zink-Ionen auf die Aktivität von DgcZ wurde darüber hinaus untersucht, indem bei steigenden Konzentrationen von $ZnSO_4$ im Medium die

Fähigkeit der Bakterien zur Bildung eines PGA-Biofilms ermittelt wurde: Wird Zink extern hinzugegeben, hemmt es die PGA-Biofilmbildung in einer DgcZ- und c-di-GMP-abhängigen Art und Weise. Die *in vivo*-Ergebnisse bestätigen damit die *in vitro*-Experimente und belegen, dass die Diguanylat-Zyklase DgcZ allosterisch durch Zink reguliert wird. Die Bedeutung dieses regulatorischen Mechanismus ist noch offen; mögliche Erklärungsansätze wären, dass er den Bakterien hilft, zwischen Nischen mit hohen und niedrigen Zink-Konzentrationen zu unterscheiden, oder den metabolischen Zustand der Bakterienzelle selbst widerspiegelt.

Neben diesen Studien zur allosterischen Kontrolle wurde die physiologische Rolle von DgcZ untersucht, denn dessen primäre Funktion und die Bedingungen, unter denen das Protein aktiv ist, sind nach wie vor nicht ausreichend verstanden. DgcZ-Lokalisationsstudien im Rahmen dieser Arbeit zeigen, dass es bei einer Kombination von Kohlenstoffmangel und alkalischem pH (8,7) zu einer Lokalisation an einem Pol der Bakterienzelle kommt. Diese Lokalisation konnte nur bei sich nicht teilenden Bakterien beobachtet werden und ist bei erneuter Nährstoffgabe reversibel. Auf eine eventuelle Funktion dieses Phänotyps gibt es bis jetzt allerdings keine Hinweise.

Des Weiteren wurden Co-Immunpräzipitation-Experimente durchgeführt, in deren Verlauf 11 Proteine identifiziert werden konnten. Unter diesen 11 Proteinen war auch FrdB, eine Untereinheit des Fumarat-Reduktase-Komplexes (FRD), für die anschließend eine Interaktion mit DgcZ mittels eines bakteriellen Zwei-Hybrid-System bestätigt werden konnte. Darüber hinaus erwies sich der FRD-Komplex als essenziell in einer Superoxid-stimulierten Zunahme von DgcZ abhängigen Biofilmen, was auf eine neue Rolle dieses Komplex einerseits und von oxidativem Stress andererseits in der DgcZ-abhängigen Biofilm-Bildung hindeutet.

Abschließend wurde die Rolle von DgcZ in der durch CpxAR vermittelten Oberflächenadhäsion untersucht, denn es war bekannt, dass *dgcZ* durch dieses Zweikomponentensystem transkriptionell reguliert wird. Der Cpx-Komplex wiederum ist für die Oberflächendetektion verantwortlich und stimuliert die Zelladhäsion durch einen bislang unbekannten Mechanismus. Diese Arbeit zeigt nun eine Beteiligung von DgcZ in der Cpx-vermittelten Oberflächenadhäsion und belegt damit eine physiologische Funktion dieser Diguanylat-Zyklase im Übergang von Oberflächendetektion zur Adhäsion.

1. Introduction

1.1 *Escherichia coli* - A "Model Organism"

Discovered in 1884 by Theodor Escherich, *Escherichia coli* (*E. coli*) is the most thoroughly studied bacterial species. A rod-shaped Gram-negative bacterium colonizing the gastrointestinal tract of warm-blooded animals, *E. coli* is a favored organism for investigation because it is relatively easy to identify, isolate and culture (Blount, 2015). *E. coli* strains can be cultured on media containing inorganic salts and a carbon source as well as on complex media, such as lysogeny broth (LB), which supports faster growth (Sezonov *et al.*, 2007).

Strains of *E. coli* are ubiquitous in humans and constitute normal gastrointestinal flora. Nonpathogenic strains form a mutualistic relationship in mammalian hosts, providing vitamin K and other useful vitamins utilized by hosts (Blount, 2015). Pathogenic strains of *E. coli* are also quite common and are capable of invading other parts of the body, causing urinary tract infections, neonatal sepsis and meningitis, and diarrheal diseases (Kaper *et al.*, 2004).

E. coli's dual nature as commensal or pathogen makes the bacterium an important target for molecular and microbiological research efforts. The relative simplicity of introducing genomic mutations and the availability of non-pathogenic strains enable investigation of *E. coli* in bacterial physiology as well as basic research. Most of our knowledge concerning fundamental mechanisms, including gene transcription, translation and DNA replication, was obtained using this organism (Blount, 2015). Furthermore, the increasing knowledge of *E. coli* physiology makes this organism suitable for pharmaceutical and biotechnological purposes.

1.2 Bacterial biofilms

Under favorable laboratory conditions, in shaking flasks, *E. coli* grows as a planktonic single-celled organism. In natural habitats however, conditions differ widely and often only support suboptimal growth. To counter the diverse constraints present in nature, a widespread bacterial survival strategy consists in the production of biofilms: communities of bacteria encased within a heterologous matrix often composed of exopolysaccharides, flagella, proteins and eDNA (Hobley *et al.*, 2015). Biofilms protect bacteria from desiccation (White *et al.*, 2006), antibiotics and host defenses (Hobley *et al.*, 2015). In *E. coli,* for example,

DePas *et al.* (2014) demonstrated that biofilm formation protects bacteria against killing by *Caenorhabditis elegans* and *Myxococcus xanthus*. The protection conferred to pathogenic bacteria within a biofilm is of significant clinical relevance.

Bacteria living in biofilms are more resistant to antibiotics, host immune responses, and constitute an existential threat to human health (Fux *et al.*, 2005). Many chronic infections are linked to bacterial biofilms (Bjarnsholt, 2013). *Pseudomonas aeruginosa* biofilms, for instance, are well-documented sources of chronic infection in the lungs of patients with cystic fibrosis (Ciofu *et al.*, 2015). *E. coli* biofilm formation is also widely studied. *E. coli* strains produce submerged biofilms on plastic and glass surfaces (Wang *et al.*, 2004, Boehm *et al.*, 2009), pellicle biofilms at air-liquid interface (Andersson *et al.*, 2013), and macrocolonies on agar plates (Serra *et al.*, 2013; 2013b).

Biofilms vary considerably in terms of their structure and composition. Macrocolonies are mainly composed of curli fibers, flagella and the polysaccharide cellulose (Serra *et al.*, 2013; 2013b). Submerged biofilms, instead, are mainly composed of the exopolysaccharide poly-β-1,6-N-acetyl-D-glucosamine (PGA) (Wang *et al.*, 2004). Other components of *E. coli* biofilms are colanic acid, the adhesin Antigen43 (Ag43) and type 1 fimbriae (Beloin *et al.*, 2008; Hobley *et al.*, 2015).

Biofilm formation results from a temporal sequence of highly regulated events that begins with surface sensing and attachment and continues with biofilm maturation (Fig. 1). Biofilm dispersal is conclusive step of the "biofilm life cycle" (Kaplan, 2010) (Fig. 1). In response to favorable conditions or mechanical stress, cells detach from the mature biofilm and spread into the environment.
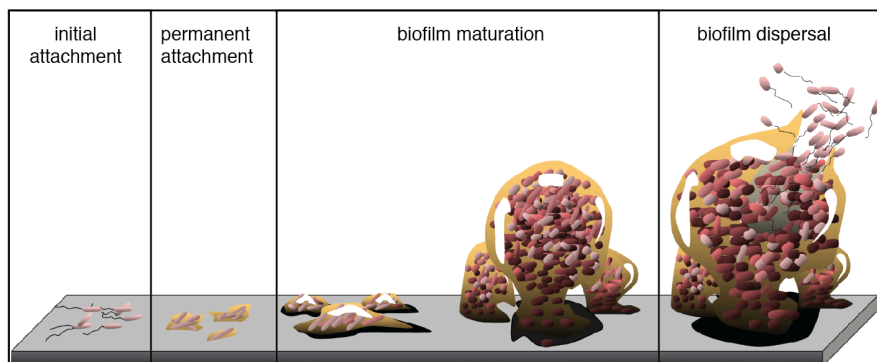
Figure 1. Schematic representation of *E. coli* biofilm formation on abiotic surfaces. Biofilm formation begins with surface sensing and initial attachment to an abiotic surface. This initial, transient encounter is followed by permanent attachment. Bacteria attached to the surface then produce several exopolysaccharides and adhesins, promoting cell to cell interactions, which lead to biofilm maturation. In response to favorable conditions or mechanical stress, biofilm dispersal may occur. This mechanism allows bacteria to spread and colonize new sites. Figure adapted from Monroe, 2007.

1.2.1 The Cpx complex and surface sensing

Bacteria process and alter their behavior in response to external signals. Chemotaxis, for example, describes the phenomenon whereby bacteria integrate complex environmental signals in order to follow nutrient gradients (Adler, 1966; Khan *et al.*, 1995). Bacteria also sense and respond to signals indicating surface presence (Belas, 2014). During initial adhesion to abiotic surfaces, *E. coli* "senses" the surface through the lipoprotein NlpE which facilitates this first, transient surface attachment (Otto and Silhavy, 2002).

Although the mechanism employed by NlpE for surface recognition remains unclear, several theories have been proffered to explain its function. Otto and Silhavy (2002) hypothesize the protein may be involved in sensing damage to the outer membrane that occurs upon contact of the cell with a hydrophobic surface. An alternative theory, proposed by Hirano *et al.*, (2007), suggests NlpE is an outer membrane lipoprotein and "monitors" the structural integrity of Pili, Curli, or other extracellular components. This theory presumes that the signal associated with surface sensing stimulates the partial unfolding of NlpE, resulting in Cpx complex activation (Hirano *et al.*, 2007).

The Cpx complex is a two-component system that senses and responds to multiple perturbations of the cell envelope, including bacterial adhesion to surfaces (Otto and Silhavy, 2002). This complex also responds to elevated pH, misfolded proteins, variations in lipoprotein production, indole, copper and ethanol (Raivio, 2014). The Cpx complex comprises the sensory transmembrane protein CpxA and the cytoplasmic transcriptional regulator CpxR (Raivio and Silhavy, 1997). While inactive, CpxA functions as a phosphatase on CpxR, keeping the system dormant. Once inducing conditions exist, CpxA acts as an autokinase, and additionally phosphorylates CpxR (Raivio and Silhavy, 1997). CpxR is a transcriptional regulator and in its phosphorylated form affects the transcription of target genes with functions that include protein folding and degradation, bacterial adherence, motility, multidrug efflux and DNA repair (Dorel *et al.*, 2006; Raivio *et al.*, 2013).

During initial adhesion of *E. coli* to abiotic surfaces, CpxR-mediated gene regulation leads to bacterial adhesion (Otto and Silhavy, 2002). The precise mechanisms and genes involved in CpxR-dependent surface adhesion are unknown and require additional study.

1.2.2 Bacterial attachment to the surface

Bacterial attachment to the surface initiates biofilm formation. Similar to other bacteria, *E. coli* is capable of forming biofilms on diverse surfaces by selectively using a combination of exopolysaccharides, flagella and proteinaceous structures (Beloin *et al.*, 2008).

Surface attachment is also influenced by the properties of the medium, such as ionic strength (Janjaoren *et al.*, 2013) and flow speed (Wang *et al.*, 2013). The sheer diversity and number of factors influencing surface attachment hamper efforts to provide a general description of the attachment process. For the purpose of this chapter, the submerged biofilm model, explored at length in this study, will be described.

E. coli cells attach to surfaces in two steps: an initial reversible adhesion and a permanent attachment (Agladze *et al.*, 2005; Beloin *et al.*, 2008) (Fig. 1). The initial attachment is reversible and sometimes transient, lasting from seconds to minutes, giving the bacterial cells an opportunity to inspect the environment before permanently adhering or releasing from the surface (Agladze *et al.*, 2005). These permanently attached bacteria adhere longer, remain surface associated and initiate biofilm development (Agladze *et al.*, 2005).

Initial attachment by *E. coli* is achieved by weak electrostatic interactions between the bacterial envelope and the surface, and is influenced by pH, ionic strength of the medium and temperature (Beloin *et al.*, 2008). Flagellar rotation is another factor influencing the initial attachment of *E. coli* to abiotic surfaces (McClaine and Ford, 2002).

Permanent attachment is mediated by bacterial surface structures such as flagella (Friedlander *et al.*, 2013), the exopolysaccharide PGA (Agladze *et al.*, 2005), curli fimbriae, and others (Beloin *et al.*, 2008).

The proprieties of the surface itself, such as hydrophobicity and roughness, influences both initial and permanent attachments to abiotic surfaces (Beloin *et al.*, 2008).

1.2.2.1 Role of flagella for bacterial adhesion

Flagella are mostly known for their role in bacterial motility. In several bacterial species flagella also contribute to biofilm formation (Belas, 2014). In some species, including *Vibrio cholerae* and *Caulobacter crescentus*, a single flagellum is directly involved in surface mechanosensing (Watnick *et al.*, 2001; Li *et al.*, 2012; Belas, 2014).

In *Escherichia coli* there is no evidence for the direct involvement of flagella in surface

mechanosensing. In this organism, however, flagella and their rotation influence bacterial attachment under different flow speeds and ionic strength of certain media (McClaine and Ford, 2002). Friedlander *et al.* (2013) reported that flagella act as structural components during *E. coli* attachment to surfaces with crevices of different sizes. These same researchers also demonstrated how flagella of *E. coli* increase attachment to hydrophobic surfaces and decrease adhesion to hydrophilic surfaces (Friedlander *et al.*, 2015).

Yoshihara *et al.* (2015) reported that on glass surfaces, *E. coli* attachment was not influenced by flagella or motility; although once attached, *E. coli* possessing flagella capable of rotation required stronger mechanical forces to detach from the surface. Despite evidence for a direct role of *E. coli* flagella in surface mechanosensing is missing, flagella do have a role in bacterial attachment to certain surfaces (e.g. hydrophobic) under specific conditions.

1.2.2.2 Role of poly-GlcNAc (PGA) for surface attachment of *E. coli*

After initial attachment, the interaction between bacteria and surface is stabilized by several bacterial surface structures, including the exopolysaccharide poly-GlcNAc (PGA) (Agladze *et al.*, 2005). PGA is synthetized by the PgaABCD machinery and consists of monomers of N-Acetylglucosamine (GlcNAc) linked by β-1,6 bond (Wang *et al.*, 2004) (Fig. 2). PgaC and PgaD are inner membrane proteins that form a heterodimeric complex, responsible for PGA polymerization from UDP-GlcNAc precursors, after binding the second messenger cyclic dimeric GMP (c-di-GMP) (Itoh *et al.*, 2008; Steiner *et al.*, 2013) (Fig. 2). PgaB is required for partial N-deacetylation of PGA, which is exported through the porin PgaA, located in the outer membrane of *E. coli* (Itoh *et al.*, 2008) (Fig. 2). Expression of the *E. coli pgaABCD* operon is controlled on transcriptional and translational levels.

Transcription of the operon is activated by the regulator NhaR (Cerca and Jefferson, 2008), while translation is controlled by the carbon storage regulator CsrA (Wang *et al.*, 2005). CsrA inhibits the initiation of translation of both *pgaA-D* and *nhaR* mRNA binding their 5′UTR (Wang *et al.*, 2005; Pannuri *et al.*, 2012).
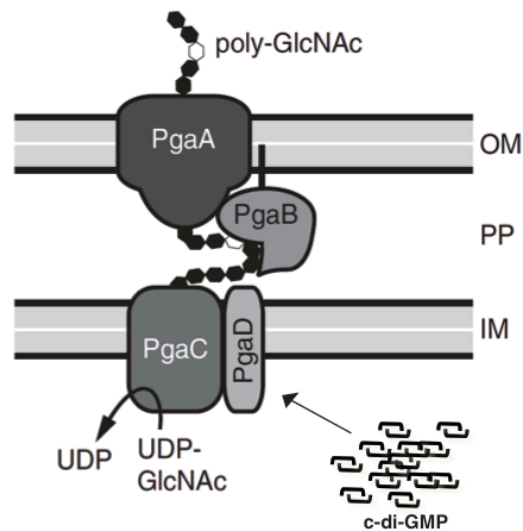
Figure 2. Illustration of the PgaABCD machinery. Schematic representation of the *E. coli* Pga machinery. See text for details. IM, inner membrane; PP, periplasm; OM, outer membrane. Adapted from Steiner *et al.,* (2013).

PGA production and its effects are often studied in the *csrA::Tn5* strain background that carries a truncated and partially active version of CsrA (Romeo *et al.*, 1993). In this strain, PGA is responsible for the permanent attachment to the surface (Agladze *et al.*, 2005) and for biofilm formation (Wang *et al.*, 2005; Boehm *et al.*, 2009). Initial data for an involvement of PGA in permanent adhesion were provided by Agladze *et al.*, (2005), after deleting the *pgaC* gene and assaying the mutated strain for initial and permanent attachment to the surface. *PgaC* deletion had no impact on the initial adhesion of the *csrA::Tn5* strain to glass surfaces, but the PGA deficient bacteria were drastically impaired in permanent attachment (Agladze *et al.*, 2005).

1.2.3 Biofilm maturation

Biofilm maturation requires three-dimensional growth of bacteria permanently attached to the surface (Beloin *et al.*, 2008). This process is characterized by bacterium–bacterium interactions, leading to the formation of a heterogeneous environment in which bacteria exhibit distinctive physiological traits absent or less pronounced in their planktonic counterparts.

E. coli biofilms, such as macrocolonies and submerged biofilms, are characterized by diverse matrix components including surface adhesins and exopolysaccharides (Beloin *et al.*, 2008).

The outer membrane protein Antigen 43 in *E. coli* K-12 is the most thoroughly studied surface adhesin. Ag43 promotes cell-to-cell adhesion, which leads to three-dimensional biofilm development (Kjaegaard *et al.*, 2000). In *E. coli* K-12, the *yfaL*, *yeeJ*, *ypjA*, and *ycgV* genes encode four additional putative adhesins whose overproduction resulted in increased biofilm formation (Roux *et al.*, 2005; Beloin *et al.*, 2008).

The precise physiological conditions which govern the expression of these four genes in K-12 bacteria are not well understood (Roux *et al.*, 2005). Another significant component of mature biofilms are exopolysaccharides which form the biofilm matrix, a hydrated viscous layer protecting bacteria from desiccation.

In *E. coli* strains, the biofilm matrix is mainly composed of the exopolysaccharides cellulose, PGA and colanic acid, and of the proteinaceous curli fimbriae (Beloin *et al.*, 2008). Cellulose, a glucose polymer, along with curli fibers and flagella are the main components of *E. coli* macrocolonies (Serra *et al.*, 2013; 2013b).

The distribution of cellulose, curli and flagella within macrocolonies is heterogeneous. Bacteria at the bottom of the macrocolony are in post-exponential growth phase and are elongated with abundant flagella (Serra *et al.*, 2013b). At the top of the macrocolony, where nutrients are limited or absent, bacteria assume a round shape and the biofilm matrix is enriched with curli and cellulose (Serra *et al.*, 2013b).

PGA and colonic acid are not involved in macrocolony biofilms formation. PGA is essential for permanent surface attachment and as part of the matrix of submerged biofilms (Wang *et al.*, 2004; Agladze *et al.*, 2005; Boehm *et al.*, 2009). In contrast to PGA, colanic acid is not required in bacterial surface attachment, but is produced in mature biofilms to facilitate the development of biofilm architecture (Domka *et al.*, 2007; Danese *et al.*, 2000).

1.3 The carbon storage regulator (Csr) system in *E. coli*

Escherichia coli lives in the lower intestine of warm-blooded organisms and in the external environment. In these habitats, availability of nutrients, temperature, and other conditions change often. Bacteria have therefore evolved to rapidly adapt to these fluctuating environmental cues. Adaptation often involves extensive metabolic changes coordinated by global regulators, which often inversely regulate antagonistic pathways.

The switch between motile and sessile lifestyle during biofilm formation in *E. coli* is controlled, in part, by the global regulator protein CsrA (Carbon Storage Regulator A), a

central component of the csr system (Timmermans and Van Melderen, 2010; Wang *et al.*, 2005; Wei *et al.*, 2001; Jonas *et al.*, 2008).

Identified in 1993 by a transposon mutagenesis screen, the *csrA* gene was initially described as a pleiotropic gene affecting glycogen biosynthesis, gluconeogenesis, cell size, and surface properties (Romeo *et al.*, 1993). The *csrA* gene encodes a 61 amino acid regulatory protein which controls several processes including biofilm formation (Wang *et al.*, 2005), secondary metabolite production (Jonas *et al.*, 2008; Boehm *et al.*, 2009), and motility (Wei *et al.*, 2001). An estimated 130 bacterial species contain CsrA homologues grouped in the CsrA/RsmA protein family (Mercante *et al.*, 2006).

CsrA is an RNA-binding protein and acts by either stimulating or repressing the translation of target mRNAs. The protein generally binds to the 5' UTR of a target transcript, altering its stability and/or repressing the translation initiation (Yakhnin *et al.*, 2011). Repression by CsrA typically involves a direct binding of the protein to the Shine-Dalgarno sequence and blocking of ribosome binding (Yakhnin *et al.*, 2011). Exceptions are found in the cases of the *sdiA* and *pgaABCD* mRNAs.

In the first case, CsrA inhibits mRNA translation by binding exclusively within the *sdiA* coding region (Yakhnin *et al.*, 2011). And in respect to *pgaABCD*, the protein binds to the 5' UTR of the mRNA and unfolds a secondary structure that sequesters an entry site for the termination factor Rho, resulting in the premature stop of transcription (Figueroa-Bossi *et al.*, 2014). CsrA binding can also increase the stability of mRNAs, as in the case of the *flhDC* mRNA (Wei *et al.*, 2001).

The activity of CsrA is tightly controlled by the CsrB and CsrC sRNA (Timmermans and Van Melderen, 2010). CsrB and CsrC have 18 and 9 CsrA binding sites respectively, and inhibit protein activity through a titration mechanism (Liu *et al.*, 1997; Weilbacher *et al.*, 2003). Sequestration of the CsrA by CsrB-C reduces the concentration of available protein, thereby compromising the proteins' ability to bind and regulate target mRNAs.

McaS, a small RNA binding protein, employs a similar inhibitory mechanism on CsrA (Jørgensen *et al.*, 2013). Interestingly CsrB, CsrC, and McaS are all highly expressed at the onset of stationary phase (Timmermans and Van Melderen, 2010; Thomason *et al.*, 2012).

1.3.1 Inverse regulation of motility and biofilm formation by CsrA

CsrA inversely regulates motility and biofilm formation (Wang *et al.*, 2005; Wei *et al.*, 2001; Jonas *et al.*, 2008) (Fig. 3). The protein regulates motility positively, by stabilizing *flhDC* mRNA, which encodes the flagellar master regulators FlhC and FlhD (Wei *et al.*, 2001). The effect of CrsA on biofilm formation is negative and occurs at multiple points (Fig. 3). CsrA inhibits: i) the translation of the *pgaABCD* mRNA, encoding the PgaABCD complex, responsible for PGA production (Wang *et al.*, 2005; Itoh *et al.*, 2008); ii) the translation of the *nhaR* mRNA, coding for a *pgaABCD* transcriptional regulator (Pannuri *et al.*, 2012), and iii) the translation of the *dgcZ* and *dgcT* mRNAs, coding for the diguanylate cyclases DgcZ and DgcT (Jonas *et al.*, 2008), which produce the second messenger cyclic dimeric GMP (c-di-GMP), that regulates PGA production (Boehm *et al.*, 2009). The inverse regulation of motility and PGA production by CsrA is relevant in biofilm formation under specific physiological conditions.
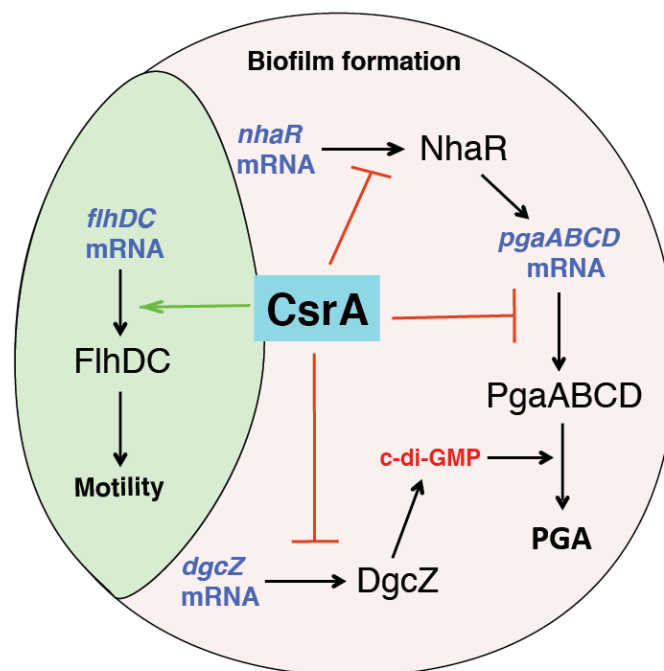
Figure 3. Inverse regulation of motility and PGA-mediated biofilm formation by CsrA. Schematic representation of the action of CsrA on *flhDC* mRNA (motility) (green arrow) and on *nhaR*, *dgcZ* and *pgaABCD* mRNAs encoding proteins involved in biofilm formation (red arrows). CsrA stabilizes the *flhDC* mRNA (Wei *et al.*, 2001) and inhibits the translation of the *nhaR*, *pgaABCD* and *dgcZ* mRNAs (Pannuri *et al.*, 2012; Wang *et al.*, 2005; Jonas *et al.*, 2008).

1.4 The bacterial second messenger c-di-GMP

Cyclic di-GMP (c-di-GMP) (bis-(3'-5')-cyclic dimeric guanosine monophosphate) is a secondary messenger, regulating cellular processes including biofilm formation, motility and virulence (Fig. 4). In 1987, Benziman and co-workers discovered c-di-GMP as an allosteric activator of the cellulose synthase in *Gluconacetobacter xylinus* (formerly *Acetobacter xylinus*) (Ross *et al.*, 1987). At present, this regulatory molecule is recognized in a large number of bacterial species.

Cyclic di-GMP is produced from two molecules of GTP by diguanylate cyclases (DGCs) enzymes, and then degraded to pGpG by phosphodiesterases (PDEs) (Schirmer and Jenal, 2009) (Fig. 4). The number of DGCs and PDEs varies between species; for example *Escherichia coli* contains 29, *Pseudomonas aeruginosa* has 41, *Vibrio cholerae* 72 and *Salmonella enterica* 19 (Boyd and O'Toole 2012). DGCs harbor a distinctive GGDEF domain, while PDEs contain either EAL or HD-GYP domains (Tal *et al.*, 1998; Simm *et al.*, 2004; Ryan *et al.*, 2006; Schirmer and Jenal, 2009) (Fig. 4).
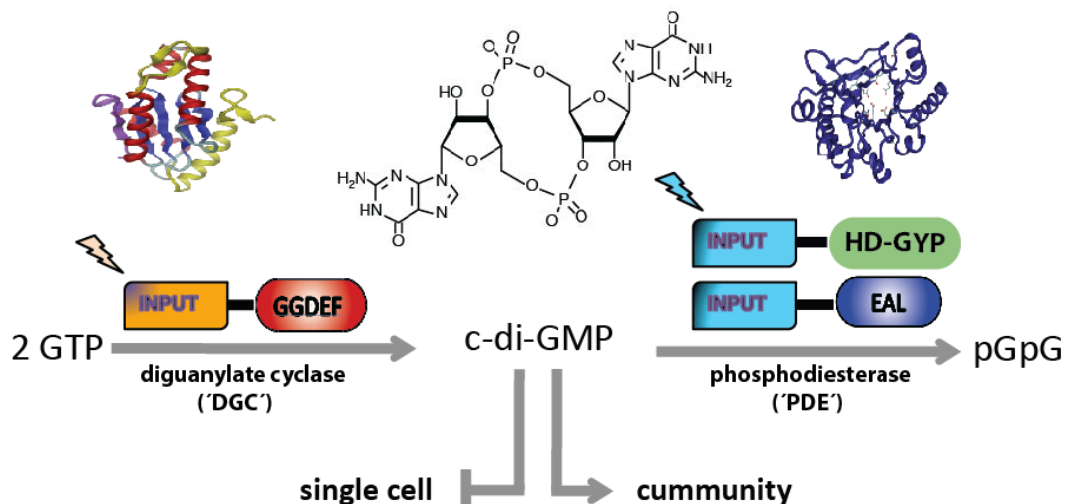
Figure 4. Production and degradation of c-di-GMP. The second messenger c-di-GMP is synthesized from two molecules of GTP by diguanylate cyclases (DGCs) and degraded by c-di-GMP specific phosphodiesterases (PDEs) to linear pGpG. DGC activity is mediated by GGDEF domains, whereas PDE activity is provided by the EAL or HD-GYP consensus motifs. Both DGCs and PDEs contain input domains which respond to environmental cues. Among other functions, c-di-GMP regulates the transition from motile to sessile lifestyle. Figure adapted from Alex Boehm's work.

The GGDEF domain, characteristic of DGCs, is located in the protein active site (A-site) and is responsible for GTP binding (Schirmer and Jenal, 2009). In every example studied, dimerization is needed for DGC activity. Once dimerization occurs, the GGDEF domains come into proximity and two GTP molecules are condensed to produce c-di-GMP. DGCs are subject to allosteric inhibition when c-di-GMP binds the protein inhibitory site (I-site) (Christen *et al.*, 2006). The I-site, located in the GGDEF domain, consists of a RxxD motif. At high concentrations, c-di-GMP binds this I-site preventing over-consumption of GTP and limiting excessive accumulation of the second messenger (Christen *et al.*, 2006).

The EAL domain, present in c-di-GMP specific PDEs, catalyzes the asymmetric opening of the c-di-GMP macrocycle through hydrolysis of an ester bond to yield the linear dinucleotide 5′-phosphoguanylyl-(3′-5′)-guanosine (pGpG) (Schirmer and Jenal, 2009). EAL-containing PDEs exhibit high specificity for their substrate and require either Mg^{2+}, or Mn^{2+} to operate.

The HD-GYP-containing PDEs represent another group of PDEs. These HD-GYP PDEs are less abundant than EAL-containing PDEs and there is limited information due to the few crystal structures solved (Lovering *et al.*, 2011; Bellini *et al.*, 2014; Rinaldo *et al.*, 2015). The HD-GYP domain is characterized by a bi-metal (Rinaldo *et al.*, 2015) or a tri-iron binding site involved in catalysis (Bellini *et al.*, 2014). Distinct from EAL-containing PDEs, the c-di-GMP binding site of HD-GYP PDEs allows for the interaction of both hydrolysable phosphates of c-di-GMP with the metal center, resulting in complete hydrolysis of the molecule to GMP (Bellini *et al.*, 2014).

Whole genome sequencing revealed an abundant and wide distribution of GGDEF, EAL and HD-GYP domains among bacteria (Galperin 2005). The GGDEF and EAL domains identified were often associated with receiver domains of two-component, phosphorylation systems (Galperin 2006). These receiver domains connect extra- and intracellular signals to produce or degrade c-di-GMP, which acts as second messenger to regulate cellular functions (Hengge 2009) (Fig. 4).

Cyclic di-GMP controls the transition between planktonic and sessile "lifestyle" in many bacterial species, stimulating the synthesis of various exopolysaccharides, adhesins and inhibiting motility (Hengge 2009) (Fig. 4). This second messenger also regulates other bacterial functions, such as virulence and cell cycle progression (Tischler and Camilli, 2005; Ryan *et al.*, 2006; Duerig *et al.*, 2009; Lori *et al.*, 2015).

1.4.1 c-di-GMP effectors

To orchestrate these functions, c-di-GMP binds cognate receptor proteins and elicits structural changes to alter their activity. Cyclic di-GMP receptors are diverse and include PilZ proteins (Amikam and Galperin, 2006; Hengge 2009), proteins with degenerate GGDEF (Duerig *et al.*, 2009) or EAL domains (Navarro *et al.*, 2009) and transcriptional factors (Tschowri *et al.*, 2014). The PilZ protein family represents the largest class of c-di-GMP receptors.

The PilZ domain is present in numerous proteins controlling bacterial motility, and the production of cellulose or alginate (Boehm *et al.*, 2010; Hengge 2009). PilZ domains are frequently linked to GGDEF, EAL and/or HD-GYP domains; or alternatively to a domain producing a molecular output, such as the BcsA protein, involved in bacterial cellulose production (Amikam and Galperin, 2006).

In reference to *E. coli*, YcgR provides the most thoroughly studied PilZ protein. Upon c-di-GMP binding, YcgR undergoes a conformational change that allows the protein to interact with the FliG-MotA interface, thereby regulating swimming speed (Boehm *et al.*, 2010; Paul *et al.*, 2010).

Proteins with degenerate GGDEF or EAL domains may still bind the second messenger and function as c-di-GMP receptors (Duerig *et al.*, 2009; Navarro *et al.*, 2009). The PopA protein of *Caulobacter crescentus*, for example, contains a degenerate GGDEF domain (ATEVF) and binds c-di-GMP through its I-site. Once bound to c-di-GMP, PopA relocates to the stalked cell pole where the protein induces the degradation of CtrA, a replication initiation inhibitor, thereby promoting entry into the S-phase of the cell cycle (Duerig *et al.*, 2009). FimX from *Pseudomonas aeruginosa* instead uses a degenerate EAL domain for c-di-GMP binding (Navarro *et al.*, 2009).

Another distinct class of c-di-GMP effectors includes transcriptional factors regulated by the second messenger. The BldD transcription factor of *Streptomyces venezuelae*, for example, binds tetrameric c-di-GMP, dimerizes and then binds DNA, repressing bacterial development and sporulation (Tschowri *et al.*, 2014). Aside from effector proteins, c-di-GMP also binds riboswitches and regulates gene expression at post-transcriptional level (Sudarsan *et al.*, 2008). Research efforts have now identified two types of c-di-GMP riboswitches in Vibrio *cholerae* and *Clostridium difficile* species.

1.4.2 c-di-GMP signalling in *Escherichia coli*

The c-di-GMP network in *E. coli* K-12 is the subject of extensive and ongoing research efforts. Genomic analysis revealed 29 GGDEF/EAL encoding genes – 12 code for GGDEF domains, 10 for EAL, and seven for GGDEF and EAL domains (Povolotski and Hengge, 2012). Combined biochemical and sequencing data elucidated the roles of these proteins as either c-di-GMP synthases, or hydrolases (Povolotski and Hengge, 2012). Accordingly, 12 of these proteins were classified as DGCs, 13 as PDEs and four as enzymatically inactive proteins (Povolotski and Hengge, 2012).[1]

The 25 active DGCs and PDEs in *E. coli* precisely regulate cellular c-di-GMP concentrations under different growth conditions. In *E. coli* K-12 MG1655, the second messenger regulates cell motility (Boehm *et al.*, 2010; Paul *et al.*, 2010), PGA (Itoh *et al.*, 2008; Steiner *et al.*, 2013) and curli fimbriae production (Lindenberg *et al.*, 2013), as well as the activity of PNPase (Polynucleotide Phosphorylase) (Tuckerman *et al.*, 2011).

Motility is regulated through the PilZ-protein YcgR (Boehm *et al.*, 2010; Paul *et al.*, 2010), described in section 1.4.1.

PGA is produced by the PgaABCD complex in presence of c-di-GMP (Itoh *et al.*, 2008; Steiner *et al.*, 2013). The binding of the second messenger to PgaCD stabilizes the heterodimeric complex stimulating PGA production (Steiner *et al.*, 2013).

Curli fimbriae, encoded by the *csgBAC* and *csgDEFG* operons, are transcriptionally activated by the CsgD regulator. Transcription of *csgD* depends on c-di-GMP levels and the transcriptional factor MlrA (Lindenberg *et al.*, 2013). MlrA interacts with DgcM (YdaM), a diguanylate cyclase, and PdeR (YciR), a phosphodiesterase. At low c-di-GMP concentrations, PdeR inhibits MlrA activity; while at high concentrations of the second messenger, PdeR inhibition of MlrA activity is relieved and *csgD* transcription occurs (Lindenberg *et al.*, 2013). Through the DgcM-PdeR-MlrA complex, c-di-GMP controls transcription of *csgD* and of the curli operons *csgBAC* and *csgDEFG*.

Polynucleotide Phosphorylase (PNPase) is an enzyme involved in mRNA processing and degradation in bacteria. In *E. coli* PNPase interacts with the diguanylate cyclase DgcO (DosC) and the phosphodiesterase PdeO (DosP) and its activity is controlled by c-di-GMP (Tuckerman *et al.*, 2011).

---

[1] Hengge *et al.* (2016) recently introduced a systematic nomenclature for GGDEF and EAL containing proteins in *E. coli*. This nomenclature will be used throughout this work. The corresponding traditional designations are highlighted in brackets

Cellulose biosynthesis in *E. coli* species is another mechanism controlled by c-di-GMP. Cellulose production is stimulated by c-di-GMP binding the PilZ domain of BcsA (Amikam and Galperin, 2006). For maximal production of cellulose, *E. coli* requires another c-di-GMP effector protein, BcsE (Fang *et al.*, 2014). BcsE contains a GGDEF I-site like domain called GIL, which also binds the second messenger (Fang *et al.*, 2014).

E. coli MG1655 does not produce cellulose because of a single nucleotide polymorphism (SNP) in the *bcsQ* gene, which is essential in this process (Serra *et al.*, 2013b). The *bcsQ* mutation in MG1655 introduces a premature stop codon in the gene, resulting in a truncated and inactive protein (Serra *et al.*, 2013b).

1.4.2.1 Coordinated regulation of DGCs and PDEs production and activity in *Escherichia coli*

The presence of multiple DGCs and PDEs acting on several target mechanisms requires tight regulation to avoid redundancy and ensure the specificity of the signal. Achieving this specificity ensures that at a certain time, or a specific spatial compartment, the bacterium has a set of active proteins or "modules" composed of DGCs, PDEs, and c-di-GMP receptors (Hengge 2009). An example of a c-di-GMP module acting locally in *E. coli* is the aforementioned DgcM-PdeR-MlrA system (Lindenberg *et al.*, 2013).

Recently, six PDEs were identified in a screening designed to find PDEs controlling *E. coli* motility (Reinders *et al.*, 2015). Locked-on (constitutively active) mutants of these six PDEs regulated motility and influenced the c-di-GMP "global pool" of the bacterium (Reinders *et al.*, 2015). Interestingly, Reinders *et al.* (2015) did not identify any PdeR mutation in the screening. This finding agrees with previously reported data indicating PdeR involvement in c-di-GMP local signalling (Reinders *et al.*, 2015; Lindenberg *et al.*, 2013). Another explanation for the absence of PdeR locked-on mutants in this screening may result from the unsaturated nature of the screening (Reinders *et al.*, 2015).

Based on current understanding, one may reasonably posit a concomitant presence of "global" and "local" pools of c-di-GMP regulating various mechanisms in *E. coli*.

The interactions between c-di-GMP modules involved in regulation of different mechanisms can be avoided by "temporal separation". Temporal separation of c-di-GMP control modules occurs in *E. coli* through specific gene expression patterns and sensory

domains, which are only active under particular conditions (Hengge 2009). Such a temporal distribution of c-di-GMP modules is observed during the switch between flagellar motility and adhesion at the beginning of stationary phase (Pesavento *et al.*, 2008). In the exponential growth phase, PDE PdeH (YhjH) is produced and active, keeping c-di-GMP levels low and the bacteria motile. In post-exponential phase, the production of DGCs DgcE (YegE) and DgcQ (YedQ) raises c-di-GMP concentrations which inhibit motility (Pesavento *et al.*, 2008).

The transition between exponential and stationary phase together with the temporal separation of c-di-GMP modules is partially regulated by CsrA. During the exponential phase, CrsA acts on *flhDC* mRNA resulting in increased expression of the PDE-encoding gene *pdeH* (Wei *et al.*, 2001; Pesavento *et al.*, 2008). With onset of the stationary phase, the CsrB-C and McaS sRNA sequester CsrA (Liu *et al.*, 1997; Thomason *et al.*, 2012; Jørgensen *et al.*, 2013), resulting in increased translation of the *dgcZ* (*ydeH*) and *dgcT* (*ycdT*) mRNAs, encoding DGCs (Jonas *et al.*, 2008). CrsA sequestration may also negatively affect *pdeH* expression. The decreased activity of the *pdeH* promoter observed at the beginning of the stationary phase, when sequestration of CsrA occurs, supports this hypothesis (Sommerfeldt *et al.*, 2009).

These examples show how the coordinated regulation of DGCs and PDEs production and activity allows c-di-GMP control of multiple processes in *Escherichia coli*.

1.5 Function and regulation of the diguanylate cyclase DgcZ

DgcZ (known previously as YdeH) is the main DGC involved in PGA production (Boehm *et al.*, 2009; Steiner *et al.*, 2013). Transcription of *dgcZ* is activated by the regulator CpxR (Yamamoto and Ishihama, 2006; Price and Raivio, 2009; Raivio *et al.*, 2013). The precise physiological conditions influencing the CpxR-mediated transcriptional activation of *dgcZ* and the relevance of this regulation for bacteria are not fully understood. After transcription, *dgcZ* mRNA translation is inhibited by the carbon storage regulator CsrA (Jonas *et al.*, 2008; Boehm *et al.*, 2009).

The role of DgcZ-derived c-di-GMP in the stabilization of the PgaCD complex and biosynthesis of PGA has been described at length (Steiner *et al.*, 2013; Boehm *et al.*, 2009). But many questions remain. What physiological conditions permit DgcZ production and activation? And are there additional mechanisms regulating protein activity or localization? This study addresses these open questions.

1.5.1 *In vitro* evidence for Zn^{2+} regulation of DgcZ activity

Diguanylate cyclases possess GGEDF domains coupled with input domains (Galperin, 2006). The N-terminal domain of DgcZ is homologous to a domain first identified in the soluble *Helicobacter pylori* chemoreceptor TlpD, named CZB for its ability to bind zinc (Draper *et al.*, 2011). The CZB domain exists in more than 3,600 bacterial species (pfam family PF13682), and is often associated with chemoreceptors involved in chemotaxis (MCPs).

DgcZ binds zinc ions through a 3His/1Cys motif present in the CZB domain. It is unclear if this domain has a structural or a functional role (Draper *et al.*, 2011). Because DgcZ only possesses a catalytic GGDEF and a CZB domain, understanding the function of the CZB domain provides valuable insights into the activation and regulatory functions of this DGC.

With this motivation, researchers from the Biozentrum Basel (Franziska Zähringer, Tilman Schirmer and Urs Jenal) began a set of *in vitro* experiments to ascertain the function of the CZB domain within DgcZ.

Crystalizing the CZB and GGDEF domains, together with a DgcZ mutant (C52A), aided in the completion of a model for the diguanylate cyclase DgcZ (Zähringer *et al.*, 2013) (Fig. 5A). The protein crystallized as a homodimer, with one zinc ion tightly associated to each DgcZ monomer. Each zinc ion was coordinated by three conserved histidines (H22, H79, and H83) and one cysteine (C52), all located in the CZB domain (Fig. 5A). This structural data confirmed previous observations regarding the capability of the CZB domain (of TlpD) to bind Zn^{2+}, but did not provide evidence to support a structural, or functional, role for the zinc ions bound to DgcZ. To test if Zn^{2+} has an active role in the control of DgcZ protein activity, this researcher performed *in vitro* activity tests in the presence of EDTA, a zinc-chelating agent (Fig. 5B).

The addition of EDTA increased the diguanylate cyclase activity of both the wild-type protein and of the DgcZ (C52A) mutant more than 2-fold (Fig. 5B) (Zähringer *et al.*, 2013).
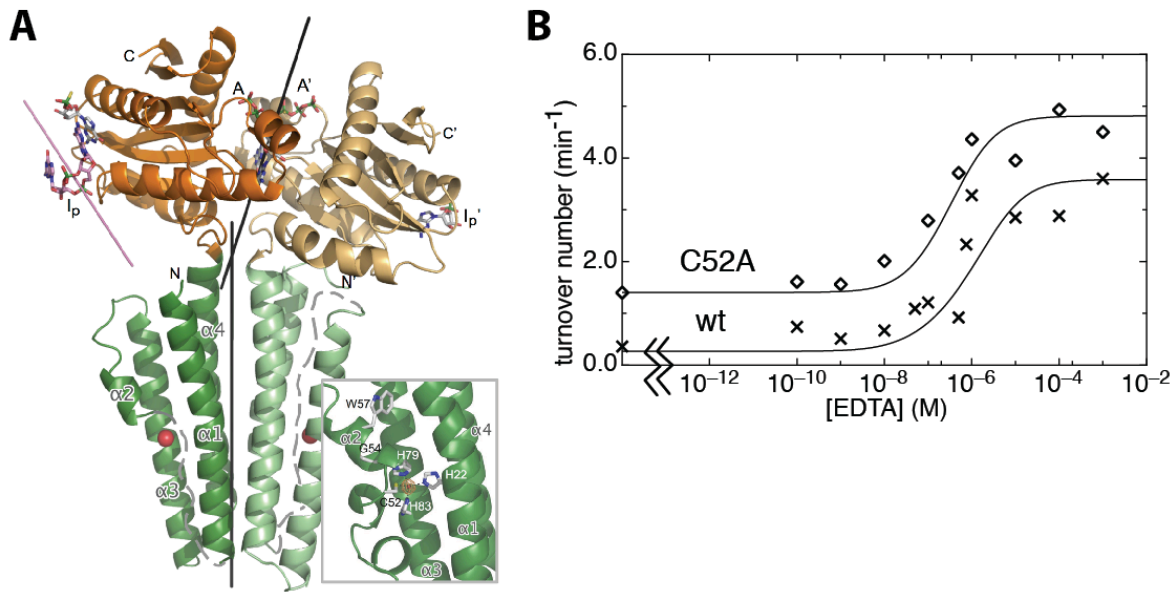
Figure 5. Structure of diguanylate cyclase DgcZ and *in vitro* analysis of protein activity upon addition of EDTA. (A) Structure of full-length DgcZ$_{C52A}$. The N-terminal CZB and the GGDEF domains are colored in green and orange, respectively. The subunits of the dimer are distinguished by color hue, termini are indicated. Black lines indicate the noncrystallographic dyads of the CZB and GGDEF dimer, the magenta line represents a local dyad that would generate an adjacent dimer in the crystal (omitted for clarity) with a c-di-GMP molecule on the axis mediating the interaction. Disordered segments are marked as dashed lines. The zinc ions bound to the CZB domains are depicted as red spheres. Substrate analog GTPαS molecules are bound to the active half-sites A and A` and to the inhibition sites (Ip and Ip0). Inset: high-resolution structure of the separated DgcZ$_{CZB}$ domain, close-up view onto the zinc site in monomer B. The zinc-coordinating residues (H22, C52, H79, and H83) and the conserved residues G54 and W57 are shown in stick representation. Overall, the domain structure is virtually identical to the CZB dimer of full-length DgcZ$_{C52A}$. (B) DgcZ activity in the presence of zinc chelator EDTA. Inhibition of wild-type DgcZ (crosses) and DgcZ$_{C52A}$ (diamonds) diguanylate cyclase activity, expressed as turnover number, is relieved by zinc sequestration to EDTA. Figure adapted from Zähringer *et al.,* 2013.

1.6 Study Objectives

Diguanylate cyclases (DGCs) synthesize c-di-GMP, a common and important second messenger shown to regulate bacterial motility, biofilm formation, virulence, cell differentiation, and other processes. Bacterial species possess several DGCs that are subjected to multiple regulatory steps, ensuring a robust, fine-tuned signalling response. DgcZ is the principle diguanylate cyclase controlling the production of the exopolysaccharide poly-GlcNAc (PGA), a crucial component in *Escherichia coli* surface attachment. The N-terminal domain of DgcZ is a homologue of the zinc-binding domain CZB of TlpD in *Helicobacter*

pylori and displays Zn^{2+} binding affinity. Additional *in vitro* evidence suggests a functional role for zinc in the regulation of DgcZ activity.

This study aims to elucidate the role of zinc in DgcZ regulation *in vivo*, and to better understand the physiological conditions influencing DgcZ production and the role of this diguanylate cyclase in the surface adhesion process.

One aim is to test the effects of zinc on the activity of DgcZ *in vivo* by employing protein variants carrying mutations in the amino acids involved in zinc binding and by the zinc addition to the bacterial growth medium. The goal of these approaches is to confirm initial *in vitro* data suggesting an inhibitory effect of zinc ions on DgcZ activity.

Another aim is to understand under which growth conditions the protein activity is important for the bacterium, which mechanisms are controlled by DgcZ and whether yet unexplored factors such as protein localization and protein-protein interactions regulate the protein function.

This work aims also to investigate the role of CpxR, a transcriptional regulator, shown to stimulate *dgcZ* expression, in relation to DgcZ-mediated surface attachment and biofilm formation.

This in-depth analysis of DgcZ regulation aims to improve our understanding of the physiological relevance of this diguanylate cyclase.

2. Material and Methods

2.1 Material

2.1.1 *E. coli* strains

Table 1. Strains used in this study

Strain designation	Genotype	Reference
MG1655	Wt	(Blattner *et al.*, 1997)
Tr1-5	*csrA::Tn5*(kan)	(Romeo *et al.*, 1993)
AB400	*csrA::Tn5*(kan)	(Boehm *et al.*, 2009)
AB3321	*csrA::Tn5*(kan), Δ*dgcZ*	This work
AB2010	*csrA::Tn5*(kan), *dgcZ*(H79,H83L)	This work
AB1062	*csrA::Tn5*(kan), *pgaD-3xFlag*	(Boehm *et al.*, 2009)
AB1063	*csrA::Tn5*(kan), Δ*dgcZ*, *pgaD-3xFlag*	(Boehm *et al.*, 2009)
AB1484	*csrA::Tn5*(kan), *dgcZ*(E208Q), *pgaD-3xFlag*	This work
AB3085	*csrA::Tn5*(cat), *dgcZ*(C52A), *pgaD-3xFlag*	This work
AB3089	*csrA::Tn5*(cat), *dgcZ*(H79L), *pgaD-3xFlag*	This work
AB3417	*csrA::Tn5*(cat), *dgcZ*(H83L), *pgaD-3xFlag*	This work
AB3090	*csrA::Tn5*(cat), *dgcZ*(H22L), *pgaD-3xFlag*	This work
AB3091	*csrA::Tn5*(cat), *dgcZ*(H79L,E208Q), *pgaD-3xFlag*	This work
AB3092	*csrA::Tn5*(cat), *dgcZ*(H22L,E208Q), *pgaD-3xFlag*	This work
AB3412	*csrA::Tn5*(kan), *dgcZ*(H79L,H83L), *pgaD-3xFlag*	This work
AB3088	*csrA::Tn5*(cat), *dgcZ*(H79L,H83L,E208Q), *pgaD-3xFlag*	This work
AB2012	*csrA*::Tn5(kan), *dgcZ*(H79L,H83L), Δ*pgaABCD*	This work
AB1057	*csrA*::Tn5(kan)::*Frt*, Δ*relA*::*Frt*, Δ*spoT*::*Frt*	(Boehm *et al.*, 2009)
AB1089	*csrA*::Tn5(kan)::*Frt*, Δ*relA*::*Frt*, Δ*spoT*::*Frt*, Δ*dgcZ*	(Boehm *et al.*, 2009)
AB3239	*csrA*::Tn5(kan)::*Frt-cat-Frt*, Δ*relA*::*Frt*, Δ*spoT*::*Frt*, *dgcZ*(H79L,H83L)	This work
AB1123	*csrA*::Tn5(kan)::*Frt*, Δ*relA*::*Frt*, Δ*spoT*::*Frt*, Δ*araB*	This work
AB1124	*csrA*::Tn5(kan)::*Frt*, Δ*relA*::*Frt*, Δ*spoT*::*Frt*, Δ*araB*, λatt::P$_{ara}$-*dgcA*-bla	This work
AB1072	*csrA::Tn5*(kan), *pgaD-GFP*	This work

AB1073	*csrA::Tn5*(kan), *ΔdgcZ, pgaD-GFP*	This work
AB3367	*csrA::Tn5*(kan), *dgcZ-mVENUS*	This work
AB3348	*dgcZ::PRha_ccdB-kan*	This work
AB3320	*csrA::Tn5*(kan), *dgcZ(+)*	This work
AB1299	*csrA::Tn5(kan), dgcZ(E208Q)*	(Boehm *et al.*, 2009)
AB3401	*csrA::Tn5*(kan), *dgcZ(+), pgaD-3xFlag*	This work
AB3408	*csrA::Tn5*(kan), *dgcZ(H79L,H83L)-mVENUS*	This work
AB3409	*csrA::Tn5*(kan), *dgcZ(H79L,H83L,E208Q)-mVENUS*	This work
GL60	*ibpA–mCherry::Frt-kan-Frt*	(Li and Young, 2012)
AB3403	*csrA::Tn5*(kan), *dgcZ-mVENUS, ibpA-mCHERRY*	This work
AB3369	*ΔcpxR*	This work
AB3402	*csrA::Tn5(kan), dgcZ-mVENUS, pgaD-3xFlag*	This work
AB1718 (Δ7)	*ΔpdeH, ΔpdeL, ΔpdeA, ΔpdeR, ΔpdeN, ΔpdeC, ΔpdeF*	This work
AB1872 (Δ9)	*ΔpdeH, ΔpdeL, ΔpdeA, ΔpdeR, ΔpdeN, ΔpdeC, ΔpdeF, ΔpdeB, ΔpdeI*	This work
AB3383	*ΔpdeH, ΔpdeL, ΔpdeA, ΔpdeR, ΔpdeN, ΔpdeC, ΔpdeF, csrA::Tn5*(kan), *pgaD-3xFlag*	This work
AB3384	*ΔpdeH, ΔpdeL, ΔpdeA, ΔpdeR, ΔpdeN, ΔpdeC, ΔpdeF, ΔpdeB, ΔpdeI, csrA::Tn5*(kan), *pgaD-3xFlag*	This work
AB3424	*ΔpdeI, csrA::Tn5*(kan), *pgaD-3xFlag*	This work
AB3425	*ΔpdeB, csrA::Tn5*(kan), *pgaD-3xFlag*	This work
AB3420 (Δ2)	*ΔpdeB, ΔpdeI*	This work
AB3426	*ΔpdeB, ΔpdeI, csrA::Tn5*(kan), *pgaD-3xFlag*	This work
BTH101	*Δcya*	(Battesti and Bouveret, 2012)
AB3411	*csrA::Tn5*(kan), *dgcZ-mVENUS, frdA-mCHERRY*	This work
AB3405	*csrA::Tn5*(kan), *dgcZ-mVENUS, frdB-mCHERRY*	This work
AB629	*ΔdgcZ*	(Boehm *et al.*, 2009)
AB3365	*ΔfrdA*	This work
AB3370	*ΔdgcZ, ΔfrdA*	This work
AB3389	*ΔfrdA, csrA::Tn5*(kan)	This work
AB3391	*ΔdgcZ, ΔfrdA, csrA::Tn5*(kan)	This work
AB3390	*ΔfrdB, csrA::Tn5*(kan)	This work
AB3392	*ΔdgcZ, ΔfrdB, csrA::Tn5*(kan)	This work

AB3413	*frdA::ccdB-kan*	This work
AB3414	*frdA::ccdB-kan, csrA::Frt*	This work
AB3415	*frdA*(+), *csrA::Tn5*(kan)	This work
AB3416	Δ*frdA^{Frt}, csrA::Tn5*(kan)	This work
AB3372	Δ*dgcZ,* Δ*cpxR*	This work
AB3418	Δ*cpxR, csrA::Tn5*(kan)	This work
AB3419	Δ*dgcZ,* Δ*cpxR, csrA::Tn5*(kan)	This work

2.1.2 Plasmids

Table 2. Plasmids used in this study

Plasmid name	Feature	Reference
pBAD18	Expression vector	(Guzman *et al.*, 1995)
pDL-mVENUS	Vector used for amplification of *mVENUS* template	Gifted from Daniella Cavalcanti de Lucena (unpublished)
pWBP20911	Vector used for amplification of *mCHERRY* template	(Charoenpanich *et al.*, 2015)
pKD45	Vector used for amplification of *kan-ccdB* construct	Gifted from K. Datsenko and B. Wanner (unpublished)
pKD46	λ-RED recombination plasmid	(Datsenko and Wanner, 2000)
pCP20	Plasmid used to remove the kanamycin resistence cassette	(Cherepanov and Wackernagel, 1995)
pDgcZ	Expression vector (pBAD18) for *dgcZ*	This work
pBAD-DgcZ-mVENUS	Expression vector for *mVENUS* fusion to *dgcZ*	This work
pCJ30	Expression vector	(Bibikov *et al.*, 1997)
pYfbR-mCHERRY	Expression vector for *mCHERRY* fusion to *yfbR*	This work
pNlpE	Expression vector (pCJ30) for *nlpE*	This work
pBAD-DgcZ(E208Q)-mVENUS	Expression vector for *mVENUS* fusion to *dgcZ*(E208Q)	This work
pBAD-GGDEF-mVENUS	Expression vector for *mVENUS* fusion to the nucleotide sequence encoding the GGDEF-domain	This work

pBAD-CZB-mVENUS	Expression vector for *mVENUS* fusion to the nucleotide sequence encoding the CZB domain	This work
pBAD-DgcA (pAB551)	Expression vector for *dgcA* (*C. crescentus*)	(Boehm *et al.*, 2009)
pKT25	Standard plasmid for bacterial two-hybrid	(Battesti and Bouveret, 2012)
pKNT25	Standard plasmid for bacterial two-hybrid	(Battesti and Bouveret, 2012)
pUT18	Standard plasmid for bacterial two-hybrid	(Battesti and Bouveret, 2012)
pUT18C	Standard plasmid for bacterial two-hybrid	(Battesti and Bouveret, 2012)
pUT18-zip	Standard plasmid for bacterial two-hybrid	(Battesti and Bouveret, 2012)
pKT25-zip	Standard plasmid for bacterial two-hybrid	(Battesti and Bouveret, 2012)
pKT25-DgcZ	Plasmid for bacterial two-hybrid	This work
pKT25-CZB	Plasmid for bacterial two-hybrid	This work
pKT25-GGDEF	Plasmid for bacterial two-hybrid	This work
pKT25-FrdA	Plasmid for bacterial two-hybrid	This work
pKT25-FrdB	Plasmid for bacterial two-hybrid	This work
pKNT25-DgcZ	Plasmid for bacterial two-hybrid	This work
pKNT25-FrdA	Plasmid for bacterial two-hybrid	This work
pKNT25-FrdB	Plasmid for bacterial two-hybrid	This work
pUT18-DgcZ	Plasmid for bacterial two-hybrid	This work
pUT18-FrdA	Plasmid for bacterial two-hybrid	This work
pUT18-FrdB	Plasmid for bacterial two-hybrid	This work
pUT18C-DgcZ	Plasmid for bacterial two-hybrid	This work
pUT18C-FrdA	Plasmid for bacterial two-hybrid	This work
pUT18C-FrdB	Plasmid for bacterial two-hybrid	This work

2.1.3 Oligonucleotide primers

Table 3. Oligonucleotide primers used to construct *dgcZ* mutants

Primer name	Sequence	Use
dgcZ-pKD45_rev_new	GAATCGTTGACACAGTAGCATCAG TTTTCTCAATGAATGTTAAACGGA GCacccggatattatcgtgaggatgcG	Generation of *dgcZ::PRha-ccdb-kan* strain

dgcZ_KO_pKD45_fwd	GatcaagaagacaacggaaattgatgccatcttgttaaatctcaatTCATTTCGAACCCCAGAGTCCCGC	
1651-dgcZ_test_fwd	Gccggaccagatgatcaaca ttagtgg	Generation of *dgcZ*(+) strain
1652-dgcZ_test_rev	tgactaatgaacggagataatccctcacc	
dgcZ_H79L_fwd	ggattctgccCTTcaacatatgcataac	Generation of *dgcZ*(H79L) strain
dgcZ_H79L_rev	gttatgcatatgttgAAGggcagaatcc	
dgcZ_H83L_fwd	caacatatgCTTaactgtggtcggg	Generation of *dgcZ*(H83L) strain
dgcZ_H83L_rev	cccgaccacagttAAGcatatgttg	
dgcZ_E208Q_fwd	cgctacgggggcCaagaatttatc	Generation of *dgcZ*(E208Q) strain
dgcZ_E208Q_rev	gataaattcttGgcccccgtagcg	
dgcZ_C52A_fwd	ccattcttatggactgGCGcagtttggtcggtgg	Generation of *dgcZ*(C52A) strain
dgcZ_C52A_rev	ccaccgaccaaactgCGCcagtccataagaatgg	
dgcZ_H22L_fwd	gctatcgatgccCTCtaccagtggc	Generation of *dgcZ*(H22L) strain
dgcZ_H22L_rev	gccactggtaGAGggcatcgatagc	
SacI_NcoI_dgcZ_FWd	tatagagctcGGAGTGCCATGGatgATCAAGAAGACAACGGAAATTGATG	Generation of *dgcZ-mVENUS* strain
P2_dgcZ_mVenus	GGGGGAATTCGGTACCCATCCTAGGAATCTCCTTTCTAGAatgAACTCGGTTAATCACATTTTGTTCGTCA	
P3_dgcZ_mVenus_optim	TaccgaattccccctcgatatcgggcccggcctatctggcctgggagctggacttccttcactgATGGTGAGCAAGGGCGAGGAG	
P4_mVenus_rev	tataAAGCTTTTACTTGTACAGCTCGTCCATGCCG	
P0_dgcZ_fwd_recomb	ACTGTGAAAAAGGAGTGGCAATGATCAAGAAGACAACGGAAATTGATG	Recombination of *dgcZ-mVENUS* strain and mutants
P5_mVenus_recomb	GAATCGTTGACACAGTAGCATCAGTTTTCTCAATGAATGTTAAACGGAGCtataAAGCTTTTACTTGTACAGCTCGTCCA	
Oligonucleotides are shown from 5' to 3'		

Table 4. Oligonucleotide primers used to construct *frdA* and *frdB* mutants

Primer name	Sequence	Use
frdA_pkd45_fwd	CTTACCCTGAAGTACGTGGCTGTG GGATAAAAACAATCTGGAGGAATG TCtcatttcgaaccccagagtcccgc	Generation of *frdA::PRha-ccdb-kan* strain
frdA_pkd45_rev(2)	CCACCTCAATTTTCAGGTTTTTCAT CtcaGCcatTCGCCTTCTCCTTCTTaccc ggatattatcgtgaggatgcG	
frdA_mCHERRY_f wd	CTTACCCTGAAGTACGTGGCTGTG GGATAAAAACAATCTGGAGGAATG TCgtgCAAACCT TTCAAGCCGATCTTG	Generation of *frdA-mCHERRY* strain
frdA_mCHERRY_r ev2	CCACCTCAATTTTCAGGTTTTTCAT CtcaGCcatTCGCCTTCTCCTTCTttacttgt aca gctcgtccatgcc	
frdA_fwd	CAGGTACTTACCCTGAAGTACGTG GCT	Generation of *frdB::Frt* and *frdB*(+) strain
frdA_rev_recom	GTCATAAGGCACTTCATAGAATGC GCT	
frdB_pkd45_fwd	AGCGGATGCAGCCGATAAGGCGGA AGCAGCCAATAAGAAGGAGAAGG CGAtcatttcgaa ccccagagtcccgc	Generation of *frdB::PRha-ccdb-kan* strain
frdB_pkd45_rev	ACGTCATTGGCCGTACATACGGTTT ACGTTTAGTCGTCATGTTGCACTCC acccggatat tatcgtgaggatgcG	
frdB_mCHERRY_f wd	AGCGGATGCAGCCGATAAGGCGGA AGCAGCCAATAAGAAGGAGAAGG CGAatgGCTGAGATGAAAAACCTGA AAAT	Generation of *frdB-mCHERRY* strain
frdB_mCHERRY_re v	ACGTCATTGGCCGTACATACGGTTT ACGTTTAGTCGTCATGTTGCACTCC ttacttgtac agctcgtccatgcc	
Oligonucleotides are shown from 5' to 3'		

Table 5. Oligonucleotide primers used for cloning and mutagenesis

Primer name	Sequence	Use
SacI_NcoI_dgcZ _FWd	tatagagctcGGAGTGCCATGGatgATC AAGAAGACAACGGAAATTGATG	Cloning of *dgcZ-mVENUS* in pBAD18
P4_mVenus_rev	tataAAGCTTTTACTTGTACAGCTCG TCCATGCCG	
dgcZ_HindIII_re v	atatAAGCTTttaAACTCGGTTAATCA CATTTTGTTCGTC	Cloning of *dgcZ* in pBAD18
SacI_NcoI_dgcZ _FWd	tatagagctcGGAGTGCCATGGatgATC AAGAAGACAACGGAAATTGATG	
nlpE_pcj30_Bam	GCTGCAGGATCCGGTGAAAAAAG	Cloning of *nlpE* in pCJ30

HI_fwd	CGATAGTGACAGCGA	
nlpE_pcj30_HindIII_rev	CCAAGCTTGttaCTGCCCCAAACTACTGCAATCC	
yfbR_BamHI_fwd	CTAGAGGATCCCAAACAGAGCCATTTCTTTGCCCATCT	Cloning of *yfbR-mCHERRY* in pCJ30. In addition, primer P4_mVENUS_rev was used
yfbR_KpnI_rev	CTTAGGTACCcgAGCGGTGAATCCTGGCTAATCTCAT	
mCHERRY_KpnI_fwd	cgGGTACCGGTGAGCAAGGGCGAGGAGCTG	
dgcZ_BamHI_fwd	tataGGATCCAatgATCAAGAAGACAACGGAAATTGATG	Cloning of *dgcZ* in BTH plasmids
dgcZ_KpnI_rev	CTTAGGTACCcgAACTCGGTTAATCACATTTTGTTCGTCA	
CZB_KpnI_rev	CTTAGGTACCcgGCTACGGATCGTCAGCAAATAAATTT	Cloning of CZB domain of *dgcZ* in BTH plasmids. dgcZ_BamHI_fwd was used in addition
GGDEF_BamHI_fwd	CTAGAGGATCCCGGAGTGCCTGTGatgAATATGGATGTTTTGACGGGATTGC	Cloning of GGDEF domain of *dgcZ* in BTH plasmids. DgcZ_KpnI_rev was used in addition
frdA_BamHI_fwd	CTAGAGGATCCCCAAACCTTTCAAGCCGATCTTGC	Cloning of *frdA* in BTH plasmids.
frdA_KpnI_rev	CTTAGGTACCcgGCCATTCGCCTTCTCCTTCTTATTG	
frdB_BamHI_fwd	CTAGAGGATCCCGCTGAGATGAAAAACCTGAAAATTGAGG T	Cloning of *frdB* in BTH plasmids.
frdB_KpnI_rev	CTTAGGTACCcgGCCATTCGCCTTCTCCTTCTTATTG	
SacI_dgcZ_GGDEF_FWd	tatagagctcGGAGTGCCTGTGatgAATATGGATGTTTTGACGGGATTGC	Cloning of GGDEF-mVENUS in pBAD. In addition, primer P4_mVENUS_rev was used
CZB-mVenus_rev_P2	gggggaattcggtacccatcctaggaatctcctttctagaATGgctacggatcgtcagcaaataaattttgt	Cloning of CZB-mVENUS in pBAD. In addition, primer SacI_NcoI_dgcZ_FWd was used
Linker used for the *dgcZ-mVENUS* construct	catTCTAGAAAGGAGATTCCTAGGATGGGTACCgaattccccctcgatatcgggcccggcctatctggcctgggagctggacttccttcactg	
Oligonucleotides are shown from 5' to 3'		

2.1.4 Chemicals and enzymes

Chemicals were purchased from Carl Roth, Sigma-Aldrich, Merck, Roche and QIAGEN. Enzymes were purchased from New England Biolabs (NEB), Roche or Fermentas.

2.1.5 Growth media, solutions and buffers

LB medium

LB medium was prepared using 10 g/L Tryptone (BD), 5g/L Yeast extract (BD) and 5 g/L NaCl (Carl Roth). LB agar was prepared by adding 15 g/L Agar (BD). The medium was then autoclaved at 120 °C for 20 minutes.

LB spent medium

LB spent medium was prepared by sterile filtration of LB medium collected after *E. coli* growth. 50 mL of LB medium was inoculated with 500 µL (1:100 dilution) of a culture containing the *dgcZ-mVENUS/csrA::Tn5* strain (Table 1) grown over-night. This culture was then grown under shaking conditions at 37 °C for 24 hours. The OD_{600} ranged from 4.5 to 5.2. This culture was centrifuged at 5,000 rpm for 20 minutes and the supernatant was filtered using a 0.22 µm PES syringe filter (Sarstedt) to obtain sterile spent medium. Before use, the spent medium was tested to assure that each aliquot of was sterile and not supporting bacterial growth.

Buffered LB medium

Buffered LB medium was prepared by adding K_2HPO_4 (50 mM) and KH_2PO_4 (15 mM) to the LB medium. When necessary, the pH was adjusted to the desired value by the addition of HCl, or NaOH. The medium was then sterile filtered using a 0.2 µm filter.

MMA medium

10X MMA	Required for 1.0 L
K_2HPO_4	105.0 g
KH_2PO_4	45.0 g
$(NH_4)2SO_4$	10.0 g
Tri-sodium citrate - 2 H_2O	5.0 g

The above ingredients were dissolved in ddH_2O to a final volume of 1.0 L and autoclaved before use (Miller, 1972).

MMA 1X was obtained through the dilution of 10X MMA in sterile ddH_2O and the addition of $MgSO_4$ to a concentration of 1 mM. When indicated, the pH was adjusted by addition of HCl or NaOH. The medium was sterile filtered using a 0.2 µm filter.

Minimal medium plates contained 15.0 g/L agar, $MgSO_4$ (1 mM) and MMA 1X (Miller, 1972). MMA medium and agar were supplemented with 0.2% rhamnose, unless otherwise indicated.

TSS (Transformation and Storage Solution)

2X TSS	For 250 mL
Bacto-Tryptone	2.0 g
Yeast Extract	1.25 g
NaCl	1.25 g
PEG 8000	50 g

The 2X TSS solution was prepared as described by Chung *et al.* (1989). The above ingredients were dissolved in 125 mL ddH_2O. Then 25 mL of both $MgSO_4$ (1 M, stock solution) and DMSO (99.8%, stock solution) were added. This solution was brought to a pH of 6.5, and a final volume of 250 mL by adding distilled water. Before use, the solution was sterile filtered using a 0.2 µm filter.

Antibiotics

Antibiotic solutions were prepared and used at the concentrations indicated below:

Antibiotic	Stock solution	Final concentration	Solvent
Ampicillin	100 mg/mL	100 μg/mL	ddH$_2$O
Kanamycin	50 mg/mL	50 μg/mL	ddH$_2$O
Streptomycin	75 mg/mL	75 μg/mL	ddH$_2$O

All antibiotic solutions were sterilized using filters with a pore size of 0.2 μm and stored in aliquots at -20 °C.

Z-buffer

Component	For 1 L	Final concentration
Na$_2$HPO$_4$ ∘ 2 H$_2$O	10.5 g	0.06 M
NaH$_2$PO$_4$	4.78 g	0.04 M
KCl	0.75 g	0.01 M
MgSO$_4$ (stock solution 1 M)	1.0 mL	0.001 M
β-mercaptoethanol	2.7 mL	0.05 M

The ingredients mentioned above were dissolved in 800 mL ddH$_2$O and pH was adjusted to 7.0 by addition of HCl or NaOH. Finally, ddH$_2$O was added to a final volume of 1.0 L (Miller, 1972).

2.2 Methods

2.2.1 Cultivation of microbial cells

Bacterial strains used in this work are listed in Table 1. Bacteria were grown in LB medium at 37 °C under shaking conditions (250 rpm), unless otherwise indicated.

2.2.2 Generation of *E. coli* mutants

Site-directed mutagenesis (2.2.3) and P1 transduction (2.2.4) were used to generate *E. coli* mutants.

The *csrA::Tn5* mutation was introduced by P1 transduction using an AB400 donor strain (Boehm *et al.*, 2009). Since the *csrA*::Tn*5* mutation can result in the appearance of suppressors, the strains were P1 transduced before use. P1 transduction was also applied to replace the native *pgaD* allele with *pgaD-3xFlag-kan* and delete genes using P1 lysates derived from strains of the Keio collection (Baba *et al.*, 2006).

The Δ7 and the Δ9 strains, carrying 7 or 9 deletions of PDE-encoding genes, for instance, were generated by several cycles of P1 transductions using as donor the strains of the Keio collection. Each cycle was followed by removal of the kanamycin resistance cassette using the pCP20 plasmid (Cherepanov and Wackernagel, 1995).

Site-directed mutagenesis allowed for the creation of all the novel mutations described in this thesis. In particular, with this procedure were generated all the *dgcZ* mutants, including the fusions to *mVENUS*, and the *mCHERRY* fusions to *frdA-B*.

2.2.3 Site-directed mutagenesis of *E. coli*

Site-directed mutagenesis was achieved using the λ-RED recombination technique described by Datsenko and Wanner (2000).

A two-step recombineering procedure was required to generate scarless mutations. First, a construct carrying the *kan* resistance cassette fused to a counterselectable marker (the L-rhamnose inducible *ccdB* toxin gene), replaced the target gene. In the second step, the desired mutated allele replaced this *kan-ccdB* element. Selection was performed on minimal medium plates containing 0.2% L-rhamnose. The *kan-ccdB* element was amplified from the pKD45 plasmid with specific primers indicated in Table 3 and 4.

All integrations generated by λ-RED-mediated recombineering were confirmed by DNA sequencing.

2.2.3.1 Preparation of electrocompetent *E. coli* for λ-RED recombination

Electrocompetent *E. coli* cells for λ-RED recombination were prepared as described by Datsenko and Wanner (2000). An overnight culture of a strain carrying the RED helper plasmid pKD46 was diluted 1:100 in LB medium supplemented with ampicillin (100 μg/mL), and then incubated with agitation at 30 °C. At an OD_{600} of 0.2, the expression of λ-RED genes (γ, β, exo) was induced by 0.2% L-arabinose (stock solution 20%) and incubation was continued to an OD_{600} of 0.5. The culture was rapidly cooled in an ice water bath by gently swirling the culture flask for 10 minutes. These cold cells were transferred to chilled 50 mL tubes. The bacteria were sedimented by centrifugation at 4,000 rpm and 4 °C for 10 minutes (Heraeus Multifuge X3R). After centrifugation, the pellet formed was washed three times with ice-cold 10% glycerol. Finally, the cells were concentrated 100-fold compared to the initial culture volume and kept on ice.

2.2.3.2 Transformation of electrocompetent *E. coli* for λ-RED recombination

A Biorad model MicroPulserTM enabled the transformation of electrocompetent *E. coli* by electroporation (Dower *et al.*, 1988). 100 μL of fresh electrocompetent cells and 50-250 ng of purified linear donor DNA were first transferred to ice-cold 1 mm HiMaX cuvettes (EP-101 cell projects). *E. coli* cells were electroporated with one pulse of 2.5 kV for 5 ms. The bacterial cells were immediately re-suspended in 1 mL of LB medium. Bacteria were then incubated at 37 °C under shaking conditions for 1 hour. Half of this culture was then sedimented by centrifugation at 13,000 rpm for 1 minute (Eppendorf Centrifuge, 5418). The pellet formed was resuspended in 100 μL of LB medium and plated on agar containing an appropriate antibiotic. After overnight incubation at 37 °C, recombinants were isolated from the plates.

2.2.4 P1 transduction

Phage-mediated bacterial transduction methods facilitate the transfer of genetic elements from one strain to recipient strains of the same, or closely related, species. In *E. coli*, phage-induced transduction is commonly achieved using P1vir, an obligate, virulent and

mutated phage (referred to as "P1").

Infection begins with phage attachment and entry into a bacterial cell. Once inside the cell, the phage begins the lytic cycle, which is characterized by replication of phagic DNA, the production of phagic particles and the lysis of the bacterial cell. Through self-assembly of the phage P1, approximately 100 kb of DNA is integrated by a headful packaging mechanism. Despite the existence of specific Pac recognition sites, bacterial fragments are accidently incorporated into about 3% of all phage particles. Upon infection of recipient strains, the donor DNA integrates into the recipient genome via homologous recombination (double crossover). Since the transfer and integration of a specific genetic element is a rare event, antibiotic markers are employed to select successful phage-induced transduction events.

Prior to P1 transduction (adapted from Miller, 1992), an overnight culture containing the recipient strain was diluted 1:100 in 5 mL LB medium and incubated with agitation at 37 °C until an OD_{600} of 0.5 was reached. Subsequently, a final concentration of 10 mM $CaCl_2$ (stock solution 1 M) was added and the suspension was vortexed briefly.

100 µL P1 lysate containing donor constructs were used to infect 1 mL recipient cells. The suspension was mixed by vortex and incubated on the benchtop for 15 minutes. To stop infection, sodium citrate was added to 100 mM (stock solution 1 M) to chelate calcium. Phenotypic expression was done at 37 °C with agitation for 1 hour, and plated on selective agar plates containing sodium citrate (20 mM, final concentration). Colonies were picked and streaked twice on selective agar plates to prevent carrying over of phages.

2.2.4.1 Preparation of P1 lysates

The following procedure used to prepare P1 lysates, adapted from Miller (1992), began by incubating a strain carrying the donor construct at 37 °C under shaking conditions (250 rpm) over night in LB medium. The following day, the culture was diluted 1:100 in 7 mL of LB medium and grown, as described above, to an OD_{600} of 0.2-0.3. After adding $CaCl_2$ (stock solution 1 M) to a final concentration of 10 mM, the culture was infected with 10 µL of the *E. coli* K-12 MG1655, P1 starter lysate and briefly vortexed. The culture was again incubated for approximately 3 to 4 hours at 37 °C with agitation. Incubation was interrupted when the culture turned clear, indicating bacterial lysis. To assure complete bacterial lysis, 250 µL $CHCl_3$ were added and the sample was vortexed for ten seconds. The bacterial cell debris was then sedimented by centrifugation at 5,000 rpm for 10 minutes. The supernatant was

transferred to a new glass tube supplemented with 50 μL CHCl₃ and stored at 4 °C before use.

2.2.5 Construction of protein fusions to mVENUS and mCHERRY

The fluorescent protein *mVENUS* differs from *VENUS* because the A206K mutation prevents protein dimerization (Zacharias *et al.*, 2002; Nagai *et al.*, 2002). Generating *dgcZ-mVENUS* fusions for the purpose of this work, first required amplifying *mVENUS*.

mVENUS was amplified from the plasmid template pDL-mVENUS (D. Cavalcanti De Lucena, unpublished) using the primers P3_dgcZ_mVenus_optim, and P4_mVenus_rev. For *dgcZ*, the primers SacI_NcoI_dgcZ_FWd and P2_dgcZ_mVenus were used. Once amplified, the *dgcZ* fragment was digested with SacI, and EcoRI, whereas *mVENUS* was digested with EcoRI and HindIII.

Using the SacI and HindIII restriction sites, the digested *dgcZ* and *mVENUS* fragments were inserted into the pBAD18 plasmid. The resulting pBAD-DgcZ-mVENUS plasmid served as the template in PCR amplification of the *dgcZ_mVENUS* construct applied for recombineering. This cloning strategy resulted in the insertion of a DNA sequence of 93 nucleotides encoding a flexible linker of 31 amino acids (sequence provided by D. Cavalcanti De Lucena and indicated in Table 5) between *dgcZ* and the *mVENUS* coding region.

The plasmid carrying *yfbR-mCHERRY* was obtained by cloning *yfbR* and *mCHERRY* into pCJ30 (Bibikov *et al.*, 1997). Using the yfbR_BamHI_fwd and yfbR_KpnI_rev primers, the *yfbR* gene was amplified and then digested with the BamHI and KpnI restriction enzymes. *mCHERRY* was amplified from the template pWBP20911mCherry (Charoenpanich *et al.*, 2015) using mCHERRY_KpnI_fwd and P4_mVENUS_rev and digested with KpnI and HindIII.

Digested *yfbR* and *mCHERRY* fragments were inserted into the pCJ30 vector, using the KpnI and HindIII restriction sites. This same strategy was applied to generate *frdA-* and *frdB-mCHERRY*.

The plasmids for the bacterial two-hybrid (BACTH) assays were constructed inserting the bait and prey sequences into the pKT25, pKNT25, pUT18, pUT18C vectors using the restriction sites for BamHI and KpnI (Battesti and Bouveret, 2012).

Primers used for amplification of bait and prey sequences are listed in Table 5. All plasmids and constructs were sequenced before use.

2.2.6 Polymerase chain reaction (PCR)

The polymerase chain reaction (PCR) is a technique by which small samples of DNA can be quickly amplified, that is, increased to quantities that are large enough for *in vitro* analysis (Saiki *et al.*, 1986). PCR reactions were usually performed in a total volume of 50 µL, using *Taq* DNA Polymerase provided by Sigma. The Q5 DNA Polymerase (NEB), possessing 3´- 5´ exonuclease activity, was employed for cloning purposes. The necessary reagents for PCR using *Taq* DNA Polymerase are included below:

Reagent	Final volume
10X Thermo Polymerase Buffer (Sigma)	5 µL
dsDNA template	>10 ng
Oligonucleotide primer 1 (10 µM)	2.5 µL
Oligonucleotide primer 2 (10 µM)	2.5 µL
dNTP mix (2 mM)	5 µL
Taq DNA Polymerase (Sigma, 5 U/µL)	1 µL
ddH$_2$O	to 50 µL Vf

In PCR reactions using Q5 DNA Polymerase, however, 10 µL 5X Q5 Reaction Buffer (NEB) replace the 10X Thermo Polymerase Buffer, and 0.5 µL Q5 DNA Polymerase were added to each reaction, instead of 1 µL *Taq*.

Annealing temperatures varied in accordance with the primers used and were calculated for each reaction using either the Jena Bioscience calculator (*Taq*) or the NEB Tm Calculator (Q5). Elongation times of the product changed in response to the length of the gene of interest and were calculated with 1 min/kb (*Taq*) or 30 sec/kb (Q5). PCR reactions were performed using the thermal cycling parameters described below:

Step	Temperature	Time	Cycles
1. Initial denaturation	95 °C	5 min	1X
2. Denaturation	95 °C	30 sec	31X
3. Primer annealing	55 °C	30 sec	
4. Extension	72 °C	30-60 sec / kb	
5. Final Extension	72 °C	10 min	1X

For colony PCR, the reaction mixture in each tube contained ddH$_2$O, 10X reaction buffer, oligonucleotides and dNTPs as previously described. Selected colonies were transferred to PCR tubes for use as templates. Next, *Taq* DNA Polymerase was added and thermal cycling was initiated in the manner described above.

2.2.7 Restriction and ligation of DNA fragments for cloning

PCR products and plasmids were digested using the "FastDigest" restriction enzymes (ThermoFisher Scientific) and protocols recommended by the manufacturer. In most cases, the reaction mixture was incubated at 37 °C for 2 to 3 hours. After incubation, the digested product was loaded on a 1% agarose gel and purified using a QIAquick Gel Extraction Kit (QIAGEN). The DNA concentration was quantified using a NanoDrop spectrophotometer.

The ligation reaction was prepared using T4 DNA Ligase (ThermoFisher Scientific) as described below:

Reagent	Final volume/concentration
Vector DNA	25 ng
Insert DNA	(10 x ng Vector x kb insert)/kb Vector
T4 DNA Ligase 10X Buffer	2 µL
T4 DNA Ligase	1 µL
dH$_2$0	to 20 µL Vf.

The reaction was incubated over night at 4 °C. The following day, 10 µL of the reaction mixture were transformed into chemical competent *E. coli* DH5α cells. The transformed cells were plated on LB plates with the corresponding antibiotic and incubated at 37 °C for 24 hours. Single colonies were then chosen and used to isolate the generated construct.

2.2.8 Plasmid DNA preparation

Plasmid DNA was isolated using the "Plasmid DNA Purification" kit and protocol provided by Macherey-Nagel, the manufacturer.

Briefly, 6 mL of an overnight culture were harvested by centrifugation for 30 seconds at 14,000 rpm (Eppendorf Centrifuge 5418). The pellet was resuspended in 250 μL Buffer A1, which was followed by the addition of 250 μL of Buffer A2. The suspension was gently mixed by inverting the tube six to eight times, and incubated at room temperature for 4 to 5 minutes until the lysate was clear. The lysis reaction was stopped by adding 300 μL of the Buffer A3 to the solution and inverting the tube six to eight times. The suspension was then centrifuged for 10 minutes at 14,000 rpm and the supernatant was transferred to the provided column and centrifuged for 1 minute at 14,000 rpm. The column was washed by 500 μL of Buffer AQ (supplemented with ethanol) and the flow-through was discarded. The column was centrifuged once more to remove any remaining buffer and dry the silica membrane.

Plasmid DNA was eluted by adding of 30 μL ddH$_2$O to the column, which was then centrifuged for 1 minute at 14,000 rpm. The concentration of plasmid DNA was quantified using a NanoDrop spectrophotometer. Plasmids were stored at -20 °C.

2.2.9 TSS-Transformation of *E. coli*

TSS-Transformation is a quick and efficient method to introduce plasmid DNA into *E. coli* strains (Chung *et al.*, 1989). A single colony of the target strain (or a 1:100 dilution from an overnight culture) was inoculated in two mL of LB medium and grown until reaching an OD$_{600}$ value between 0.3 and 0.8. The culture was then chilled on ice for 10 minutes, and an equal volume of ice-cold 2X TSS was added. The bacterial suspension was then vortexed and incubated on ice for another 10 minutes. At least 10 ng of plasmid DNA was added, and then the suspension was mixed by vortexing. The mixture was then incubated on ice for 30 minutes. When selecting for ampicillin-resistant bacteria, 200 μL of culture was immediately placed on selective plates. To select for bacteria carrying different resistance markers, the transformants were incubated at 37°C for 1 hour under shaking conditions to allow phenotypic expression and then 200 μL of culture was placed on selective plates.

2.2.10 Congo red assay

Congo red is a dye used in microbial research to stain amyloid fibers (curli) and bind the exopolysaccharide PGA (Serra *et al.*, 2013; Steiner *et al.*, 2013). To prepare this assay, a

10% solution of Congo red in distilled water was mixed with liquid LB agar (1:20 dilution) and plates were immediately poured. The Plates were then irradiated with UV light in a sterile hood for 20 minutes and stored for 24 or more hours at 4 °C before use. Single colonies were streaked on Congo red plates and incubated at 37 °C overnight. A Nikon D3300 digital camera was then used to photograph the plates. Adobe Photoshop software was used to decrease the red color intensity of these photographs.

2.2.11 Western blot

Bacterial culture methods are described in the legend of each figure. At specific times, the optical densities of these cultures were measured, and 200 to 500 µL of culture were centrifuged at 13,000 rpm for 1 minute. Supernatants were discarded and pellets were resuspended in adequate volumes of SDS-sample buffer 1X. Sample concentrations were normalized to an OD_{600} value of 5.0. Samples were vortexed for 10 seconds and boiled for 5 minutes.

Gel electrophoresis and blotting were conducted using standard protocols. PgaD-3xFlag was detected in Western blots using monoclonal, anti-M2 mouse, and HRP-conjugated rabbit anti-mouse antibodies (DakoCytomation). Both antibodies were diluted 1:10,000 in a solution of PBS 1X containing 0.1% tween and 5% non-fat milk. Detecting DgcZ and GroEL by Western blotting required the primary antibodies anti-DgcZ (T. Schirmer and U. Jenal, unpublished), diluted to 1:2,000 and anti-GroEL, diluted to 1:10,000 (SIGMA). The HRP-conjugated, anti-rabbit (1:10,000) served as the secondary antibody for both DgcZ and GroEL blots. In every case, the primary antibody was incubated overnight at 4 °C, while the secondary antibody was incubated at room temperature for 1 hour. After incubation with both the primary and secondary antibodies, the membranes were washed three times for 5 minutes with a PBS 1X solution containing 0.1% tween. Western blots were developed using a ECL Kit (Pierce) and documented with an ImageQuant LAS 4000 (GE Healthcare).

2.2.12 Attachment assay

Attachment assays are used to measure bacterial biofilm formation (Boehm *et al.*, 2009; Zahringer *et al.*, 2013). Bacteria were grown on LB plates overnight at 30 °C, and single

colonies were inoculated in 200 µL of LB medium in a 96-well plate (BD Falcon - 353072). These plates next underwent static incubation at 30 °C for 24 hours. Cell density was recorded at 600 nm using a TECAN Infinite M200 Pro plate reader, the supernatants were discarded, and then the plates were filled with distilled water using a multichannel pipet. This water was removed, and the plates were dried for 15 to 20 minutes. Each well was then filled with 200 µl of crystal violet solution (0.1% in H2O, 1-propanol, methanol [96.7: 1.66:1.66]) and incubated at room temperature with moderate shaking (100 rpm) for at least 30 minutes. The wells were washed twice with water to remove the staining solution and dried, again for 15 to 20 minutes.

Retained crystal violet solution was redissolved in 200 µl of 20% acetic acid and quantified at 600 nm in a plate reader. If any measurement was outside the dynamic range of the plate reader, then the crystal violet solutions were diluted 1:4 in 20% acetic acid and measured once again.

Normalized attachment values describe the ratio of the optical density of dissolved crystal violet, which corresponds to the attached biomass, divided by the cell density. Generally, a single data point is derived from at least six replicates. Error bars for normalized attachment values represent the standard error of the means.

2.2.13 Quantification of intracellular c-di-GMP concentrations

Bacterial cultures grown overnight in LB medium at 37 °C under shaking conditions (250 rpm) were diluted 1:100 in 20 mL of LB medium and grown under the same conditions. After 9 hours OD_{600} values of 3.1 to 3.2 were measured, and after 48 hours, an OD_{600} value of 4.5 was recorded. At both time points, 5 mL of each culture were transferred to a cold, 15 mL Falcon tube, and centrifuged at 4 °C for 10 minutes at 2,500 g. The pellet was resuspended in 1 mL of LB medium and transferred into 2 mL Safe-Lock tubes (Eppendorf), which were centrifuged at 4 °C for 20 minutes at 2,500 g.

The supernatant was removed, and the pellet resuspended in 300 µL of solution A (acetonitrile / methanol / water - 2:2:1) and cooled on ice for 15 minutes.

The tube was incubated at 95 °C for 10 minutes and then placed on ice for 5 minutes. After centrifugation for 10 minutes at 4 °C and 20,800 g, the supernatant was collected and stored on ice.

The pellet was resuspended in 200 μL of solution A, incubated on ice for 15 minutes, and then centrifuged for 10 minutes at 4 °C and 20,800 g. 200 μL of supernatant was collected and then added to the 300 μL of previously collected supernatant.

Once again, the pellet were resuspended in 200 μL of solution A, incubated for 15 minutes on ice and then centrifuged for 10 minutes at 4 °C and 20,800 g. 200 μL of supernatant was collected and added to the 500 μL of previously collected supernatant for a total volume of 700 μL. The tube containing 700 μL of supernatant, was then incubated overnight at -20 °C.

The following day, this tube was centrifuged at 4 °C for 10 minutes at 20,800 g and the supernatant was collected. The sample was then lyophilized for 2 hours at 30 °C, and sent for c-di-GMP quantification at a specialized mass spectrometry facility.

As described by Burhenne and Kaever (2013), the sample was analyzed by liquid chromatography-tandem mass spectrometry.

2.2.14 Microscopy

Bacterial cultures were grown as indicated in the figure legends. 4 μl of each culture were placed on 1% agarose pads (in PBS 1X) for observation. Differential interference contrast (DIC) and total internal reflection fluorescence (TIRF) microscopy was applied to examine individual bacterial cells. A Nikon Eclipse Ti-E inverse microscope was used. The microscope was equipped with 100X CFI Apo TIRF Oil objective (numerical aperture of 1.49), and AHF HC filter sets F36-528 (excitation band pass 500/24 nm, beam splitter 520 nm, emission band pass 542/27 nm) and F36-504 (excitation band pass 562/40 nm, beam splitter 593 nm, emission band pass 624/40 nm). A Multiline Argon laser (Melles Griot) 65 mW (MHX00171) and a Sapphire laser 561 nm - 50 mW (MHX00146) were used as light sources for mVENUS and mCHERRY microscopy, respectively. Exposure times ranged from 50 to 300 ms.

Images were acquired with an Andor iXon3 885 EMCCD camera. Image acquisition and adjustment was done with the Nikon NIS elements 4.0 software and with ImageJ. For time-lapse fluorescence microscopy bacterial stationary phase cultures (4 μL) were spotted onto agarose pads (LB, 1% agarose) and were grown at 30 °C under the microscope. Images were acquired every 15 minutes.

2.2.14.1 Microfluidics

Details about the preparation and the set up of the microfluidic system used for this experiments have been described elsewhere (Arnoldini *et al.*, 2014; Wang *et al.*, 2010).

The *E. coli dgcZ-mVENUS/ibpA-mCHERRY/csrA::Tn5* strain (Table 1) was cultured in LB medium at 37 °C to an OD_{600} of 0.2 and salmon sperm DNA and BSA were added to the preculture to a final concentration of 75 μg/mL and 25 μg/mL respectively to prevent excessive biofilm formation within the flow chamber device. 1 mL of this cell suspension was then spinned down for 1 minute at 8,000 rpm and the resulting cell pellet was recovered in 20 μL of the residual LB. 1 μL of this suspension was transferred into the main channel and the applied medium flow flushed the cells into the side channels. With the help of two programmable syringe pumps (NE-1000; New Era Pump Systems Inc.) a medium gradient from fresh (F) to spent (S) LB medium was driven. The following program was applied: (i) 2 hours constant flow of F 0.7 mL/h and S 0.1 mL/h, (ii) 3 hours of a gradient from F 0.7 mL/h to F 0.0 mL/h and from S 0.1 mL/h to S 0.7 mL/h, (iii) 16 hours constant flow of S 0.3 mL/h, (iv) 1 hour of a gradient from S 0.3 mL/h to S 0.0 mL/h and from F 0.0 mL/h to F 0.7 mL/h, and (v) 20 hours constant flow of F 0.7 mL/h.
The microfluidic device was mounted on an automated Olympus BX81 microscope equipped with an UPLFN100O2PH/1.3 phase-contrast oil objective and an incubator chamber set to 37 °C (Cube and Box incubation system, Life Imaging Services, Reinach, Switzerland). mVenus (U-N41028 filter (Chroma); excitation band pass 500/20 nm, beam splitter 515 nm, emission band pass 535/30 nm) and mCherry (U-N49008 (Chroma); excitation band pass 560/40 nm, beam splitter 585 nm, emission band pass 630/75 nm) fluorescence and phase contrast images were taken every 12 minutes. Image analysis was finally performed using the CellM software (Olympus) and Fiji / ImageJ.

2.2.15 Co-immunoprecipitation (CoIP)

The *dgcZ-3xFlag* and *dgcZ*(wt) strains, both in the *csrA*::Tn*5* background, were cultured in 200 mL of LB broth at 30 °C under shaking conditions to an OD_{600} of 0.65. For the stationary phase condition, bacteria were cultured in 50 mL LB for 48 hours (OD_{600} of 4.5). 37% formaldehyde was added to a final concentration of 0.2% and cultures were shaken for 15 minutes. Glycine (1.875 M) was added to a final concentration of 0.375 M and cultures

were shaken for 5 minutes. Bacteria were collected in 50 mL tubes and centrifuged at 4,000 g for 10 minutes at 4 °C. Bacterial pellets were then resuspended in 24 mL (6 mL for stationary phase condition) TE buffer supplemented with 0.1% sarkosyl and centrifuged as before. Pellets were washed twice with 50 mL (12.5 mL for stationary phase condition) cold PBS 1X, frozen in liquid nitrogen and stored at -80 °C. Before use, pellets were resuspended in 4 mL of lysis buffer (50 mM Tris-HCl, pH 7.4, 150 mM NaCl, 1 mM EDTA, 1% TRITON X-100, 0.2 mM PMSF) and disrupted using a French press. Cell lysates were then centrifuged at 100,000 g for 1 hour at 4 °C. 40 µL of the ANTI-FLAG M2 resin (Sigma #A2220) were added to the cleared lysates and incubated overnight with shaking at 4 °C.

The suspensions were centrifuged; the beads were resuspended in 500 µl Wash buffer (Flag Immunoprecipitation Kit - SIGMA) and transferred to spin columns, followed by six washes in 500 µL of the same buffer. Samples were then incubated with a solution of 150 ng/µL of 3xFLAG Peptide (Sigma #F4799) in 100 µL Wash buffer at 4 °C for 30 minutes with occasional gentle shaking. Proteins were collected by centrifugation at 8,200 g for 1 minute at 4 °C and analyzed by Mass Spectrometry. Lysates from the *dgcZ*(wt) strain grown under the same conditions as the *dgcZ-3xFlag* strain were used as negative controls.

The initial list of co-immunoprecipitated proteins was filtered by removing proteins present in the negative controls. In two additional filtering steps, first all hits identified by less than three peptides were discarded and second only hits identified by at least two unique peptides were kept. Further details and the complete dataset, including the hits with a low score not present in the negative controls, are listed in Table S1 and S2, in the appendix and in the CoIP dataset, in the attached CD-ROM.

2.2.16 Bacterial two-hybrid

For all BACTH experiments the *E. coli* BTH101 strain (Battesti and Bouveret, 2012) was grown at 30 °C on LB plates supplemented with Amp (100 µg/mL), Kan (50 µg/mL), Str (75 µg/mL), X-Gal (40 µg/mL) and 500 µM IPTG. The BTH101 strain was cotransformed with plasmids encoding the T25- and T18- protein fusions and grown overnight on LB (Amp, Kan, Str, X-Gal, IPTG) plates at 30 °C. Single colonies of each combination were streaked on new plates and incubated overnight at 30 °C. Subsequently, bacteria from these plates were resuspended in PBS 1X to an OD_{600} of 0.1 and 10 µL of each solution were spotted on new

plates. Bacteria were grown for 40 hours at 30 °C and pictures were acquired with a Nikon D3300 camera.

2.2.17 ß-galactosidase assay

Bacteria from the same plates used for the BACTH experiments were used for the β-galactosidase assays. Bacteria were resuspended in PBS 1X and OD_{600} was normalized to 1.0. 200 µL of bacterial suspensions were harvested by centrifugation and resuspended in an equal amount of Z-buffer (Miller, 1972). 20 µL of 0.1% SDS and $CHCl_3$ were added for permeabilization and cell suspensions were vortexed for 10 seconds.

Tubes were left for 15 minutes with open lid to allow phase separation. 100 µl of the upper phase were mixed with 100 µL of Z-buffer. OD_{600} was measured for normalization. 25 µL of ONPG were added and adsorption at 405nm was recorded. Miller units were measured as $1,000 \times ((OD_{600} \times (T \times V(in\ mL) \times OD_{405})^{-1})$.

T represents the time of the reaction in minutes and V the volume, in this case 0.2 mL.

2.2.18 Aerobic and anaerobic growth curves

Pre-cultures of the *E. coli* strains MG1655, Δ*dgcZ*, Δ*frdA* and Δ*frdA*/Δ*dgcZ* were grown in LB medium at 37 °C for 24 hours. The following day, 1µL of each pre-culture was inoculated in 99 µL of LB medium in a 96-well plate (Greiner - 655161) The plate was sealed with a plastic sheet and incubated in a TECAN (infinite F200 Pro) reader at 37 °C under shaking conditions (amplitude 3.5 mm, frequency 424.1 rpm). OD_{600} was measured and recorded every 15 minutes. Error bars are standard error of the means from six biological replicates.

For the anaerobic growth curves, pre-cultures of the *E. coli* MG1655, Δ*dgcZ*, Δ*frdA* and Δ*frdA*/Δ*dgcZ* strains were grown aerobically in MMA 1X supplemented with 0.4% glucose at 37 °C for 24 hours. For each strain, 8 µL of a pre-culture were added to a 1.5 mL eppendorf tube containing 392 µL of MMA 1X supplemented with 0.4% glycerol and 40mM fumarate. The medium was stored in an anaerobic hood from the previous day. The tubes were shaken at 300 rpm in an Eppendorf Thermomixer R at 37 °C in an anaerobic hood. OD_{600} values were

measured at specific time points using a NanoDrop. The OD_{600} values of the anaerobic curves were multiplied by eight to be comparable with values of the aerobic growth curves, detected by the TECAN reader. Error bars are SEM from three biological replicates.

2.2.19 Leifson staining

Leifson staining was used to visualize flagellar filaments of bacteria (Clark, 1976) and was performed as described by El Andari *et al.* (2015). Solutions were prepared as follows:

Solution name	Solutes	Concentrations	Solvent
Solution A	NaCl	256.8 mM	dH_2O
Solution B	tannic acid	17.6 mM	dH_2O
Solution C	pararosaniline acetate	259.1 mM	95% EtOH
	pararosaniline hydrochloride	92.64 mM	

The staining solution was prepared by mixing solution A and B (1:1 ratio) and then adding the mix to solution C (2:1 ratio).

Bacteria were grown in 2 mL of either LB medium (85 mM NaCl), or LB medium without salt (without added NaCl), at 37 °C for 24 hours until reaching the stationary phase (OD_{600} 4.5). 1 mL of each culture was transferred in a 1.5 mL Eppendorf tube and centrifuged at 5,000 rpm for 10 minutes to avoid flagellar and hook shearing. Pellets were washed once with 1 mL of PBS 1X and then resuspended in 1 mL of the same buffer.

Approximately, 10–15 µL of these cells were added to microscopy slides and were air-dried at room temperature for 2 hours. The staining solution was added and the slides were incubated at room temperature until a golden film formed on the surface of the dye, usually after 5 to 7 minutes. The microscopy slide was gently washed with water to remove the dye and then air-dried. For microscopy, a drop of oil was applied and a coverslip placed on each slide. Differential interference contrast (DIC) microscopy was performed using a Nikon Eclipse Ti-E inverse microscope.

2.2.20 Flagellin isolation

Bacteria were grown in 5 mL of LB medium, or LB medium without salt (without added NaCl), supplemented with Ampicillin (100 µg/mL) and arabinose (0.1%) at 37 °C for 24 hours under shaking conditions. 3 mL of culture were transferred in a 15 mL falcon tube and vortexed three times for ten seconds each. The cultures were then centrifuged at 5,000 rpm for 10 minutes and 1.5 mL of supernatant was transferred in 2 mL eppendorf tubes. The tubes were then centrifuged at 16,400 rpm at 4° C for 1 hour, supernatants were removed and pellets resuspended in 30 µL of sample buffer 1X. Samples were heated at 95 °C for 5 minutes and loaded (10 µL) in 10% polyacrylamide gels. After each run, the polyacrylamide gels were stained in Comassie Brilliant Blue R-250 solution (0.25%) for 4 hours and subsequently destained overnight in a solution containing 26% ethanol and 10% Acetic acid. Images were taken with a Nikon D330 camera.

2.2.21 Motility assay

The swimming behavior of bacteria was assayed on motility agar plates containing tryptone (1.0%), NaCl (0.5%) and agar (0.3%). Before pouring plates, the medium was supplemented with Ampicillin (100 µg/mL), and either arabinose (0,1%) (for the assay shown in Fig. 24C), or IPTG (200 µM) (for the assay shown in Fig. 26A). Bacteria were grown at 37 °C overnight on LB Amp plates with either arabinose or IPTG. The following day, single colonies were inoculated on motility agar plates and incubated at 37 °C for 5 to 6 hours before acquiring pictures. Each assay was repeated at least three times.

3. Results

3.1 Zn^{2+} regulates DgcZ activity *in vivo*

Zähringer *et al*. (2013) reported biochemical data suggesting Zn^{2+} inhibited DgcZ activity by binding the CZB domain. Using a series of *in vivo* experiments, this work assessed the potential of zinc to modulate DgcZ activity under physiological conditions.

3.1.1 Mutation of zinc-coordinating amino acids results in a hyperactive DgcZ variant

The crystal structure of DgcZ revealed that four amino acids coordinate Zn^{2+} binding (Fig. 5A). To study the effects of the mutation of these amino acids on protein activity, the wild-type *dgcZ* gene of *E. coli* MG1655 was replaced by alleles encoding protein mutants in the four zinc-coordinating amino acids (H22, H79, H83, and C52) using λ-RED recombination. The histidines were replaced by leucines and the cysteine was replaced by alanine. A double mutant strain, DgcZ(H79L,H83L), was also constructed. To ensure that any differences observed were because of altered c-di-GMP production, the E208Q mutation in the active site of the GGDEF domain was combined with the mutations to H22, H79, H83, and C52.

The function of DgcZ has been previously investigated in the *csrA::Tn5* strain background, which harbors a truncated and partially active CsrA protein (Romeo *et al.*, 1993; Jonas *et al.*, 2008; Boehm *et al.*, 2009). The production of a CsrA variant in this strain resulted in the derepression of *dgcZ* mRNA translation which facilitated the study of DgcZ-controlled mechanisms. For this reason, the activity of the DgcZ mutant proteins was measured in this background strain.

DgcZ controls the biosynthesis of PGA via c-di-GMP. Because levels of DgcZ positively correlate with those of PgaD proteins, PgaD levels were also used to measure the activity of DgcZ mutants (Boehm *et al.*, 2009; Steiner *et al.*, 2013).

In a strain carrying a deletion of *dgcZ,* PgaD protein levels were significantly lower when compared to a strain with the *dgcZ*(wt) gene (Fig. 6A). A similar difference in PgaD levels was also observed in strains carrying alleles encoding DgcZ active site mutants (E208Q) (Fig. 6A). In fact, the E208Q mutation rendered the protein incapable of producing c-di-GMP. Conversely, PgaD levels in *dgcZ* single mutant strains (C52A, H22L, H79L, and

H83L) were similar to a strain with the wild-type *dgcZ* gene. Interestingly, the *dgcZ* double mutant strain (H79L,H83L) displayed much higher PgaD levels than the *dgcZ*(wt) strain (Fig. 6A). The PgaD levels of the strain producing the DgcZ(H79L,H83L,E208Q) variant were comparable to those produced by a *dgcZ* deletion strain, indicating that the observed effect relies on an intact active site and ultimately on c-di-GMP production (Fig. 6A). Protein levels of GroEL, used as a control, remained constant in each sample (Fig. 6A).

PGA production serves as an indicator of c-di-GMP concentrations (Steiner *et al.*, 2013). PGA is easily detected on LB agar plates containing the PGA-binding dye Congo red (Steiner *et al.*, 2013). When analyzed on Congo red plates, the strain carrying the *dgcZ*(H79L,H83L) allele formed hyperaggregative, small colonies, which bound more dye than the *dgcZ*(wt) strain (Fig. 6B). A *dgcZ* triple mutant, with both active site and zinc-binding mutations (H79L,H83L,E208Q) did not bind Congo red or display a hyperaggragative phenotype, like both the Δ*dgcZ* and the *dgcZ*(E208Q) mutant (Fig. 6B). A strain carrying a *dgcZ*(H79L,H83L) allele and a *pgaABCD* operon deletion showed no congo red binding but formed smaller colonies than the *dgcZ*(wt) strain, which suggests the hyperaggregative phenotype is partly dependent on PGA production (Fig. 6B).

Western blot analysis together with Congo red assays demonstrate that the mutation of both of the zinc-coordinating amino acids H79 and H83 results in a hyperactive DgcZ variant.
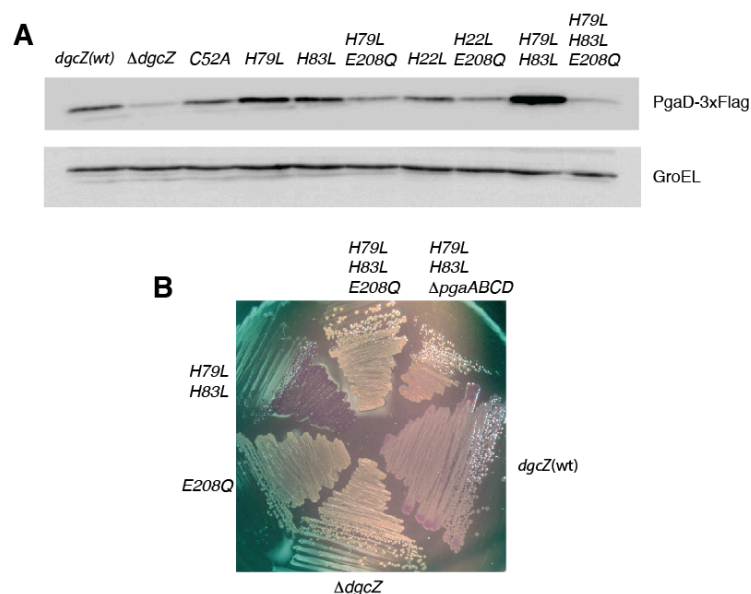
Figure 6. *In vivo* analysis of PgaD levels and PGA production by *dgcZ* mutants. (A) PgaD and GroEL Western blots. PgaD has a C-terminal triple-FLAG tag, which enabled detection by the M2 antibody. Reported by Boehm *et al.* (2009)*,* this *pgaD* allele is fully functional. DgcZ amino acid exchanges and deletions to *dgcZ* are indicated. All strains are in the *csrA::Tn5* background, to allow expression of *dgcZ* and *pgaABCD*. All strains were grown under static conditions for 24 hours in LB medium at 30 °C. (B) Picture of a Congo red agar plate after incubation at 37 °C overnight. Red channel intensity was reduced to enhance contrast. Adapted from Zähringer *et al.,* 2013.

3.1.2 Adding zinc to the growth medium reduced DgcZ-dependent biofilm formation

Mutation of the amino acids H79 and H83 resulted in a DgcZ protein variant with increased activity. Consequently, zinc concentrations in the growth medium were altered to test if these changes modulated, or inhibited protein activity.

After adding various amounts of $ZnSO_4$ to bacteria grown in LB medium, attachment assays were performed (Fig. 7). This commonly used assay assesses the ability of *E. coli* to adhere to the surface of 96-well plates and form biofilms (O'Toole *et al.*, 1999; Boehm *et al.*, 2009). Since the amount of biofilm produced in various models of 96-well plates can differ significantly (data not shown), all attachment assays presented throughout this work were performed in BD Falcon (353072) Polystyrene plates.

With the addition of zinc to the medium (500 µM final concentration), a strain harboring the wild-type *dgcZ* showed a marked decrease in biofilm formation; whereas, the *dgcZ*(H79L,H83L) strain displayed constitutively high biofilm independent of zinc concentration (Fig. 7A). Biofilm production in the Δ*dgcZ* strain was also not influenced by the addition of zinc (Fig. 7A).

Boehm *et al.* (2009) found that biofilm production is significantly increased in a strain devoid of the alarmone guanosine tetraphosphate (ppGpp) compared to a strain where ppGpp is present.

The effect of zinc on DgcZ activity was also tested in the ppGpp0 strain (Fig. 7B). In this strain, zinc exerted its effects at significantly lower concentrations than in the ppGpp[+] strain, and significant biofilm inhibition started at 25 µM with ≈75% inhibition at 200 µM zinc (Fig. 7B). In the ppGpp0 background, biofilm production of both the *dgcZ*(H79L,H83L) and Δ*dgcZ* strains were unaffected by zinc addition.

For additional confirmation that zinc affected biofilm formation via c-di-GMP, the *dgcA* gene (coding for a diguanylate cyclase) from *Caulobacter crescentus* was ectopically expressed in the ppGpp0 strain (Fig. 7C). DgcA-derived c-di-GMP, as expected, induced high levels of biofilm production even in 200 µM of zinc (Fig. 7C). Although the reason for the hypersensitivity to zinc of the ppGpp0 strain is unclear, these results demonstrate that extracellular zinc concentrations influenced DgcZ activity and PGA-dependent biofilm formation.
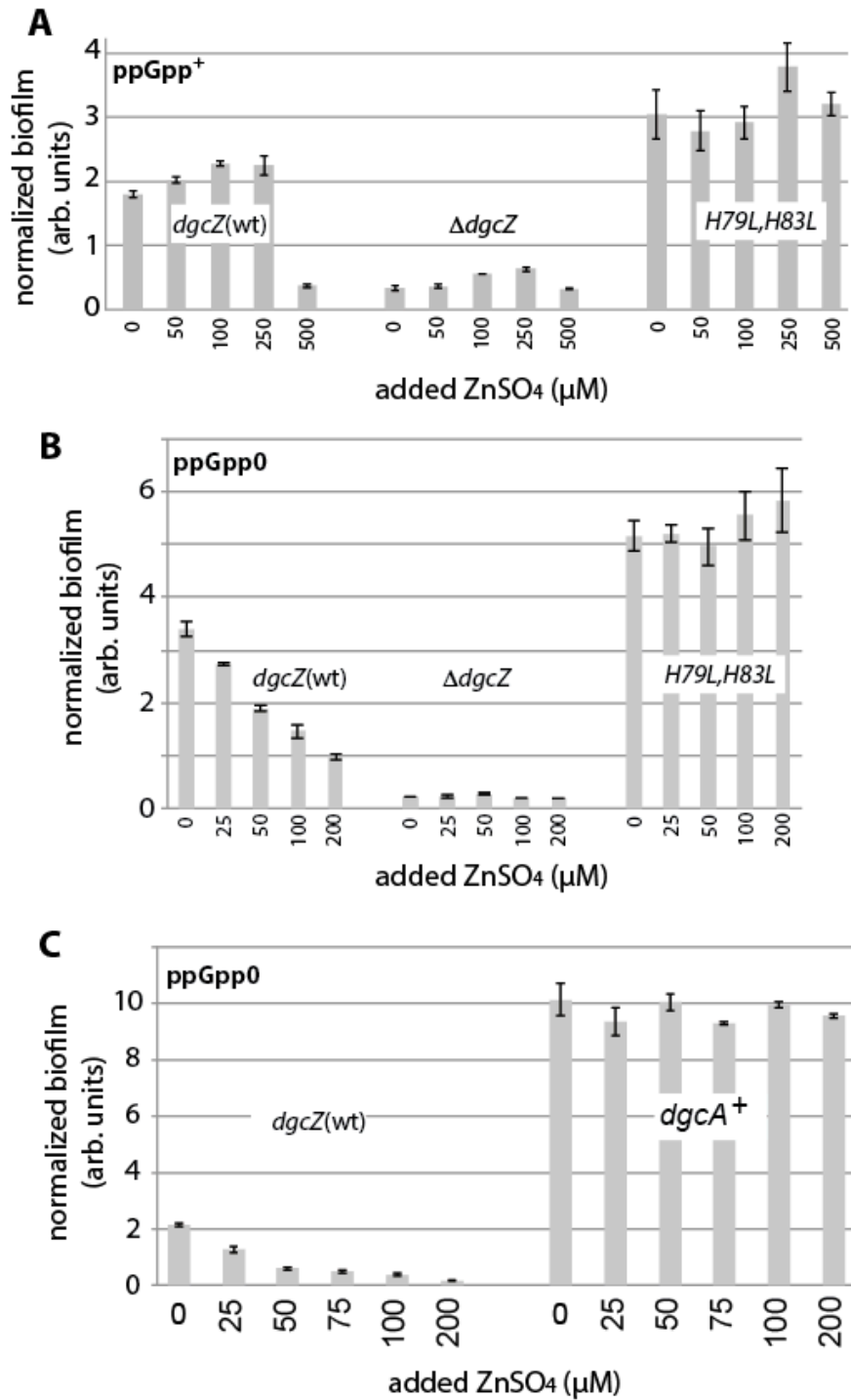
Figure 7. Zn²⁺ addition reduced DgcZ-mediated biofilm formation. Measurements of PGA-dependent biofilm formation were conducted in various concentrations of $ZnSO_4$, using the *csrA::Tn5* background. Strains in B and C are in addition $\Delta relA/\Delta spoT$ (ppGpp0). A single copy of diguanylate cyclase (*dgcA*) from *Caulobacter crescentus* was integrated at a permissive chromosomal site with an arabinose inducible promoter. L-arabinose (0.2%) was added to the LB medium used in the attachment assay in panel C. Error bars represent the SEM. Adapted from Zähringer *et al.*, 2013.

3.2 Analysis of PgaD-GFP localization

PGA production is the main process targeted by DgcZ derived c-di-GMP (Boehm *et al.*, 2009). Itoh *et al.* (2008) noted PGA production occurring at the bacterial cell poles, or throughout the bacterial cell when shaking or static cultivation conditions are applied, respectively. The factors responsible for this differential PGA production are not known. One hypothesis suggests the PgaABCD complex assembles at the bacterial cell poles, or all around the bacterial cell, depending on the cultivation conditions. The differential localization of the PgaABCD complex would lead to PGA production at different sites. Another hypothesis proffers that the PgaABCD complex is evenly distributed through the bacterial membrane, but is only active in the presence of c-di-GMP.

To discriminate between these hypotheses, the *pgaD* gene was replaced by a *pgaD-GFP* construct in the *csrA::Tn5* strain. Then, the localization of this PgaD-GFP fusion protein, which indicated PgaABCD complex localization, was analyzed. The *pgaD-GFP/csrA::Tn5* strain was grown, as described by Itoh *et al.* (2008), in LB medium under shaking conditions (250 rpm) at 26 °C for 24 hours and images captured using fluorescence microscopy (Fig. 8). PgaD-GFP showed an even localization in the bacterial cell (Fig. 8A) under conditions where PGA was only detected at bacterial cell poles by Itoh *et al.* (2008).

Biofilm formation in the *pgaD-GFP/csrA::Tn5* strain was measured using an attachment assay, which showed that the PgaD-GFP fusion protein is functional and regulated by DgcZ-derived c-di-GMP (Fig. 8B). The *pgaD-GFP/csrA::Tn5* strain, however, formed ≈25% more biofilm than the *pgaD*(wt)*/csrA::Tn5* strain in both the *dgcZ*(wt) and Δ*dgcZ* backgrounds. This observation suggests that the fusion protein may be more stable than PgaD(wt).
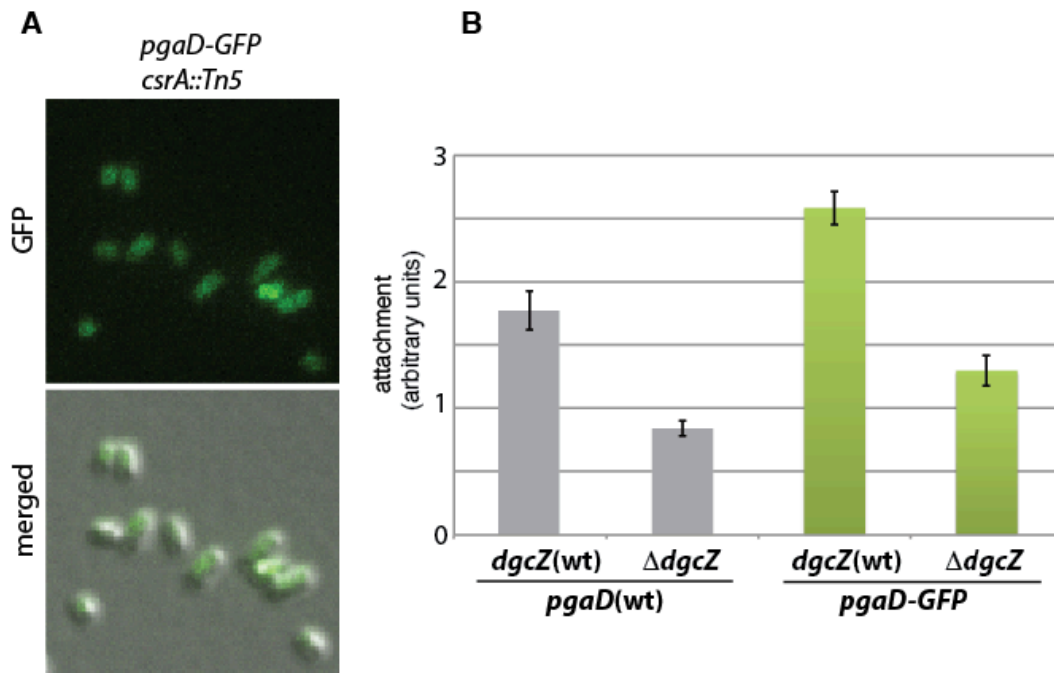
Figure 8. Localization and activity of the PgaD-GFP protein. (A) *E. coli pgaD-GFP/csrA::Tn5* cells were inoculated in 2 mL of LB medium (1:100 dilution from o/n culture), and grown at 26 °C for 24 hours under shaking conditions and fluorescence microscopy images were taken. (B) *E. coli csrA::Tn5* strains *pgaD-GFP* and *pgaD*(wt) in the *dgcZ*(wt) and Δ*dgcZ* background were grown at 30 °C for 24 hours in 96-well plates, and surface attachment was assayed. For each strain, the average derived from measurements of six wells is shown. Error bars depict the SEM.

3.3 Analysis of DgcZ-mVENUS localization

PgaD-GFP localized evenly under the conditions where PGA was observed at the bacterial poles (Itoh *et al.*, 2008), suggesting PgaABCD localization does not determine whether PGA is produced at the poles, or around the bacterial cell. An alternative hypothesis suggests that localized production of c-di-GMP is responsible for PGA biosynthesis at the poles. Since DgcZ is the major DGC involved in controlling PGA biosynthesis (Boehm *et al.*, 2009), the localization of this protein was studied using a *dgcZ-mVENUS* gene fusion.

This *dgcZ-mVENUS* fusion, located at the *dgcZ* native locus, was constructed in the *csrA::Tn5* strain background (Romeo *et al.*, 1993). The strain obtained was cultured in LB medium under shaking conditions (250 rpm) at 37 °C, and its growth was comparable to that of a *csrA::Tn5* strain with the wild-type *dgcZ* gene (Fig. 9A). Both strains grew exponentially until reaching an OD_{600} of 1.7 to 1.8, then growth slowed before stopping at an OD_{600} of 4.5 to 5.2 (Fig. 9A). In this work, OD_{600} values of 1.8 to 3.2 indicate post-exponential phase

growth, while 3.3 to 4.9 indicate the pre-stationary phase, and, when the OD_{600} remained constant (4.5 to 5.2), the bacteria are in the stationary phase (Fig. 9A).

To validate DgcZ-mVENUS protein activity, the c-di-GMP levels produced by this chimeric protein were compared to those of the wild-type protein and quantified by mass spectrometry.

Cyclic di-GMP quantification was performed at the Research Core Unit Metabolomics, located at the Institute of Pharmacology in the Hannover Medical School.

During the pre-stationary phase (9 hours, OD_{600} of 3.5), c-di-GMP concentrations were ≈25% lower in the strain with the *dgcZ-mVENUS* construct than the *dgcZ*(+) strain, which was obtained by the deletion of *dgcZ* and subsequent reintroduction of the gene at its native locus (Fig. 9B). The amount of c-di-GMP produced by a strain carrying the *dgcZ*(E208Q) allele, coding for a DgcZ active site mutant with no catalytic activity was measured as well. In this strain, the concentration of c-di-GMP was less than 22 nM, the detection limit; which suggests that under these conditions DgcZ is the main active DGC (Fig. 9B). During stationary phase (48 h, OD_{600} of 4.5), c-di-GMP concentrations for all the strains were below the detection limit (Fig. 9B).

Since biofilm formation in strains with either the *pgaD-3xFlag,* or the *pgaD*(wt) allele, are comparable (Boehm *et al.*, 2009), and PgaD protein levels correlate with c-di-GMP concentrations (Steiner *et al.*, 2013), PgaD-3xFlag levels were used to indicate intracellular c-di-GMP concentrations.

Western blots confirmed DgcZ-mVENUS activity (Fig. 9C). Levels of PgaD-3xFlag in pre-stationary phase (9 hours, OD_{600} of 3.5) were comparable in both the *dgcZ*(+) and the *dgcZ-mVENUS* strains. Only a weak PgaD-3xFlag signal was detected in the *dgcZ* active site mutant (Fig. 9C). Once all the strains reached stationary growth (24-48 hours, OD_{600} of 4.5), PgaD was no longer detected (Fig. 9C).

Furthermore, DgcZ-mVENUS activity was tested using an attachment assay (Fig. 9D). Biofilm formation in the *dgcZ-mVENUS* strain was ≈30% less than the *dgcZ*(+) strain, but almost three times more than the Δ*dgcZ* and *dgcZ*(E208Q) strains (Fig. 9D). The data demonstrates that the DgcZ-mVENUS protein is functional, although slightly less active than the wild-type protein.
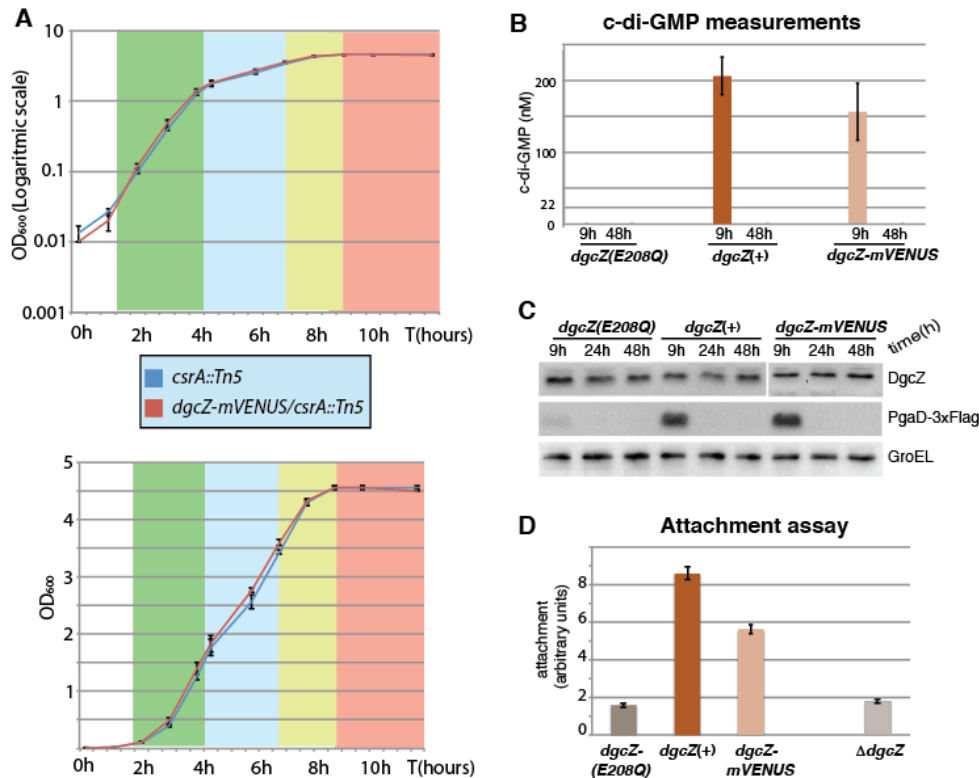
Figure 9. Activity of the DgcZ-mVENUS protein in the *csrA*::Tn5 mutant background. (A) Growth curves of the *dgcZ-mVENUS/csrA::Tn5* and *csrA::Tn5* strains in LB medium at 37 °C. OD_{600} values were registered at the above time points by spectrophotometry. Error bars represent SEM from three biological replicates. The green, blue, yellow and red colors on the chart indicate exponential, post-exponential, pre-stationary and stationary growth phases, respectively. (B) *E. coli csrA*::Tn5 cells carrying the *dgcZ-mVENUS*, the *dgcZ*(E208Q),or the complemented *dgcZ*(+) were grown for 9 hours (pre-stationary phase) and 48 hours (stationary phase) in LB medium at 37°C under shaking conditions. c-di-GMP was extracted and the concentration was determined by mass spectrometry. Three biological replicates were used for each strain. The broken line indicates the detection limit of c-di-GMP (22 nM). Error bars depict standard errors relative to the means (SEM). (C) Western blots of the strains from panel B, where *pgaD*(wt) is replaced by *pgaD-3xFlag*. Growth conditions are as in panel B. (D) Strains from panel B, and the deletion strain Δ*dgcZ* were grown at 30°C for 24 hours in 96-well plates, and surface attachment was assayed. For each strain, the average derived from measurements of the six wells is shown. Error bars represent the SEM. Adapted from Lacanna *et al.,* 2016.

DgcZ-mVENUS localization was then analyzed in cultures grown at 26 °C for 24 hours under shaking conditions similar to those employed by Itoh *et al.* (2008). Although Itoh *et al.* (2008) observed polar production of PGA, DgcZ-mVENUS displayed an even cytoplasmic localization in bacteria grown under these conditions (Fig. 10). This finding suggests that the PGA polar production previously observed (Itoh *et al.*, 2008) does not result from DgcZ proteins located at the bacterial cell poles.
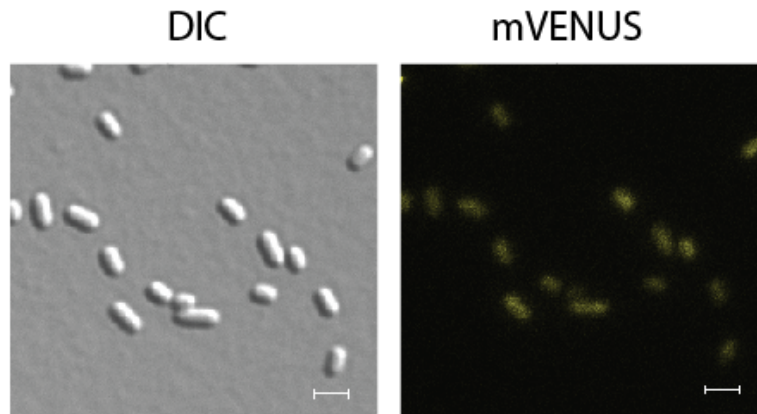
Figure 10. Localization of DgcZ-mVENUS in the *csrA::Tn5* strain background. Overnight cultures were diluted 1:100 in 2 mL of LB medium and grown under shaking conditions (250 rpm) at 26 °C for 24 hours. Bacterial cultures reached an OD_{600} of 4.5-4.6. Three independent cultures were analyzed. Size bars are 2 μm.

3.3.1 DgcZ-mVENUS localization changes during stationary phase

After observing a significant decrease in DgcZ-derived c-di-GMP levels during the stationary phase (Fig. 9 B-C), DgcZ localization was examined in different growth phases. DgcZ-mVENUS localization was analyzed in the *csrA::Tn5* strain grown under the same conditions used for c-di-GMP quantification (Fig. 11). During the pre-stationary phase (9 hours, OD_{600} of 3.5), the protein was evenly distributed in the cytoplasm. In the stationary phase (24 and 48 hours, OD_{600} of 4.5), the protein localized, almost entirely, at one cell pole in the population (Fig. 11). Occasionally, DgcZ was observed at both cell poles.

The localization of the nucleotidase YfbR, a cytoplasmic protein (Weiss, 2007), fused to mCHERRY and overproduced from the pCJ30 plasmid, was used as a control. In stationary phase (48 hours), the YfbR-mCHERRY signal displayed dispersed cytoplasmic localization in the same bacteria where DgcZ-mVENUS was localized at the cell pole (Fig. 11).
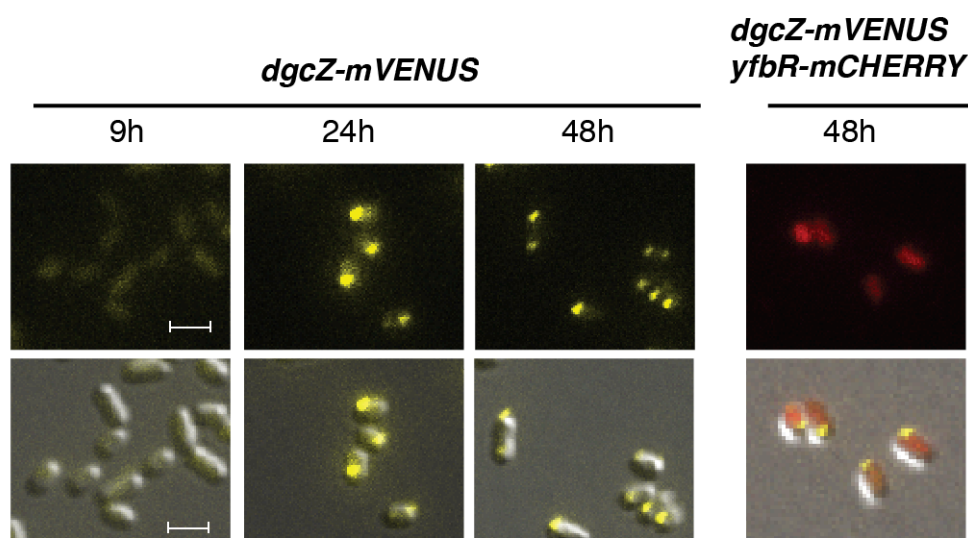
Figure 11. DgcZ-mVENUS localization in the *csrA::Tn5* mutant background in different growth phases. Fluorescence microscopy images of the *dgcZ-mVENUS*/*csrA*::*Tn5* strain with and without the plasmid pYfbR-mCHERRY. Bacterial strains were grown in LB medium at 37 °C under shaking conditions. The culture carrying pYfbR-mCHERRY was supplemented with ampicillin (100 µg/mL) and IPTG (100 µM). Size bars are 2µm and are identical in each picture. Adapted from Lacanna *et al.,* 2016.

3.3.2 Polar localization of DgcZ is independent of protein activity and concentration

After demonstrating that DgcZ polar localization occurs in the stationary phase, it was tested if this localization was affected by protein activity. Both the *dgcZ*(H79L,H83L) and *dgcZ*(H79L,H83L,E208Q) alleles, which encode for a hyperactive and an inactive variant respectively, were fused to *mVENUS* and integrated at the native *dgcZ* locus, to ensure similar expression levels of the wild-type gene. The localization of DgcZ-mVENUS and the two protein variants was then analyzed in the *csrA::Tn5* background during stationary phase (24 hours, OD_{600} 4.5) (Fig. 12A). All the DgcZ variants showed the characteristic polar localization, suggesting that protein activity does not influence localization (Fig. 12A).

Subsequent tests were performed to gauge the effect of changes in protein concentration on polar localization. The *dgcZ-mVENUS/csrA::Tn5/pgaD-3xFlag* strain was grown in LB medium at 37 °C until reaching the stationary phase (OD_{600} of 4.5). Starting 1 hour later, fluorescence microscopy images and protein samples were taken every 30 minutes (Fig. 12B).

While DgcZ protein concentrations remained constant, polar localization was observed after 2.5 hours (T5), with notable increases at 3 and 3.5 hours (T6-T7) (Fig. 12B-C). These results suggest that DgcZ localization is not caused by increasing protein concentrations.

To monitor levels of c-di-GMP, western blotting against PgaD-3xFlag was performed. PgaD was not detected in this blot. This finding indicates c-di-GMP concentrations are low and PGA is no longer produced when *E. coli csrA::Tn5* is in stationary phase, regardless of DgcZ localization.
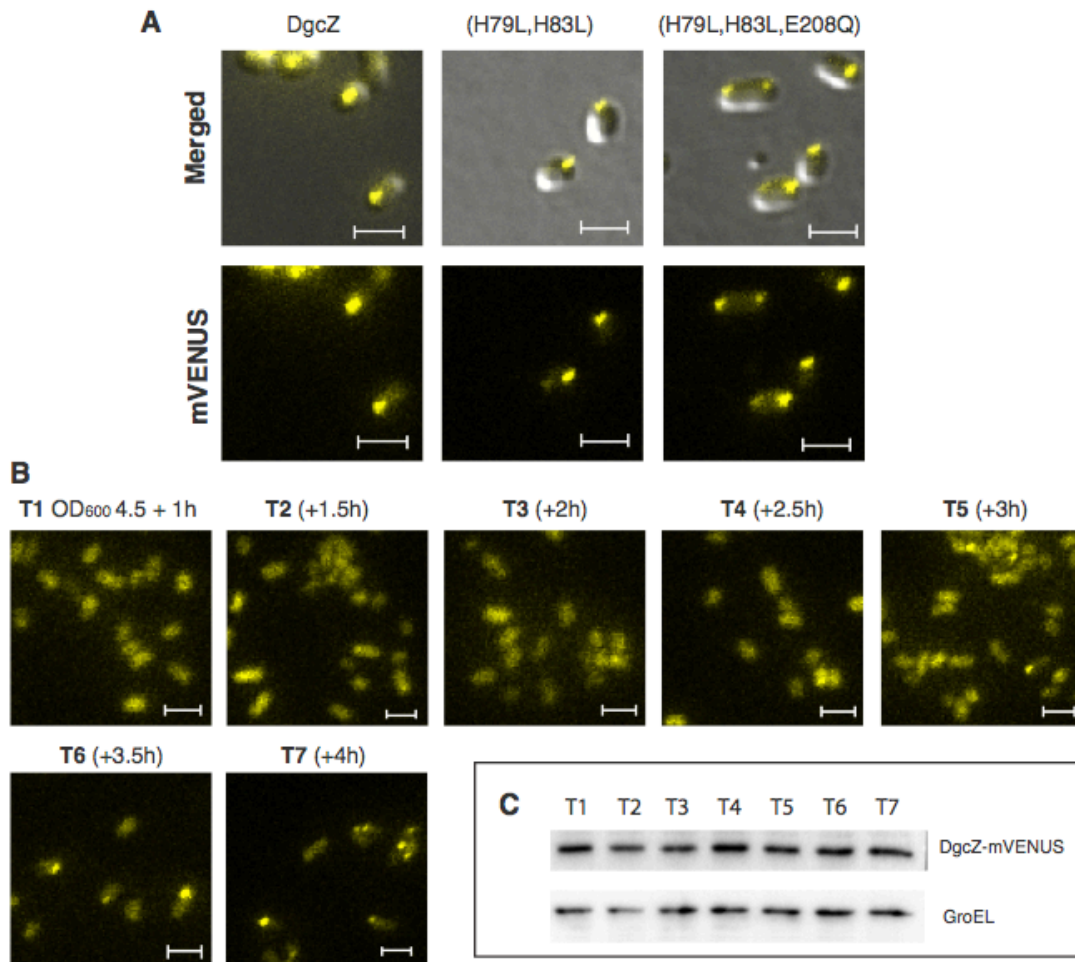
Figure 12. Polar localization of DgcZ is independent of protein activity or concentration. (A) Localization of wild-type, hyperactive (H79L, H83L) and inactive (H79L, H83L, E208Q) DgcZ proteins fused to mVENUS. All strains carry *csrA::Tn5*. Bacteria were grown at 37 °C in LB medium for 24 hours. Each picture contains identical size bars of 2 μm. (B) DgcZ-mVENUS localization in the *csrA::Tn5/dgcZ-mVENUS* strain grown in LB medium at 37 °C. Starting 1 hour after the bacterial culture reached an OD_{600} of 4.5, pictures and protein aliquots were taken every 30 minutes. Size bars are the same as those in (A). (C) Western blot detection of DgcZ and GroEL protein extracted during the experiment shown in panel B.

3.3.3 DgcZ localizes at the bacterial cell pole in response to nutrient depletion

To clarify and understand the conditions promoting DgcZ polar localization, bacterial growth and DgcZ-mVENUS localization were monitored using a microfluidic device designed to track single bacterial cells over time (Arnoldini *et al.*, 2014; Wang *et al.*, 2010)

(Fig. 13). Microfluidic systems also allow for direct observation of bacterial growth and protein localization upon sudden changes in the medium composition.

The following microfluidic experiments have been performed by Colette Bigosch, Eawag Dübendorf, Switzerland. I contributed to designing the experiments and analyzing the results.
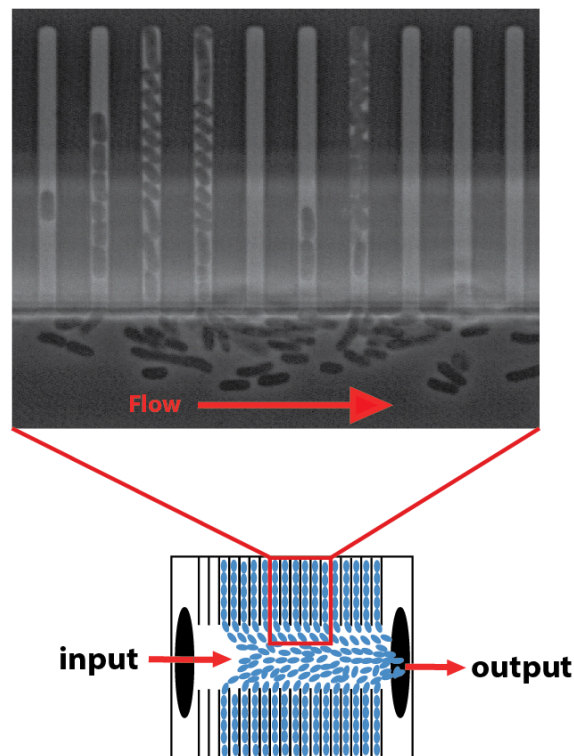
Figure 13. Snapshot and schematic representation of bacterial cells in the microfluidic system. The microfluidic system in this study consisted of a 14 chambered chip. Each chamber is composed of two opposite rows of parallel tubes. Each tube measures 1 µm in diameter and 25 µm in length. Bacteria become "trapped" in the tubes when the medium flow is applied. The medium flow supplies nutrients and removes bacteria in excess. For additional information on the design and assembly of this microfluidic system refer to Wang *et al.*, 2010.

Since DgcZ-mVENUS polar localization was observed in stationary phase, nutrient depletion was tested to determine if it induced the same phenotype. For this purpose, spent LB medium (nutrient-depleted) was prepared by growing the *csrA::Tn5* strain in LB medium for 24 hours and then filtering the medium.

The DgcZ-mVENUS-derived signal was monitored in the *csrA::Tn5* strain grown in microfluidic chambers under the following conditions:

(i)   cultivation in nutrient-sufficient medium (LB for 2 hours)

(ii)   cultivation in a gradient from fresh to nutrient-depleted (spent) medium (for 3 hours)

(iii)   cultivation in spent medium (for 16 hours)

(iv)   cultivation in a gradient from spent to fresh medium (for 1 hour)

(v)   cultivation in nutrient-sufficient medium (LB for 20 hours)

DgcZ-mVENUS-derived fluorescence was dispersed towards the end of the gradient phase (Fig. 14A - Video S1). DgcZ localization at the bacterial cell pole started after 5 hours in the spent medium phase, when bacteria ceased to grow and divide (Fig. 14A). When the fresh medium was applied to the microfluidic chamber, the DgcZ-mVENUS polar foci disappeared within 4 hours and growth resumed (Fig. 14B).

3.3.4 Once growth resumes, DgcZ polar foci are undetectable

The disappearance of DgcZ foci concomitant with bacterial regrowth required additional investigation. Stationary phase bacteria were spotted on LB agarose-coated microscopy slides, incubated at 30 °C and protein localization was analyzed. DgcZ foci vanished in all the individual cells that began to grow again but remained present in bacteria that did not resume growth (Fig. 14C). In both systems, the resumption of cell growth corresponded with the disappearance of polar DgcZ foci.
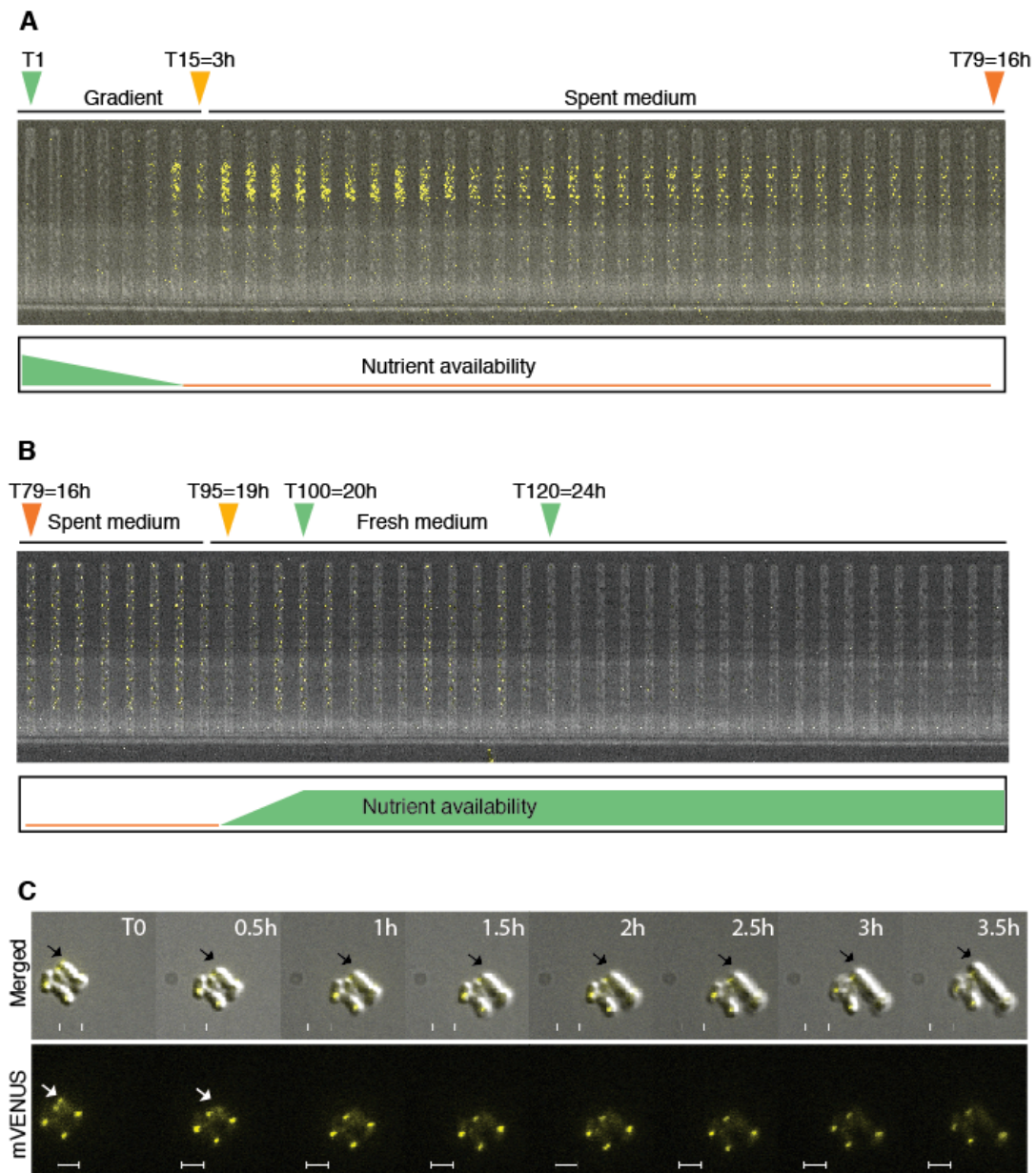
Figure 14. DgcZ polar foci observed in non-dividing bacteria vanish upon nutrient addition before growth resumes. (A) Fluorescence microscopy of the *dgcZ-mVENUS/ibpA-mCHERRY/csrA*::Tn*5* strain in microfluidic chambers. An excerpt of the experiment representing the 3 hour-long gradient from fresh to spent medium followed by 13 hours of spent medium is shown. Every 24 minutes, a photograph was taken to create the montages seen above. (B) Excerpt of microfluidic experiment. This montage illustrates the disappearance of DgcZ in response to fresh medium. (C) Fluorescence microscopy of the *dgcZ-mVENUS/csrA*::Tn*5* strain. Stationary phase bacteria (48 hours) were spotted onto a microscopy slide (LB, 1% agarose), incubated at 30 °C and images were taken every 30 minutes. White arrows show a DgcZ focus that disappeared as cell growth resumed. Black arrows indicate the respective bacterial cell in the merged channel (DIC + mVENUS). Size bars are 2 μm and identical in each picture. Adapted from Lacanna *et al.,* 2016.

3.3.5 External alkaline pH triggers DgcZ polar localization in carbon-deprived *E. coli*

The accumulation of byproducts in the spent LB medium may determine or contribute to DgcZ polar localization. To ascertain the roles of carbon starvation and accumulation of byproducts in this phenomenon, the *csrA*::Tn*5*/*dgcZ-mVENUS* strain was grown until reaching OD_{600} 2.5 and then transferred into spent LB medium, or MMA 1X (a minimal medium without carbon sources), and fluorescence microscopy was applied (Fig. 15A). In bacteria transferred to the spent LB medium, DgcZ localization at the cell pole was observed after 3 hours, and after 6 hours almost all the bacteria had polarly localized DgcZ (Fig. 15A). Polar localization was not observed in the sample in MMA 1X and the mVENUS signal was weaker (Fig. 15A).

The pH of the two media, spent LB medium and MMA 1X, differed significantly. The spent LB medium had an initial pH of 8.7, while the pH of the MMA 1X medium was 6.9. By the end of the experiment, the pH of both media increased by 0.2 and 0.1 units, respectively. The pH difference between the media prompted subsequent tests to examine the effect of pH on DgcZ localization.

Bacteria were grown in LB medium until OD_{600} 2.5 and then transferred into MMA 1X, or buffered LB spent medium. The pH of both media was adjusted to values of 6.7 and 8.7. After 5 hours, DgcZ showed polar localization in both media at pH 8.7; although, the foci in the MMA medium were smaller (Fig. 15B). At pH 6.7, both media had weaker DgcZ-mVENUS signals than at pH 8.7 and no polar foci were observed (Fig. 15B). An alkaline pH, therefore, induced DgcZ polar localization in both LB spent medium and MMA 1X.
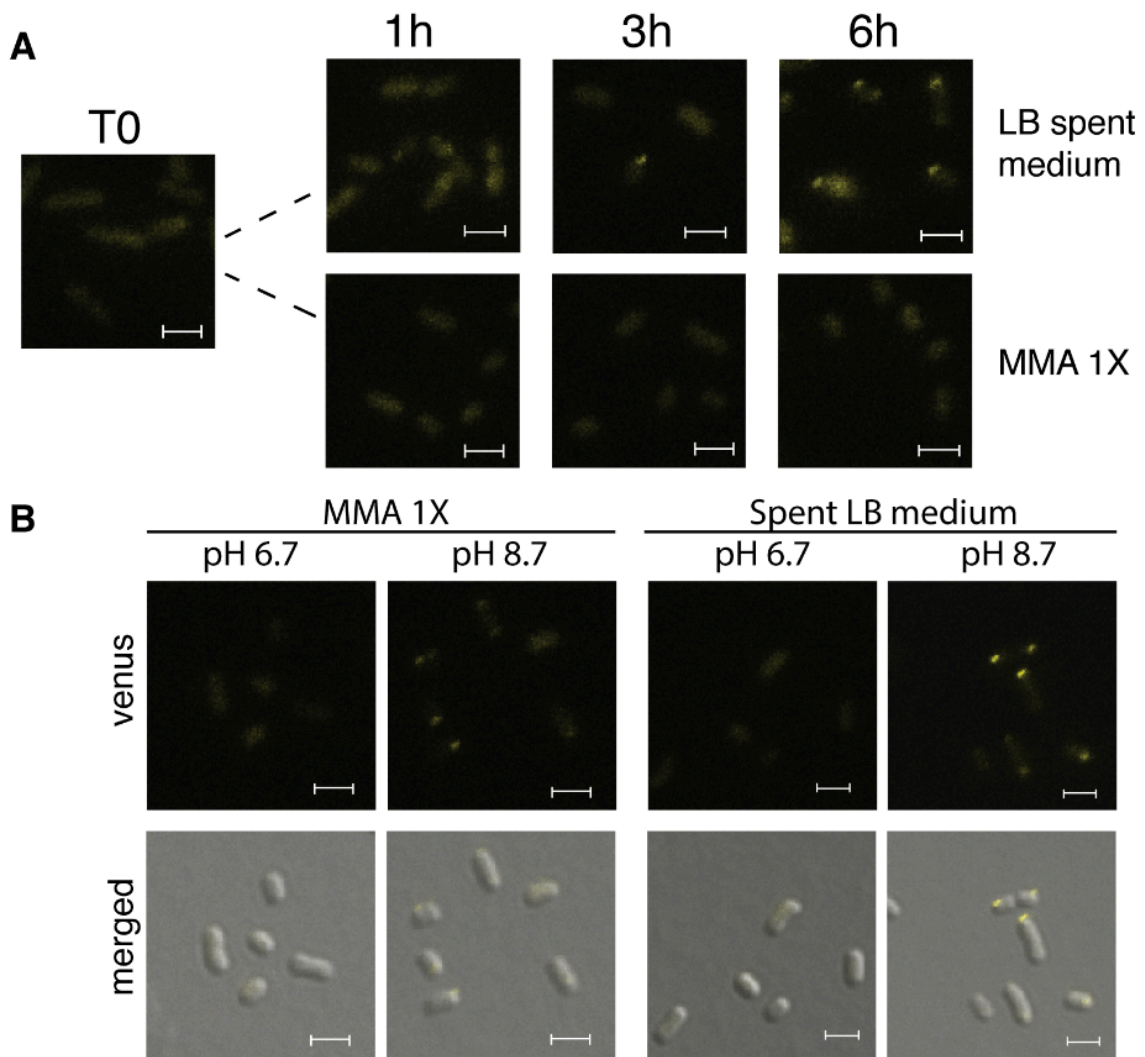
Figure 15. Effect of pH on DgcZ-mVENUS localization. (A) *E. coli dgcZ-mVENUS/ csrA*::Tn5 was grown in LB medium until OD_{600} 2.5, and resuspended in spent LB medium, or MMA 1X without carbon sources. Fluorescence microscopy images were taken after 1, 3 and 6 hours (B) The strain from panel A was grown as described above and transferred to buffered (K_2HPO_4 50 mM, KH_2PO_4 15 mM) spent LB medium or MMA 1X without carbon sources. Pictures were taken after 6 hours. Size bars are 2 μm and are identical in each picture. Adapted from Lacanna *et al.,* 2016.

E. coli growth in LB medium ceases when the carbon supply is exhausted (Sezonov *et al.*, 2007). Similar to LB spent medium, MMA 1X is a carbon-limited medium. Further, it was examined if an alkaline pH caused DgcZ polar localization only during carbon starvation, or in the presence of carbon as well. The *dgcZ-mVENUS/csrA::Tn5* strain was grown until OD_{600} 2.5 and transferred into fresh buffered LB medium with a pH of either 6.7 or 8.7, and DgcZ protein localization and bacterial growth were followed over time (Fig. 16A-B). Bacteria transferred into the LB medium with pH 8.7 displayed less growth than the bacteria resuspended in LB at pH 6.7 and showed DgcZ polar localization only after reaching

stationary phase (Fig. 16A-B). Bacteria resuspended in LB medium at pH 6.7 had weaker DgcZ-mVENUS signals and no polar localization was observed (Fig. 16A-B). This finding demonstrates that polar localization of DgcZ occurs in bacteria at an alkaline pH and only after reaching stationary phase (Fig. 16A-B).

Because of the weak DgcZ-mVENUS signal at pH 6.7, the localization of DgcZ-mVENUS overexpressed from a plasmid was investigated (Fig. 16C). At comparable inducer concentrations of 0.05% arabinose, DgcZ-mVENUS signal in stationary phase was strong and polarly localized at pH 8.7 and weak and delocalized at pH 6.7 (Fig. 16C). Increased inducer concentrations (0.2%) generated a stronger DgcZ-mVENUS signal from bacteria at pH 6.7 and the protein was evenly distributed in the cytoplasm (Fig. 16C). This observation validates the preceding results at pH 6.7, which showed a delocalized mVENUS signal.

Maurer *et al*. (2005) reported higher *dgcZ* expression at pH 8.7 than at pH 5.0 or 7.0. Alkaline pH activates the Cpx pathway, a two-component regulatory system, which initiates *dgcZ* transcription (Danese and Silhavy, 1998; Maurer *et al.*, 2005). In high pH environments, it is plausible that Cpx complex activation results in increased transcription of *dgcZ*. This might also account for the weak DgcZ-mVENUS signal detected at pH 6.7 (Fig. 15B, 16A).

The next step was to test if CpxR controlled the DgcZ-mVENUS polar localization. To overcome the effect of CpxR on the native *dgcZ* promoter, DgcZ-mVENUS was produced from a plasmid in the MG1655 and Δ*cpxR* strains. In stationary phase bacteria, DgcZ localized at the bacterial cell poles in both strains, suggesting that the protein polar localization is not controlled by CpxR (Fig. 16D).
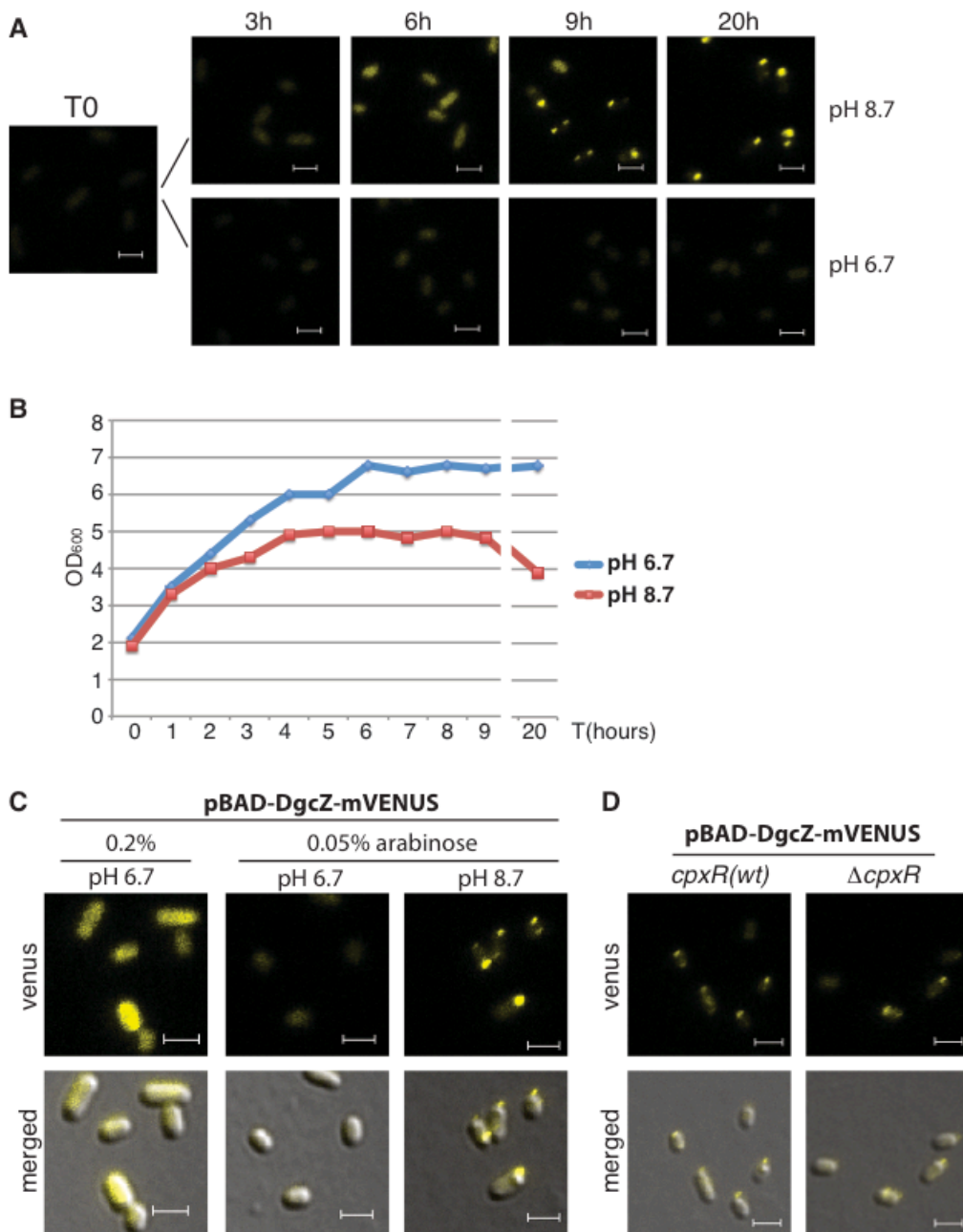
Figure 16. Localization of the DgcZ-mVENUS protein at different pH. (A) *E.coli dgcZ-mVENUS/csrA*::Tn*5* was grown in LB medium to OD_{600} 2.5, diluted (1:100) in buffered LB medium at either pH 6.7 or 8.7 and grown at 37 °C under shaking conditions. Fluorescence microscopy images were taken after 3, 6, 9 and 20 hours. (B) Growth curves from the experiment in panel A. (C) Microscopy pictures of *E.coli* MG1655 transformed with pBAD-DgcZ-mVENUS and grown in buffered LB medium at pH 6.7 or 8.7 at 37°C for 24 hours until reaching stationary phase. The medium was supplemented with 100µg/mL ampicillin and 0.2% or 0.05% arabinose was added to induce expression of *dgcZ-mVENUS*. (D) Fluorescence microscopy images of *E.coli* MG1655 *cpxR*(wt) and Δ*cpxR* transformed with pBAD-DgcZ-mVENUS and grown in LB medium at 37 °C for 24 hours. LB was supplemented with 0.02% arabinose and ampicillin. Size bars are 2 µm and identical in each picture. Adapted from Lacanna *et al.,* 2016.

3.3.6 DgcZ degradation is unaffected by protein localization

DgcZ polar foci appeared in response to alkaline pH and carbon starvation, and disappeared after restoring nutrient-sufficient conditions (Fig. 14B-C). The differential, pH-dependent localization of DgcZ enabled the investigation of DgcZ polar foci degradation when the protein was delocalized (i.e. at pH 6.7). For this purpose, the *dgcZ-mVENUS/csrA::Tn5* strain was grown in LB medium at 37 °C to OD_{600} 3.5 to allow protein production. Next, the bacteria were transferred to spent LB medium buffered at pH 6.7 or 8.7. After 3 hours, polar localization of DgcZ occurred in the bacteria at pH 8.7, while bacteria at pH 6.7 had delocalized DgcZ (Fig. 17A). Both samples were diluted in fresh LB medium and grown under shaking conditions at 37 °C. Protein samples and microscopy images were taken after 1 and 2 hours (Fig. 17A-B).

In both media, at pH 6.7 and 8.7, levels of DgcZ decreased 1 hour after dilution in fresh media, suggesting protein degradation also occurs when DgcZ is delocalized (Fig. 17A-B). As a negative control, a non-specific band in the DgcZ blot was used (Fig. 17B). In contrast to the DgcZ signal, the intensity of this band was constant (Fig. 17B).
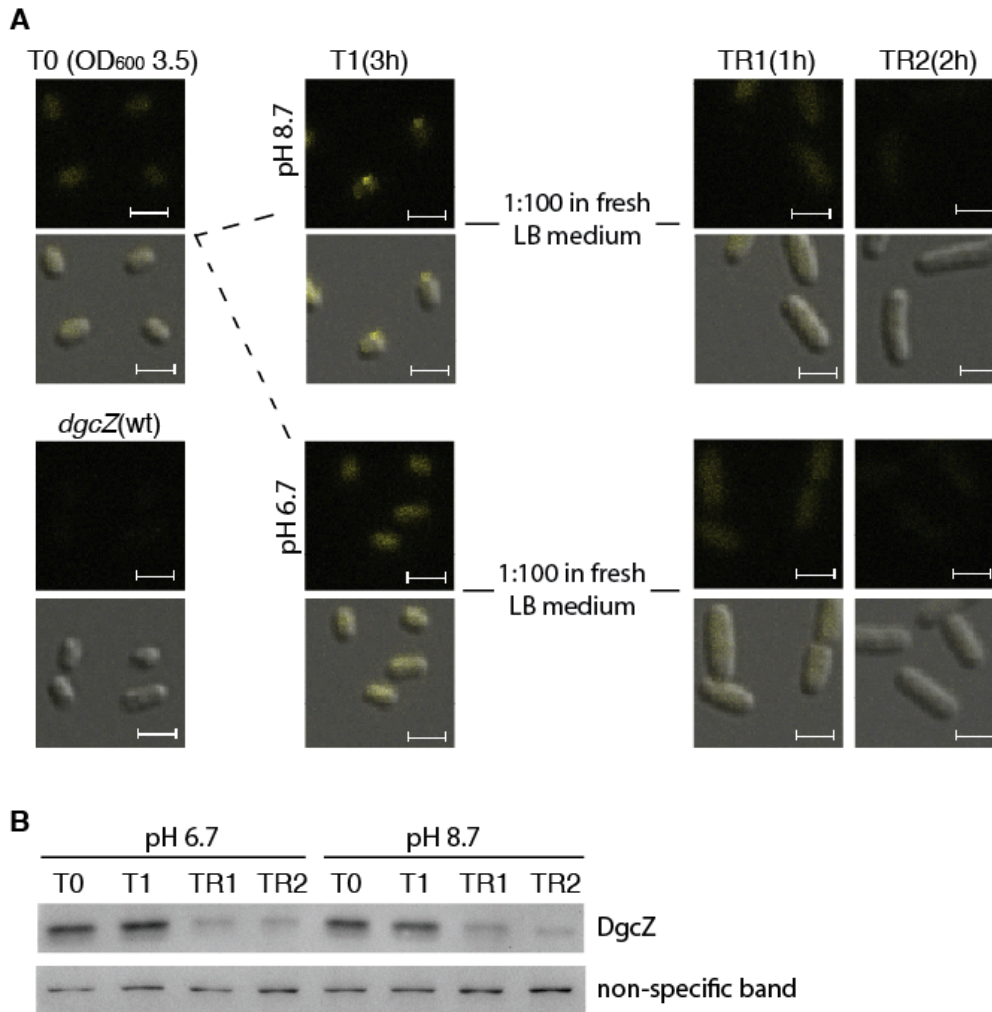
Figure 17. Decrease in DgcZ-mVENUS levels upon dilution of bacterial cultures in fresh LB medium. (A) *E. coli dgcZ-mVENUS/csrA*::Tn*5* grown in 20 mL of LB medium until OD_{600} 3.5, then transferred to buffered (K_2HPO_4 50 mM, KH_2PO_4 15 mM) spent LB medium at pH 6.7 or 8.7, and cultivated under shaking conditions at 37 °C. After 3 hours the samples were diluted (1:100) in fresh (unbuffered) LB medium, and cultivated for 2 hours. Microscopy picture were taken at the times specified above. Size bars are 2 μm, and identical in each picture. (B) Western blot detection of DgcZ from protein samples extracted during experiment described in (A). As a negative control, a non-specific band detected by the anti-DgcZ antibody is shown. Adapted from Lacanna *et al.*, 2016.

3.4 c-di-GMP concentration decreases during pre-stationary phase in the *csrA*::Tn*5* mutant background

In *E. coli* MG1655 cultured in TB medium, c-di-GMP reaches maximum concentrations at an OD_{600} of 1.34 and decreases by ≈50% over the next 3 hours (Spangler *et al.*, 2010). Using TB medium and the same conditions applied by Spangler *et al.* (2010), an OD_{600} of

1.34 corresponds to the post-exponential phase, using the criterion given in this study (Fig. 9A). Plotting a chart of the OD_{600} values indicated in Spangler *et al.* (2010) revealed a distinct change in the slope of the bacterial growth curve at an OD_{600} of 1.34 (data not shown). In the *csrA*::Tn*5* mutant background grown in LB medium, a similar drop in c-di-GMP concentrations between pre-stationary and stationary phase was observed (Fig. 9B-C).

To characterize how c-di-GMP concentrations fluctuate in different growth phases of the *csrA*::Tn*5* strain, a thorough analysis of DgcZ protein levels and PgaD concentrations (indicative of c-di-GMP amounts) during bacterial growth was performed (Fig. 18A-B). The *csrA*::Tn*5*/*dgcZ-mVENUS*/*pgaD-3xFlag* strain was grown in LB medium at 37 °C under shaking conditions and PgaD and DgcZ levels, and optical densities (OD_{600}), were monitored every hour (Fig. 18A-B). PgaD levels decreased during the post-exponential phase (OD_{600} 2.1), while DgcZ levels increased until bacteria reached stationary phase (Fig. 18A-B). Like the *E. coli* MG1655 strain grown in TB medium (Spangler *et al.*, 2010), c-di-GMP concentrations in the *csrA*::Tn*5* strain decreased in the post-exponential phase. In contrast to MG1655, the *csrA*::Tn*5* strain also showed high PgaD levels in the early exponential phase (Fig. 18A-B; Spangler *et al.*, 2010).

3.4.1 PDEs decrease c-di-GMP concentrations in post-exponential and pre-stationary phase

In the *csrA::Tn5*/*dgcZ-mVENUS*/*pgaD-3xFlag* strain, PgaD levels decreased from post-exponential phase (OD_{600} 2.1) onward, whereas DgcZ levels increased until bacteria reached the stationary phase (Fig. 18A). This result implies that the drop in PgaD levels was not caused by DgcZ degradation. PgaD levels also decreased in the *csrA::Tn5*/*dgcZ*(H79L,H83L)/*pgaD-3xFlag* strain (Fig. 18C-D).

The *dgcZ*(H79L,H83L) allele encodes a hyperactive variant of DgcZ which is unable to respond to Zn^{2+}. Thus, the decrease in PgaD and c-di-GMP levels was not caused by Zn^{2+}-dependent inactivation of DgcZ.

An increase in the activity of one or more PDEs may explain the observed c-di-GMP decrease. This hypothesis was tested using *E. coli csrA::Tn5* strains carrying deletions of seven or nine PDE-encoding genes. These strains were obtained by introducing serial deletions of genes encoding PDEs to the *E. coli* MG1655. Gene deletions, present in the Keio collection strains (Baba *et al.*, 2006), were transferred to recipient strains through P1

transductions. The Δ7 (Δ*pdeH* (*yhjH*), Δ*pdeL* (*yahA*), Δ*pdeA* (*yfeA*), Δ*pdeR* (*yciR*), Δ*pdeN* (*rtn*), Δ*pdeC* (*yjcC*), Δ*pdeF* (*yfgF*)) and Δ9 strains (Δ7, Δ*pdeI* (*yliE*), Δ*pdeB* (*ylaB*)) carry deletions of 7, or 9 PDE-encoding genes in the *E. coli* MG1655 background. Before use, *pgaD3xFlag* and *csrA::Tn5* mutations were also introduced in both strains by P1 transduction.

With *dgcZ*(+)/*pgaD-3xFlag/csrA::Tn5,* the Δ7 and Δ9 derivative strains were grown in LB medium at 37 °C. DgcZ and PgaD protein levels were monitored at specified times (Fig. 18E). DgcZ amounts increased until the stationary phase (left WB) where the concentrations remained constant (right WB) in all strains (Fig. 18E), confirming previous observations (Fig. 18A).

PgaD levels were initially higher in the Δ7 and Δ9 derivative strains compared to those detected in the *dgcZ*(+) strain (Fig. 18E). After time elapsed, PgaD levels strongly decreased in the *dgcZ*(+) and the Δ7 strains, while only a slight decrease was observed in the Δ9 strain (Fig. 18E). PgaD protein concentrations were also detected in late stationary phase (at 20, 24, and 28 hours) in the Δ9 derivative strain and the Δ7 derivative strain (to a lesser extent). As expected, in late stationary phase, PgaD levels were not detectable in the *dgcZ*(+) strain (Fig. 18E).

Further, it was tested whether the observed c-di-GMP decrease was caused by the phosphodiesterase PdeI or PdeB, not present in the Δ9 derivative strain. Strains carrying deletions in *pdeI* and *pdeB* and a Δ*pdeI*/Δ*pdeB* (Δ2) double mutant were constructed in the *pgaD-3xFlag/csrA::Tn5* background and PgaD protein levels were monitored at specified times (Fig. 18F). In the Δ*pdeI*, Δ*pdeB* and Δ2 strain, PgaD levels decreased over time (Fig. 18F), as in the *dgcZ*(+) strain.

In sum, these results show that multiple PDEs contributed to the decrease in c-di-GMP concentrations observed during post-exponential/pre-stationary phase.
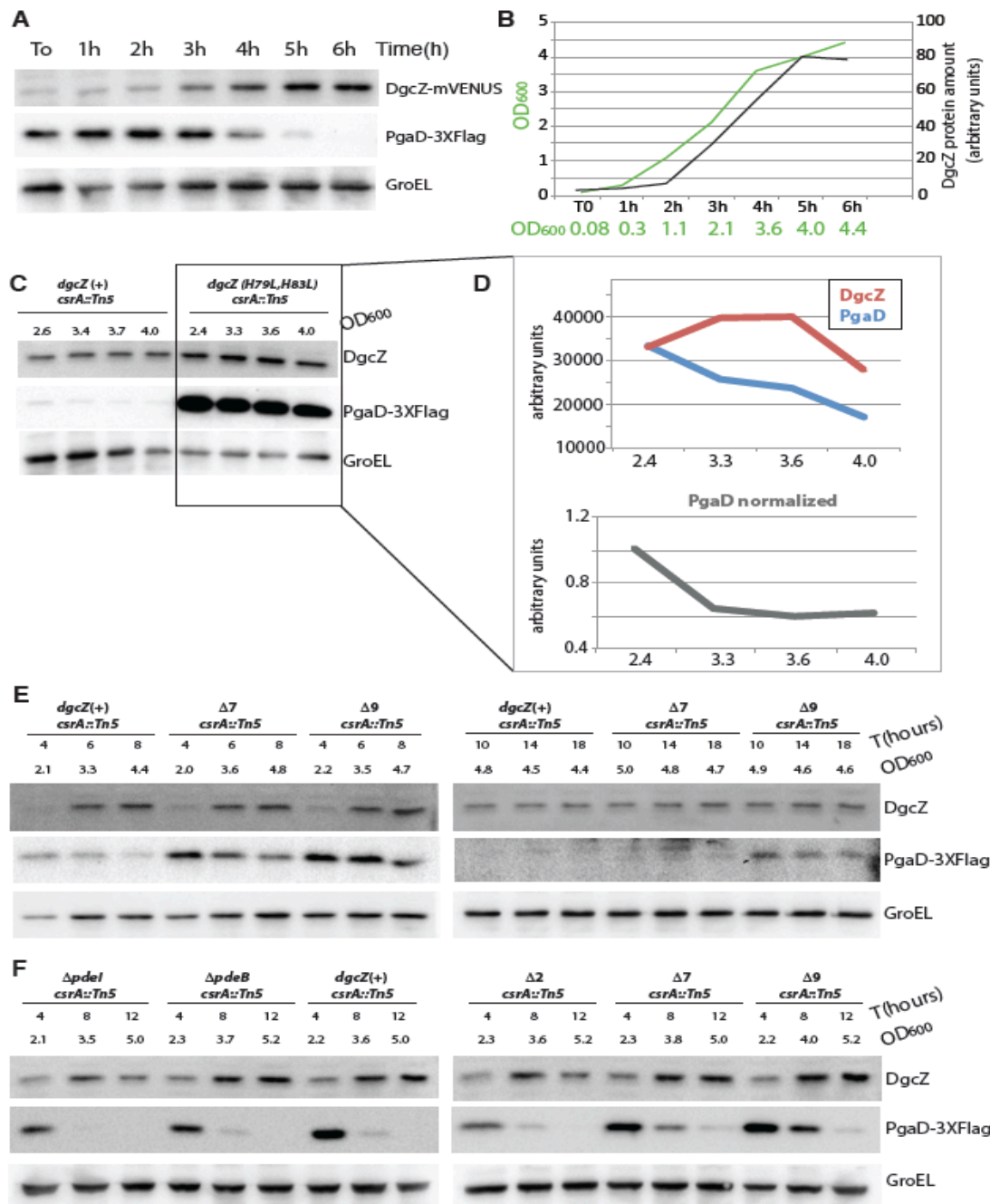
Figure 18. Decrease in PgaD protein levels in the post-exponential phase is caused by PDEs. (A) Western blot detection of DgcZ-mVENUS, PgaD-3xFlag and GroEL protein extracted from the *dgcZ-mVENUS/pgaD-3xFlag/csrA*::Tn*5* strain grown in LB medium at 37 °C. Proteins were extracted every hour until bacteria reached the stationary phase. (B) Graph indicating OD_{600} of the bacterial culture and DgcZ-mVENUS protein concentrations deduced from the experiment shown in panel A. The intensities of the DgcZ bands were quantified using ImageJ. (C) Western blot detection of DgcZ, PgaD-3xFlag and GroEL protein extracted from the *pgaD-3xFlag/csrA*::Tn*5* strains carrying either *dgcZ*(+) or the *dgcZ*(H79L,H83L) allele. (D) Analysis of Western blot in panel C. Intensities of DgcZ and PgaD bands are in the upper chart. The bottom chart shows normalized PgaD values, obtained by dividing PgaD by DgcZ signals. (E-F) Western blot detection of DgcZ, PgaD-3xFlag and GroEL proteins in the *dgcZ*(+), Δ*pdeI*, Δ*pdeB*, Δ2(Δ*pdeI*/Δ*pdeB*), Δ7 and Δ9 mutants in PDE-encoding genes in the *pgaD-3xFlag/csrA*::Tn*5* background. Strains were grown as described in (A). Adapted from Lacanna *et al.*, 2016.

3.5 Identification of potential DgcZ interaction partners

Carbon deprivation in conjunction with an alkaline pH promotes polar localization of DgcZ, but the physiological effects of this localization are unknown. To study the functions and the regulation of a protein *in vivo*, co-immunoprecipitation studies (CoIPs) are a preferred method because they reveal potential interactions with proteins and other macromolecules. With the aim of understanding the role of the polarly localized DgcZ, CoIPs using DgcZ-3xFlag as bait were performed.

Protein samples from bacteria in exponential (OD_{600} 0.6) and stationary (OD_{600} 4.5) growth phase, corresponding to delocalized and polarly localized DgcZ, were used to identify proteins that interact with DgcZ during these growth phases and localization states. OD_{600} at 0.6 was preferred over OD_{600} of 3.5 because of the higher c-di-GMP concentration present in the cells at this time (Fig 18A). It is important to note that concentrations of DgcZ differ significantly in exponential and stationary phase (Fig. 18A). The purpose of this study, however, was to identify DgcZ interaction partners in the different growth phases, not to perform a quantitative analysis. The *dgcZ*(wt)/*csrA::Tn5* strain, grown under the same conditions of the *dgcZ-3xFlag*/*csrA::Tn5* strain until an OD_{600} of 0.6 or 4.5, served as a negative control.

Mass spectrometry-based identification of co-immunoprecipitated proteins was performed by employees of the SYNMIKRO Mass Spectrometric Core Facility, Marburg.

The CoIP resulted in the identification of 65 proteins not present in the negative controls. Of these 65 proteins, 28 were from exponentially growing bacteria (Table S1), and 37 from cultures in stationary phase (Table S2). A sorted list of the proteins identified from more than two single peptides and from at least three peptides is shown below (Table 6).

Table 6. Proteins identified in DgcZ-3xFlag co-immunoprecipitation.

Name	Function	Phase
FrdB	fumarate reductase, anaerobic, iron-sulfur protein subunit	Stationary
AlaS	alanyl-tRNA synthetase	Stationary
FrdA	fumarate reductase	Stationary
GabD	succinate-semialdehyde dehydrogenase I, NADP-dependent	Stationary
YgfK	predicted oxidoreductase, Fe-S subunit	Exponential
PspD	phage shock protein, inner membrane protein	Exponential
YgeY	hypothetical protease	Exponential
TdcB	threonine dehydratase	Exponential
PflB	pyruvate formate lyase I	Exponential
TdcE	pyruvate formate-lyase 4/2-ketobutyrate formate-lyase	Exponential
GrcA	pyruvate formate lyase subunit	Exponential

3.6 DgcZ interacts with the FrdB subunit of the fumarate reductase (FRD) complex.

Among the proteins identified in stationary phase cells were two subunits of the fumarate reductase complex (FRD), FrdA and FrdB (Table 6). The FRD complex is involved in anaerobic respiration (Spencer and Guest, 1973), production of flagella and control of flagellar activity in *E. coli* (Cohen-Ben-Lulu *et al.*, 2008). Interestingly, DgcZ overproduction reduced the number of surface-attached flagella in *E. coli* MG1655 through an unknown mechanism (Jonas *et al.*, 2008). DgcZ overproduction also reduced bacterial motility (Jonas *et al.*, 2008). Identification of two subunits of the FRD complex, the high score of FrdB identification (Table S2), and DgcZ and FRD sharing flagellar motility as a regulatory target motivated further experiments to support interactions between DgcZ and FrdA-B.

A bacterial two-hybrid assay indicated a direct interaction of DgcZ with FrdB, but not with FrdA (Fig. 19A-B). The DgcZ-FrdB interaction was more evident when the *frdB* fusion genes were expressed from "high copy number" plasmids (Fig. 19A-B-C). FrdA-FrdB and DgcZ-DgcZ interactions were also examined (Fig. 19A-B). The two-hybrid assay found an interaction between FrdA and FrdB only occurred in one of the eight tested combinations (Fig. 19A-B). The inability and inherent difficulty of detecting FrdA-FrdB interactions, even though they form a complex (Iverson *et al.*, 1999), reveals the limitations of the two-hybrid assay. DgcZ-DgcZ interactions were instead detected for each combination (Fig. 19A-B).

Since the DgcZ protein consists of a GGDEF domain and a zinc binding domain (CZB), further experiments were performed to ascertain which domain interacts with FrdB. In the two-hybrid assay, the CZB domain interacted efficiently with FrdB while the GGDEF domain displayed no interaction (Fig. 19D). A β-galactosidase assay was used to quantify the strength of these interactions (Fig. 19D).
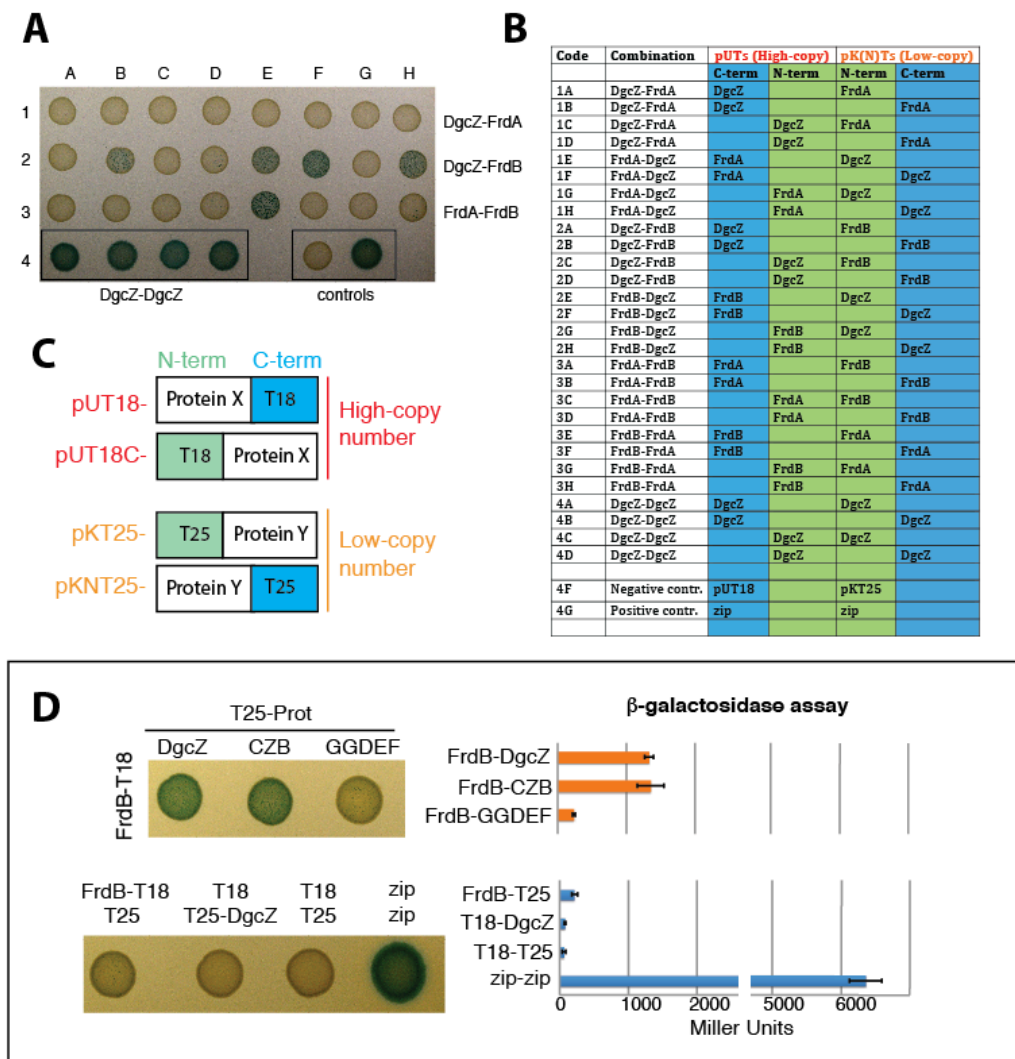
A

	A	B	C	D	E	F	G	H	
1									DgcZ-FrdA
2									DgcZ-FrdB
3									FrdA-FrdB
4									

DgcZ-DgcZ   controls

B

Code	Combination	pUTs (High-copy)		pK(N)Ts (Low-copy)	
		C-term	N-term	N-term	C-term
1A	DgcZ-FrdA	DgcZ		FrdA	
1B	DgcZ-FrdA	DgcZ			FrdA
1C	DgcZ-FrdA		DgcZ	FrdA	
1D	DgcZ-FrdA		DgcZ		FrdA
1E	FrdA-DgcZ	FrdA		DgcZ	
1F	FrdA-DgcZ	FrdA			DgcZ
1G	FrdA-DgcZ		FrdA	DgcZ	
1H	FrdA-DgcZ		FrdA		DgcZ
2A	DgcZ-FrdB	DgcZ		FrdB	
2B	DgcZ-FrdB	DgcZ			FrdB
2C	DgcZ-FrdB		DgcZ	FrdB	
2D	DgcZ-FrdB		DgcZ		FrdB
2E	FrdB-DgcZ	FrdB		DgcZ	
2F	FrdB-DgcZ	FrdB			DgcZ
2G	FrdB-DgcZ		FrdB	DgcZ	
2H	FrdB-DgcZ		FrdB		DgcZ
3A	FrdA-FrdB	FrdA		FrdB	
3B	FrdA-FrdB	FrdA			FrdB
3C	FrdA-FrdB		FrdA	FrdB	
3D	FrdA-FrdB		FrdA		FrdB
3E	FrdB-FrdA	FrdB		FrdA	
3F	FrdB-FrdA	FrdB			FrdA
3G	FrdB-FrdA		FrdB	FrdA	
3H	FrdB-FrdA		FrdB		FrdA
4A	DgcZ-DgcZ	DgcZ		DgcZ	
4B	DgcZ-DgcZ	DgcZ			DgcZ
4C	DgcZ-DgcZ		DgcZ	DgcZ	
4D	DgcZ-DgcZ		DgcZ		DgcZ
4F	Negative contr.	pUT18		pKT25	
4G	Positive contr.	zip		zip	

C

N-term   C-term

pUT18- | Protein X | T18 | — High-copy number
pUT18C- | T18 | Protein X |

pKT25- | T25 | Protein Y | — Low-copy number
pKNT25- | Protein Y | T25 |

D

T25-Prot

DgcZ   CZB   GGDEF

FrdB-T18

FrdB-T18 / T25   T18 / T25-DgcZ   T18 / T25   zip / zip

β-galactosidase assay

FrdB-DgcZ
FrdB-CZB
FrdB-GGDEF

FrdB-T25
T18-DgcZ
T18-T25
zip-zip

0   1000   2000   5000   6000   Miller Units

Figure 19. Bacterial two-hybrid assay to validate the DgcZ/FrdB interaction. (A) Validation of interactions between DgcZ and FrdA-B. N- (N-term) and C-terminal (C-term) fusions of the proteins were constructed and all combinations were tested. Growth conditions are indicated in Material and Methods. The images show the cultures spotted on LB medium agar plates supplemented with Amp (100 μg/mL), Kan (50 μg/mL), Str (75 μg/mL), X-Gal (40 μg/mL) and 500 μM IPTG. (B) Combinations used in panel A. (C) Schematic representation of plasmid features. (D) High-copy number plasmid pUT18 encoding FrdB C-terminally fused to T18 and low-copy number plasmid pKT25 encoding full-length DgcZ, CZB or GGDEF domains N-terminally fused to T25 were combined. As negative controls, pUT18-FrdB and pKT25-DgcZ combined with the empty plasmids pKT25 and pUT18, respectively. Shown on the left: Images of cultures spotted on LB medium agar plates supplemented with X-Gal and IPTG. On the right: relative β-galactosidase activities. The experiment was repeated three times and a representative plate is shown. Error bars depict the standard deviations of three biological replicates. Adapted from Lacanna *et al.*, 2016.

3.6.1 FrdA and FrdB show membrane localization

After confirming the interaction between DgcZ and FrdB using the two-hybrid assay, the localization of DgcZ, FrdA, and FrdB was investigated in the *csrA::Tn5* strain background. Fluorescence microscopy was applied to bacteria carrying *dgcZ-mVENUS* and either *frdA-* or *frdB-mCHERRY* gene fusions under the control of their native promoters (Fig. 20). FrdA- and FrdB-mCHERRY showed even membrane localization, both in pre-stationary (OD_{600} 4.0) and in stationary phase (6 hours after reaching OD_{600} 4.5) (Fig. 20). DgcZ-mVENUS displayed its characteristic localization pattern, and was dispersed in pre-stationary phase while polarly localized in stationary phase (Fig. 20).

Although these localization studies do not confirm an interaction, they cannot exclude this possibility either. Dispersed or polarly localized, DgcZ may interact with the membrane-associated FrdB.
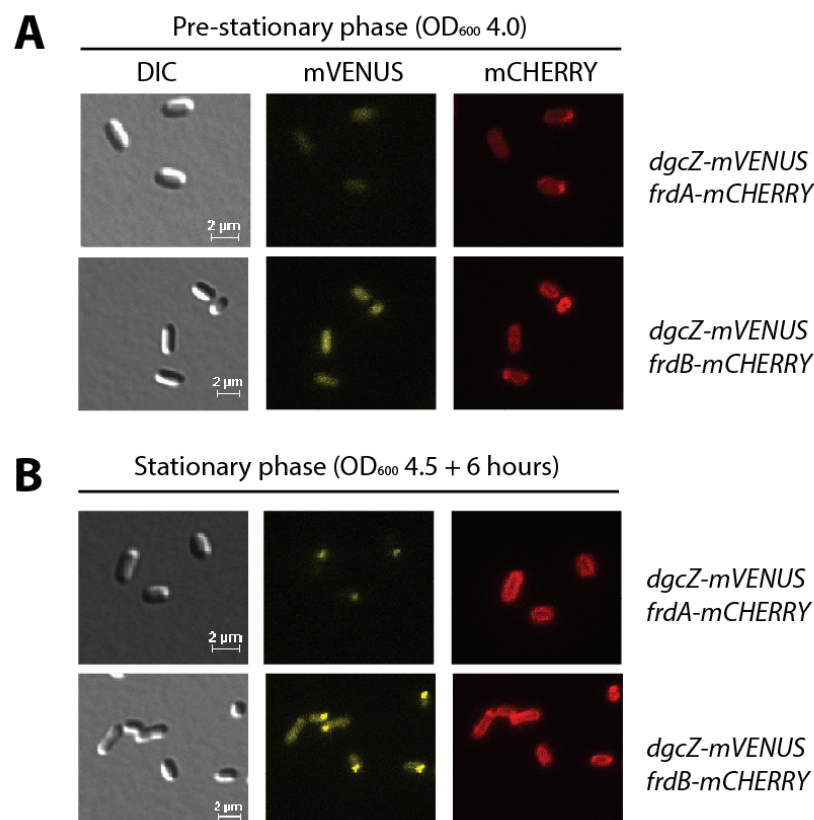

Figure 20. Fluorescence microscopy of strains co-expressing *dgcZ-mVENUS* and either *frdA-mCHERRY* or *frdB-mCHERRY*. *E. coli csrA*::Tn*5* cells with chromosomally integrated *dgcZ-mVENUS,* and either *frdA-mCHERRY* or *frdB-mCHERRY* were grown in LB medium at 37 °C. Microscopic images were taken in the pre-stationary (OD_{600} 4.0) and stationary (OD_{600} 4.5 + 6 hours) growth phase. Size bars are 2 µm. Figure adapted from Lacanna *et al.*, 2016.

3.6.2 DgcZ does not influence anaerobic growth on glycerol-fumarate

Anaerobic growth of *E. coli* on glycerol-fumarate minimal medium requires a functional FRD complex (Spencer and Guest, 1973). In this medium, glycerol serves as the carbon source and fumarate as the terminal electron acceptor (Spencer and Guest, 1973). Since the two-hybrid assay showed an interaction between FrdB and DgcZ, it was tested whether *dgcZ* deletion influenced FRD complex activity while analyzing anaerobic growth on glycerol-fumarate minimal medium at 37 °C (Fig. 21).

The growth of Δ*dgcZ* and *dgcZ*(wt) strains was measured and Δ*frdA* and Δ*frdA/ΔdgcZ* strains were used as negative controls because these strains lack a functional FRD complex (Fig. 21A). The Δ*dgcZ* strain showed a slight growth defect compared to the *dgcZ*(wt) strain, and, as expected, the Δ*frdA* and Δ*frdA/ΔdgcZ* strains did not grow (Fig. 21A). Subsequently, it was examined if the slight growth defect observed in the Δ*dgcZ* strain was specific for anaerobic conditions. For this purpose, the same strains were grown at 37 °C in LB medium under aerobic conditions (Fig. 21B). Under these conditions, the Δ*dgcZ* and Δ*frdA/ΔdgcZ* strains grew slower and reached a lower final optical density than the *dgcZ*(wt) and Δ*frdA* strains (Fig. 21B). Since both strains containing a *dgcZ* deletion displayed FRD-independent growth defects under aerobic conditions, it is possible that the growth defects observed under anaerobic conditions are also FRD-independent. Given that the FRD complex is essential for anaerobic growth on glycerol-fumarate minimal medium, if either the presence, or the absence of DgcZ-FRD interaction would alter the respiratory function of FRD, one would expect severe growth defects. Though not thoroughly tested, DgcZ most likely does not affect FRD function.
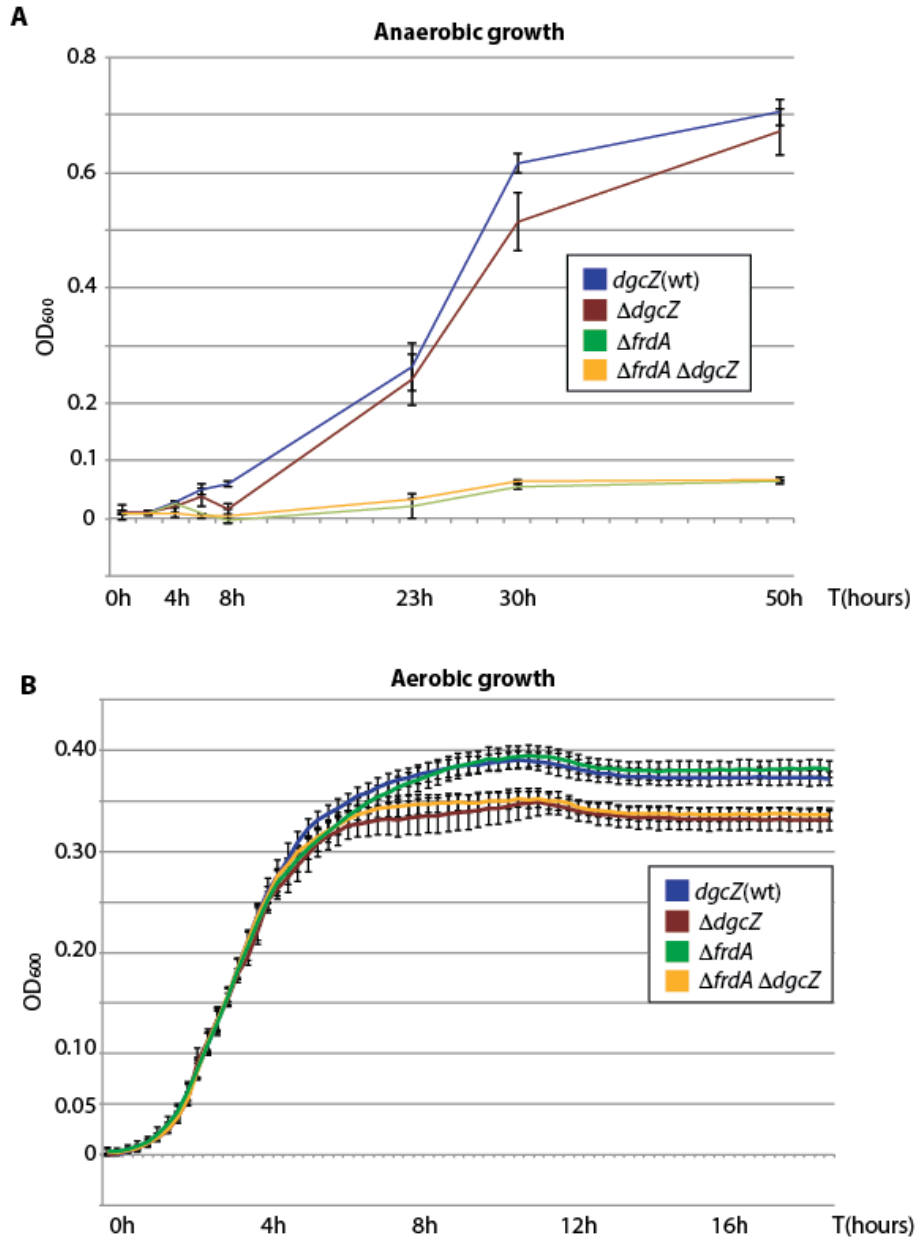
Figure 21. Anaerobic and aerobic growth of *dgcZ*(wt) and Δ*dgcZ* strains on glycerol-fumarate minimal medium and LB medium, respectively. (A) Anaerobic growth of the MG1655 *dgcZ*(wt), Δ*dgcZ*, Δ*frdA* and Δ*frdA*/Δ*dgcZ* strains at 37 °C in MMA 1X supplemented with 0.4% glycerol and 40 mM fumarate. Bacteria grown aerobically in MMA 1X supplemented with 0.4% glucose over night were diluted 50 times in 400 µl of MMA 1X (supplemented with glycerol and fumarate) in 1.5 mL eppendorf tubes. The tubes were shaken at 300 rpm in a Eppendorf Thermomixer R under the anaerobic hood and OD_{600} values were measured at the indicated time points with the help of a Nanodrop. Error bars are SEM from three biological replicates. (B) Aerobic growth of the strains from panel A in LB medium at 37 °C under shaking conditions (amplitude 3.5 mm, frequency 424.1 rpm) in a TECAN (infinite F200 Pro) reader at 37 °C. OD_{600} was measured every 15 minutes. Error bars are SEM from six biological replicates.

3.6.3 Superoxide stimulates FRD- and DgcZ- dependent biofilm formation

Since DgcZ does not appear to influence FRD function, a deletion of the *frdA* gene, creating a non-functional FRD complex, was tested to determine whether it influenced DgcZ-dependent biofilm formation in the *csrA::Tn5* background.

An attachment assay was conducted to compare biofilm formation between the wt and the Δ*frdA*, Δ*dgcZ* and Δ*dgcZ*/Δ*frdA* strains (Fig. 22). Δ*frdA* strains could not assemble a functional FRD complex and formed similar amounts of biofilm as the wild-type strains, in both *dgcZ*(wt) and Δ*dgcZ* backgrounds.
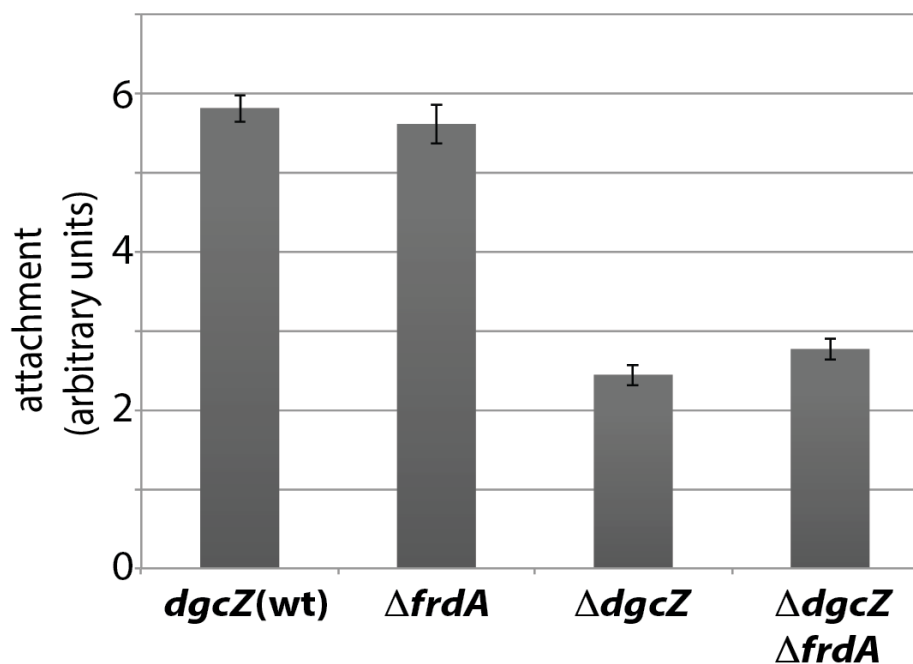

Figure 22. Effect of *dgcZ* and *frdA* deletions on biofilm formation of the *csrA::Tn5* strain. The *dgcZ*(wt), Δ*frdA*, Δ*dgcZ* and Δ*dgcZ*/Δ*frdA* strains carrying the *csrA::Tn5* mutation were grown as described in Material and Methods and then an attachment assay was performed. These results are averages of six wells inoculated with single colonies. Error bars represent the SEM. The experiment was repeated three times and generated the same results.

The FRD complex has been previously shown to generate superoxide in *E. coli* (Imlay, 1995). Paraquat (*N,N'*-dimethyl-4,4′-bipyridinium dichloride) is an organic compound known to generate superoxide in bacteria, including *E. coli* (Hassan and Fridovich, 1978). To understand the effect of FRD on DgcZ-mediated biofilm formation in the presence of paraquat, attachment assays in the *csrA::Tn5* background were performed (Fig. 23A). Without paraquat, the Δ*frdA* strain showed similar levels of biofilm as the *frdA*(wt) strain,

confirming previous observations. After adding 50 µM of paraquat, the levels of biofilm formation in the *frdA*(wt) strain increased by roughly two-fold, while only a small increase of ≈10% was detected in the Δ*frdA* strain (Fig. 23A). A strain carrying a deletion of the *frdB* gene showed the same behavior of the Δ*frdA* strain (Fig. 23A). The addition of paraquat did not influence the attachment of the Δ*dgcZ* and Δ*dgcZ*/Δ*frdA* strains (Fig. 23A).

These findings indicate that DgcZ and the FRD complex play a role in superoxide-induced increase in biofilm formation.

To substantiate the effect of the FRD complex in paraquat-stimulated biofilm formation, the *frdA* gene was deleted with a *frdA::ccdB-kan* construct and then restored. The new strain created by this process is referred to as *frdA*(+) (Fig. 23B). P1 transduction was used to insert the *csrA::Tn5* allele into this strain. A control strain, Δ*frdA*^{Frt}, was also constructed. In this control, the *frdA::ccdB-kan* element was replaced by an *Frt* site, and then *csrA* was replaced by *csrA::Tn5* via P1 transduction (Fig. 23 B). As an additional control, the *frdA::ccdB-kan* construct was transduced into the *csrA::Frt* strain (Fig. 23 B). The attachment of these strains was then assayed (Fig. 23 C-D). Similar to the *frdA*(wt) strain, the *frdA*(+) strain showed a two-fold increase in the levels of biofilm formed upon paraquat addition (Fig. 23C). Both the Δ*frdA*^{Frt} and *frdA::ccdB* strains only showed a 10% increase in biofilm upon paraquat addition (Fig. 23C-D). This finding confirms that the increase in paraquat-stimulated biofilm formation is dependent on a functional FRD complex (Fig. 23B-D).

Furthermore, paraquat also increased biofilm formation in FRD-dependent manner when DgcZ was overproduced from a plasmid (Fig. 23E). The dependence of superoxide-stimulated biofilm formation on DgcZ and FRD may indicate a functional link between this DGC and the FRD complex.
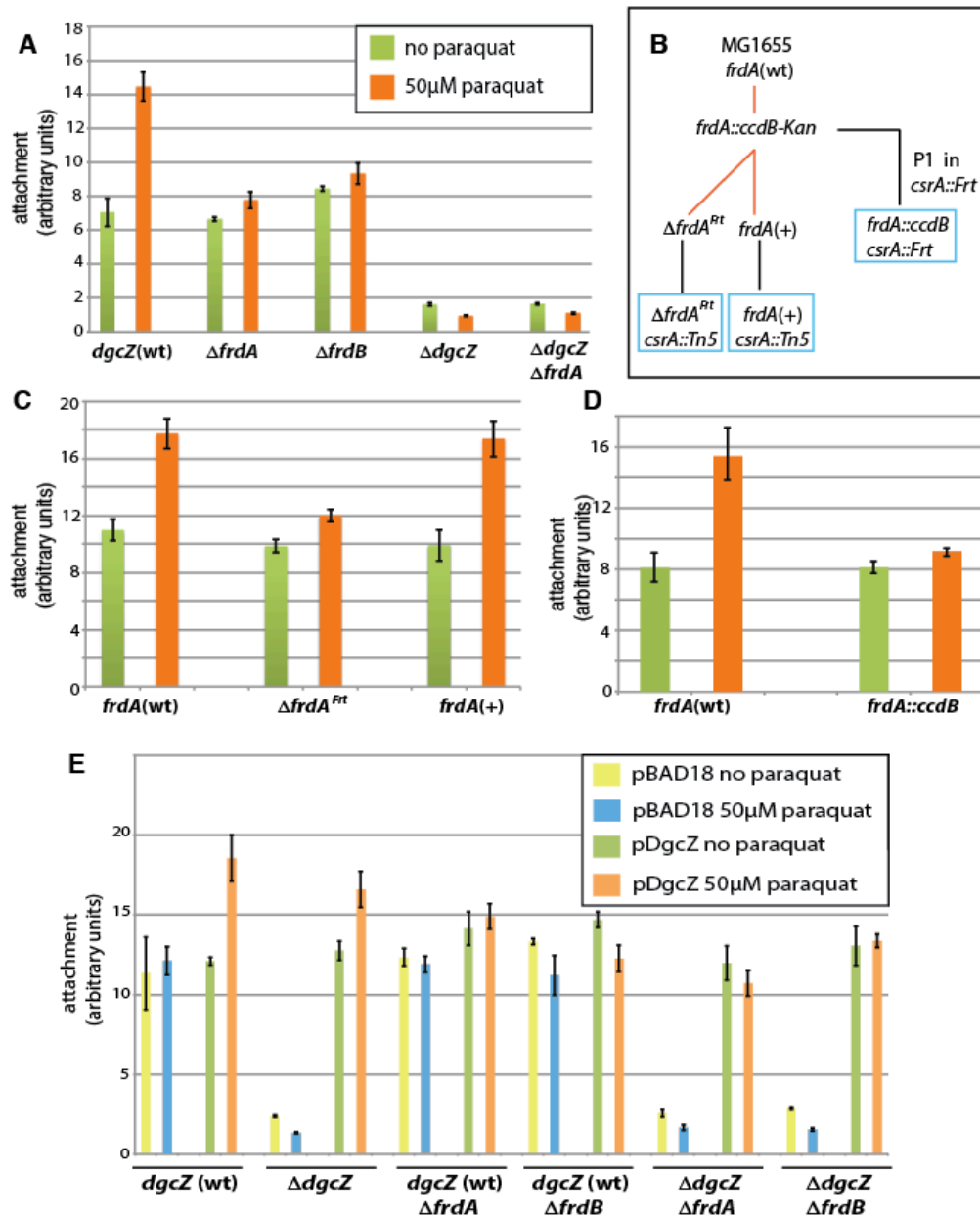
Figure 23. Paraquat enhances DgcZ-dependent biofilm formation in an FRD-dependent fashion. (A) Attachment assays of the *dgcZ*(wt)*, ∆frdA, ∆frdB, ∆dgcZ* and *∆dgcZ/∆frdA* strains carrying a *csrA::Tn5* mutation. LB medium was supplemented with 0, or 50 µM of paraquat. (B) Schematic representation of strain construction. The *frdA* gene was first deleted in *E. coli* MG1655. Then, the resulting *frdA::ccdB-Kan* strain was used as an ancestor for the *∆frdA^{Frt}* and the *frdA*(+) strains. Both strains were transduced using the P1 lysate from the *crsA::Tn5* strain. The *frdA::ccdB/csrA::Frt* strain was obtained by P1 transduction of the *csrA::Frt* strain using the lysate from the *frdA::ccdB-Kan* strain. Black arrows indicate P1 transductions and red arrows λRed-mediated recombineering. Blue boxes indicate the strains used for attachment assays. (C) Attachment assays of the *frdA*(wt), *∆frdA^{Frt}*, and *frdA*(+) strains in the *csrA::Tn5* background. (D) Attachment assays of the *frdA*(wt) and *frdA::ccdB* strains carrying the *csrA::Tn5* mutation. (E) Attachment assays of *frdA*(wt)/*dgcZ*(wt), *∆dgcZ, ∆frdA, ∆frdB, ∆dgcZ/∆frdA* and *∆dgcZ/∆frdB* in the *csrA::Tn5* background. These strains were transformed with pDgcZ, or an empty plasmid. LB medium was supplemented with Ampicillin, 0.02% arabinose and with 0, or 50 µM paraquat. Results of panels A, C, D and E are averages of five wells inoculated with single colonies. Experiments were repeated three times with the same results. Error bars represent the SEM. Figure adapted from Lacanna *et al.*, 2016.

3.7 DgcZ overproduction influences motility, but not the amount of flagella in non-attached bacteria

Jonas *et al.* (2008) found that the overexpression of *dgcZ* negatively affected the amount of flagella on surface-attached bacteria grown in LB medium without salt. The effect of DgcZ overproduction on flagella in non-attached bacteria was not described (Jonas *et al.,* 2008). The DgcZ full-length protein, as well as the CZB and the GGDEF domains were fused to mVENUS and overproduced, to evaluate their effects on the amount of flagella and motility (Fig. 24). Bacteria were growth in LB medium without salt at 37 °C for 24 hours until reaching stationary phase (OD_{600} 4.5). Then, Leifson staining was performed to visualize the bacterial flagella (Clark, 1976). There were no apparent differences in the amount of flagella detected between an *E. coli* MG1655 strain carrying a plasmid for *dgcZ-mVENUS* overexpression and a strain transformed with the empty plasmid (Fig. 24A). Strains overproducing CZB- / GGDEF-mVENUS fusions were also flagellated (data not shown). Similar results were obtained from bacteria grown in LB medium (85 mM NaCl) (data not shown).

The images obtained using Leifson staining do not allow for the quantitative analysis of flagella. For this reason, the amount of flagellin, which is the main component of bacterial flagellum, was quantified using SDS-PAGE (Fig. 24B). Flagellin was isolated by vortexing the bacteria, centrifuging and discarding bacterial pellets, and then concentrating the flagella from the supernatant by long centrifugation (1 hour). The detailed procedure is described in Material and Methods.

Bacteria were grown as for Leifson staining, flagellin extraction was performed and then comparable volumes of each sample were submitted to SDS-PAGE analysis. None of the analyzed samples contained significant differences (Fig. 24B).

Next, the effects on motility were tested. The overexpression of *dgcZ-mVENUS* reduced bacterial motility, whereas strains overproducing mVENUS fusions to the DgcZ active site mutant (E208Q), the CZB and GGDEF domain, were fully motile (Fig. 24C). As positive and negative controls, a plasmid overproducing the DGC DgcA from *Caulobacter crescentus* and the empty plasmid pBAD18 were used, respectively (Fig. 24C). Results from these experiments indicate that in non-attached bacteria DgcZ overproduction reduces motility in a c-di-GMP dependent fashion but does not affect the amount of flagella.
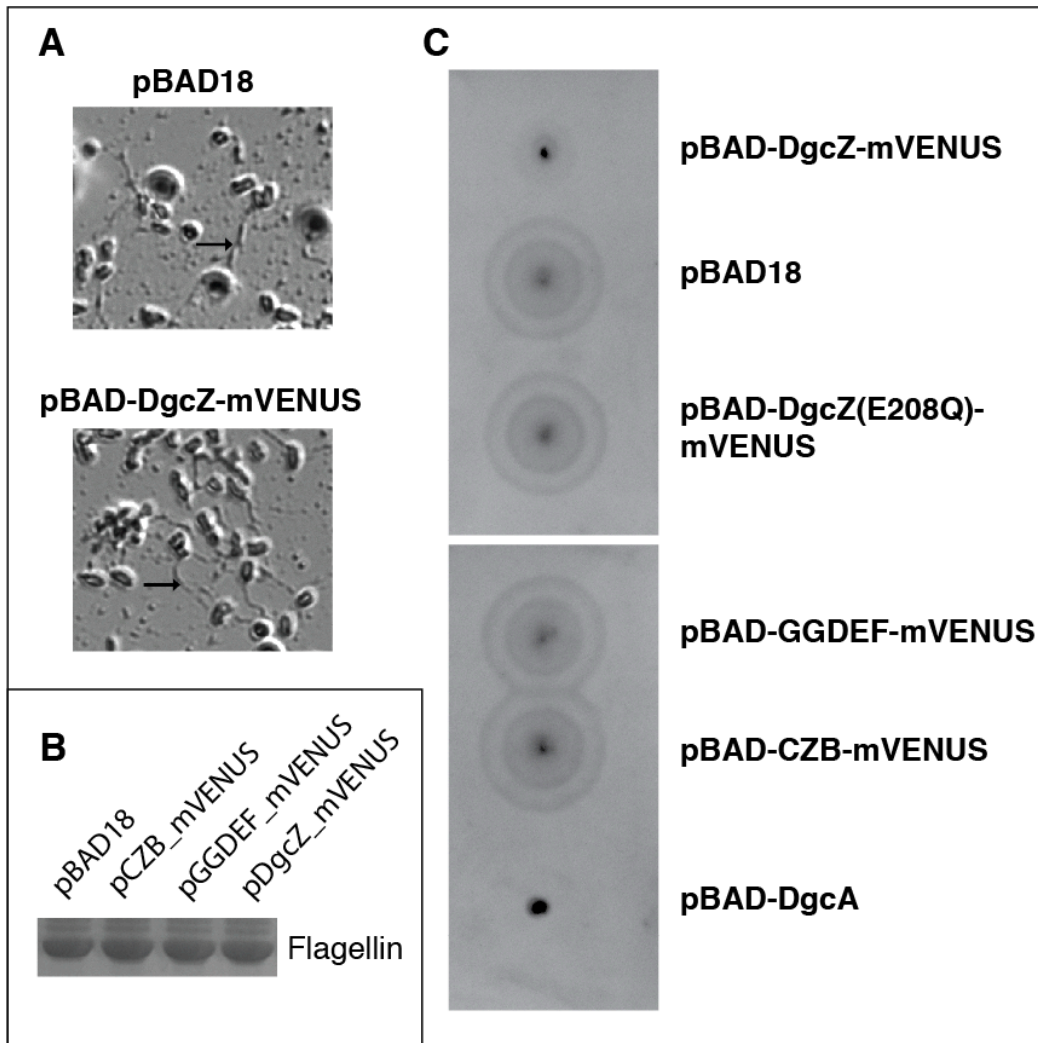
Figure 24. DgcZ overproduction affects motility, but not flagella amount in non-attached bacteria. (A) Leifson staining of *E. coli* MG1655 transformed with pBAD-DgcZ-mVENUS and with the empty plasmid pBAD18 and grown for 24 hours at 37 °C in LB without salt. (B) SDS-PAGE for the detection of Flagellin. Sample handling is described in Material and Methods. The experiment was repeated three times with the same results. (C) Motility assay of *E. coli* MG1655 transformed with plasmids carrying *mVENUS* gene fused to *dgcZ*, *dgcZ*(E208Q) and to the nucleotide sequences encoding the CZB and GGDEF domains. The empty plasmid pBAD18 and a plasmid carrying the gene encoding the DGC DgcA were used as negative and positive controls, respectively. The motility agar was supplemented with Ampicillin (100 µg/mL) and arabinose (0.1%).

3.8 The roles of CpxR and NlpE in DgcZ-dependent biofilm formation

Transcription of *dgcZ* is activated by CpxR, a component of the CpxA/R signal transduction system, in response to high levels of copper and other unknown signals (Yamamoto and Ishihama, 2005). Additionally, *dgcZ* transcription increases with the transient overproduction of the NlpE lipoprotein, a known activator of the CpxAR system (Raivio *et*

al., 2013). Since Otto and Silhavy (2002) demonstrated that the Cpx complex induced surface attachment by an unknown mechanism, and DgcZ, regulated by CpxAR, is involved in bacterial attachment, the effects of CpxR and NlpE on DgcZ-mediated biofilm formation were investigated.

3.8.1 DgcZ and CpxR contribute to biofilm formation in the *csrA*(wt) strain MG1655

In *E. coli* MG1655, *dgcZ* mRNA levels remain low but constant when grown in LB medium at 37 °C (Jonas *et al.*, 2008). Employing Western blot analysis, Boehm *et al.* (2009) reported that under conditions permissive for biofilm formation (static incubation in LB at 28 °C) DgcZ protein levels are low, but can be detected.

This observation was reconfirmed (Fig. 25A) and the effect of DgcZ on biofilm formation was examined in *csrA*(wt) strains using attachment assays (Fig. 25B).

In the *csrA*(wt) background, the Δ*dgcZ* strain formed ≈20% less biofilm than the wild-type strain (Fig. 25B). In addition, the ability to form biofilms was tested in a strain that carried a deletion of *cpxR*, a gene encoding a DgcZ transcriptional regulator, and in a Δ*cpxR*/Δ*dgcZ* double mutant. Both strains, Δ*cpxR* and Δ*cpxR*/Δ*dgcZ*, displayed reduced biofilm formation when compared to the wild-type strain (Fig. 25B). These results indicate that DgcZ and CpxR play a role in *E. coli* MG1655 biofilm formation.

3.8.2 *cpxR* deletion does not affect biofilm formation in the *csrA::Tn5* strain

The *csrA::Tn5* strain has higher levels of DgcZ protein because of the increased translation of *dgcZ* mRNA. The effect of *cpxR* deletion on biofilm was also tested in the *csrA::Tn5* background (Fig. 25C). Contrary to the results observed in the *csrA*(wt), the *cpxR* deletion had no effect on biofilm formation in this background (Fig. 25C). The Δ*cpxR* and Δ*cpxR*/Δ*dgcZ* strains formed the same amounts of biofilm as the *dgcZ*(wt) and the Δ*dgcZ* strain, respectively (Fig. 25C). The high amount of biofilm produced by the Δ*cpxR*/*csrA::Tn5* strain is most likely due to leaky transcription of *dgcZ*. The observation that the Δ*cpxR*/Δ*dgcZ* strain shows similar levels of biofilm compared to the Δ*dgcZ* strain adds additional weight to the hypothesis that the two proteins belong to the same pathway.
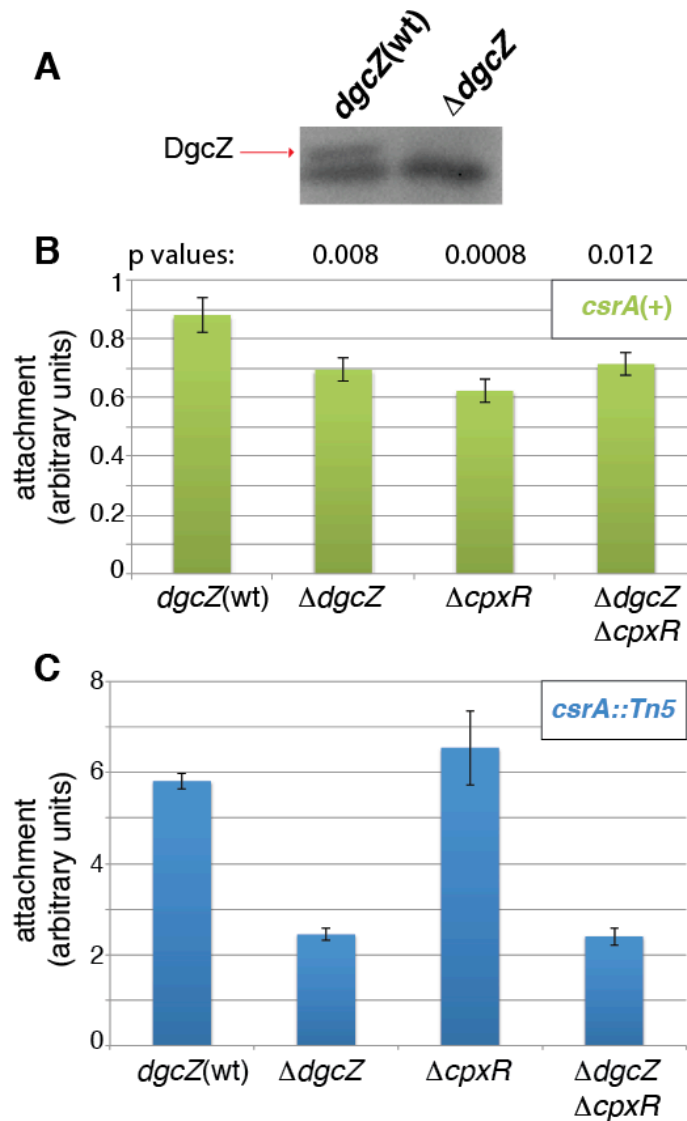
Figure 25. Effects of *dgcZ* and *cpxR* deletions on attachment of *csrA*(wt) and *csrA::Tn5* strains. (A) Western blot detection of DgcZ in *E. coli* MG1655, indicated as *dgcZ*(wt), and Δ*dgcZ*. Strains were grown for 24 hours at 30 °C under static conditions. (B) Attachment assay of MG1655, Δ*dgcZ*, Δ*cpxR*, and Δ*dgcZ*/Δ*cpxR* strains grown as in panel A. Statistical analysis for determining significance was performed using a student´s T-Test for two independent means, where each P value was obtained by comparing the mutant to the MG1655 strain. Results are averages of 12 wells inoculated with single colonies in two different experiments. Error bars represent the SEM. (C) Attachment assay of strains from panel B in the *csrA::Tn5* background. Results are averages of six wells inoculated with single colonies. Experiments were repeated three times with the same results. Error bars represent the SEM. Figure adapted from Lacanna *et al.*, 2016.

3.8.3 The effects of NlpE on biofilm formation depend on DgcZ

Since NlpE activates CpxR in response to surface sensing (Snyder *et al.*, 1995; Otto and Silhavy, 2002) and CpxR inhibits motility and stimulates *dgcZ* transcription (De Wulf *et al.*, 1999), the effects of NlpE overproduction on DgcZ-dependent regulation of motility and

biofilm formation were assessed (Fig. 26). Either the pNlpE overexpression plasmid or the empty vector pCJ30 were introduced into the *E. coli* MG1655 and the Δ*dgcZ* mutant.

NlpE overproduction repressed the motility of the *dgcZ*(wt) and the Δ*dgcZ* strain (Fig. 26A). This DgcZ-independent inhibition of motility may result from the transcriptional repression of the *motAB-cheAW* operon, which occurs upon the phosphorylation and subsequent activation of CpxR (De Wulf *et al.*, 1999).

To examine if *nlpE* overexpression affected biofilm formation, attachment assays using strains carrying either *dgcZ*(wt) or Δ*dgcZ* in the *csrA::Tn5* mutant background were performed (Fig. 26B). The *dgcZ*(wt) strain overexpressing *nlpE* produced three times more biofilm than the strain transformed with the empty plasmid. In contrast, the Δ*dgcZ* strain did not display enhanced biofilm formation upon NlpE overproduction (Fig. 26B). This finding indicates that NlpE affects this process in a DgcZ-dependent manner.
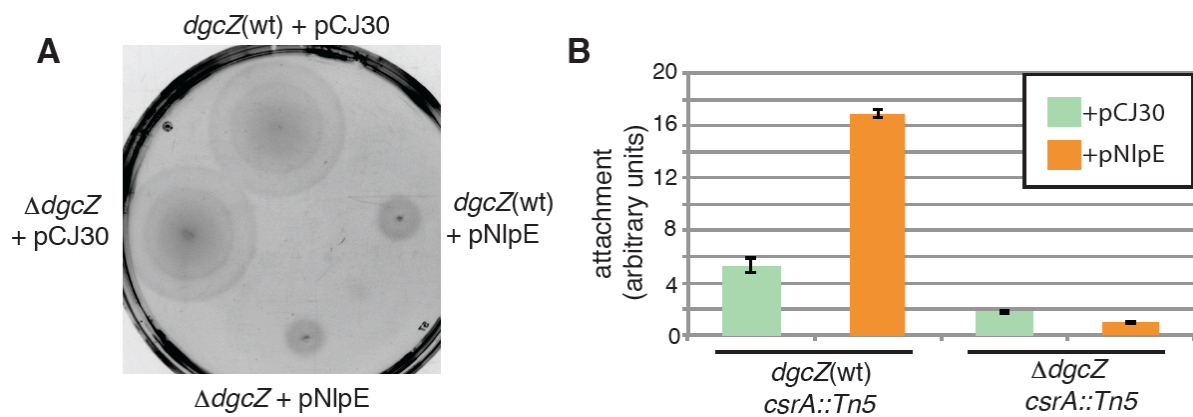

Figure 26. Effects of NlpE overproduction on motility and biofilm formation. (A) Motility of the *dgcZ*(wt) *E. coli strain* MG1655 and the *dgcZ* mutant transformed with either the pNlpE overexpression plasmid or the pCJ30 control plasmid. (B) Attachment assay of strains carrying *dgcZ*(wt) or Δ*dgcZ* in the *csrA*::Tn*5* background transformed with either pNlpE or pCJ30. Medium was supplemented with 100 µM ampicillin and 20 µM IPTG. Error bars represent the SEM. Figure adapted from Lacanna *et al.*, 2016.

4. Discussion

This work investigates the regulation and function of the diguanylate cyclase DgcZ of *E. coli*. Dyguanilate cyclases, via c-di-GMP, control in many bacteria the transition from a motile to a sessile lifestyle (Pesavento *et al.*, 2008; Kim and McCarter, 2007; Jonas *et al.*, 2010; Purcell *et al.*, 2012).

DgcZ regulates the production of the exopolisaccharide PGA, involved in bacterial adhesion to anaerobic surfaces, the first step of biofilm formation (Agladze *et al.*, 2005; Boehm *et al.*, 2009). Understanding how the DgcZ funtion is regulated is therefore of primary importance for a better comprehension of the factors triggring biofilm formation in *Escherichia coli*.

Previous studies clarified the role of CsrA in the regulation of translation of the *dgcZ* mRNA (Jonas *et al.*, 2008; Boehm *et al.*, 2009).

This work shows that the production and activity of DgcZ are regulated at multiple levels. In particular, this study reveals: i) the role of Zn^{2+} for control of DgcZ protein activity, ii) the importance of the Cpx signal transduction system for the regulation of *dgcZ* transcription, and iii) an effect of superoxide (O^{2-}) on DgcZ-dependent biofilm formation.

Additionally, this work provides a detailed analysis of the DgcZ protein levels and localization during different growth phases and a characterization of the effects of DgcZ-derived c-di-GMP on PGA production, motility, and surface adhesion. In the following sections, these findings will be discussed.

4.1 Role of Zn^{2+} in post-translational regulation of DgcZ activity

Zn^{2+} is an essential component in living organisms. This transition metal serves as a cofactor for several proteins which facilitate diverse metabolic processes (Vallee and Falchuk, 1993). For instance, some oxidoreductases, transferases, hydrolases, isomerases and ligases are zinc enzymes (Vallee and Falchuk, 1993). Since zinc is a vital trace element, bacterial cells possess efficient uptake systems to gather and harness the mineral (Hantke, 2005).

Over time, bacterial proteins developed a high affinity for zinc. These proteins rapidly capture the metal to prevent cross-reactivity with other proteins, which harms the cell (Vallee and Falchuk, 1993). Zn^{2+} ions are in fact highly reactive Lewis acids, accepting electron pairs

from other molecules, known as Lewis bases. To tightly control the metal concentration and to avoid cellular damage due to a high and toxic concentration of zinc, bacterial cells possess export systems to clear excess zinc from the cytoplasm (Outten and O'Halloran, 2001).

In most proteins, the function of zinc ions is either structural or catalytic. Altohugh, zinc-responsive proteins involved in signal transduction also exist (Patzer and Hantke, 1998; Hantke, 2005). The proteins Zur and ZntR in *E. coli*, for example, upon zinc binding, regulate transcription of the genes encoding the ZnuABC and ZntA pumps, involved in maintaining the metal homeostasis (Patzer and Hantke, 1998; Finney and O'Halloran 2003).

Recently, Draper *et al.* (2011) identified a zinc-binding domain, referred to as CZB, in the chemoreceptor TlpD of *Helicobacter pylori*. As of this writing, researchers have identified 238 bacterial species containing the CZB domain (Pfam family PF13682).

Of the 418 CZB domain-containing proteins analyzed by Draper *et al.* (2011), 46% are soluble chemoreceptors similar to the TlpD of *H. pylori*. 78% of the 418 proteins containing the CZB domain also have a methyl-accepting domain (MA), a typical characteristic of chemoreceptors. The remaining 22% are likely signalling proteins as well, because they contain GGDEF and EAL motifs, involved in c-di-GMP signalling, or other domains performing sensory functions as PAS[2], NIT[3] (a nitrate- and nitrite-sensing domain), GAF[4] (a noncatalytic cGMP-binding domain), and CHASE[5] domains (cyclase/histidine kinase-associated sensing extracellular domain).

The CZB domain is also found in the diguanylate cyclase DgcZ of *Escherichia coli* (Draper *et al.*, 2011). DgcZ, as demonstrated by Zähringer *et al.* (2013), binds zinc ions through a 3His/1Cys motif in the N-terminal CZB protein domain. *In vitro* analysis also demonstrates that DgcZ activity is allosterically regulated by zinc (Zähringer *et al.*, 2013).

Given the importance of DgcZ, this study examines the effects of zinc on DgcZ activity *in vivo*. Site-directed mutagenesis of the *dgcZ* gene reveals that the 79, and 83 histidines are involved in the zinc-mediated regulation of protein activity. A strain carrying the *dgcZ*(H79L,H83L) allele, in fact, displayed significantly higher PgaD concentrations and bound more Congo red than a strain with the wild-type DgcZ. These results strongly suggest that disrupting zinc-binding in DgcZ significantly increases its c-di-GMP production which in turn stabilizes PgaD and activates PGA production (Steiner *et al.*, 2013).

In addition, the zinc-binding disruption caused aggregation of bacteria independently of

---

[2] Taylor and Zhulin, 1999.
[3] Shu *et al.*, 2003.
[4] Galperin *et al.,* 2001
[5] Mougel and Zhulin, 2001; Anantharaman and Aravind, 2001

PGA. Since the *E. coli* strain MG1655 does not produce cellulose (Serra *et al.*, 2013b), this aggregation could be attributed to curli fimbriae, whose production is stimulated by c-di-GMP (Pesavento *et al.*, 2008). The involvement of curli fimbriae in this process, however, lacks supporting evidence.

The effect of zinc on DgcZ activity was tested directly by adding $ZnSO_4$ to the growth media and measuring biofilm formation, which correlates positively with DgcZ activity in the *csrA::Tn5* strain (Boehm *et al.*, 2009). After $ZnSO_4$ addition, a strain with the wild-type DgcZ formed less biofilm, whereas a strain carrying the DgcZ(H79L,H83L) variant displayed constitutively high biofilm production. The effects of zinc on biofilm formation were evidenced further in strains unable to produce ppGpp. The effects of zinc were specific to DgcZ. In fact, in a strain ectopically overexpressing *dgcA*, a diguanylate cyclase from *Caulobacter crescentus,* zinc did not influence biofilm production.

In summary, the results obtained through these *in vivo* experiments confirm the *in vitro* findings and demonstrate that zinc inhibits DgcZ activity.

4.1.1 Functional implications of Zn^{2+} regulation

The observation that Zn^{2+} binding to DgcZ inactivated the protein raises questions about the physiological functions of this regulation.

Zinc is essential for all living organism, but in excess, it is toxic for cells (Yamamoto and Ishihama, 2005b). Zinc homeostasis is a tightly controlled process in the bacterial cell, wherein high affinity, zinc-binding proteins govern the import and export of the nutrient (Outten and O´Halloran, 2001). For this reason, Outten and O´Halloran (2001) calculated that under normal growth conditions there is no consistent pool of Zn^{2+} in the cytoplasm. Sudden changes in Zn^{2+} concentrations, therefore, could be detected by DgcZ and used to discriminate between niches (extracellular Zn^{2+} changes), or physiological conditions (intracellular Zn^{2+} changes). In human hosts, the magnitude of zinc concentrations varies widely. In urine or plasma, for instance, zinc concentrations are high (>15 μM), but in the intestines or within host cells the availability of these ions is low (Vallee and Falchuk, 1993).

The *dgcZ* gene is highly conserved across *E. coli* genomes. As documented by Povolotsky and Hengge (2016), *dgcZ* is conserved in 56 of 61 commensal and pathogenic *E. coli* strains.

Pathogenic *E. coli* strains form biofilms in several compartments of the human body

(Kaper *et al.*, 2004). Uropathogenic *E. coli*, for example, form intracellular biofilms in bladder epithelial cells (Anderson *et al.*, 2010), where Zn^{2+} concentrations are low. This leads to speculation that *E. coli* uses zinc levels to gauge its position in the host. This would allow bacteria to form DgcZ-mediated biofilms only in appropriate niches.

Alternatively, other bacterial zinc-binding proteins may release Zn^{2+}, influencing DgcZ activity. Considering the absence of free Zn^{2+} in the cytoplasm (Outten and O´Halloran, 2001), it is conceivable that upon DgcZ production, the protein is in a zinc-depleted state and therefore active. Upon degradation of other zinc-binding proteins, DgcZ may perhaps bind the Zn^{2+} released and become inactive. And thus, Zn^{2+} may help "inform" DgcZ about the physiological state of the bacterium.

Ribosomes are a major intracellular Zn^{2+} reservoir. In *E. coli*, each ribosome can bind between 5 and 11 Zn^{2+} molecules, depending on the availability of these ions (Hensley *et al.*, 2011). L31 is one of the many ribosomal proteins capable of binding Zn^{2+} (Hensley *et al.*, 2012). By replacing L31 with the Zn^{2+}-independent paralog, YkgM, Zn^{2+} is liberated to facilitate essential cellular processes under Zn^{2+}-starvation conditions (Hensley *et al.*, 2012). Boehm *et al.* (2009) found that the addition of translation inhibitors to bacterial cells caused ribosomal stress which led to DgcZ activation; however, it was not clear how the protein sensed this ribosomal malfunction.

The discovery of Zn^{2+} as an input signal for DgcZ raises the question whether translational stress creates perturbations in Zn^{2+}-homeostasis. One hypothesis addresses this question by suggesting that antibiotic-mediated, ribosomal stress leads to the accumulation of Zn^{2+}-loaded ribosomes, by increasing the number of ribosomes or increasing the amount of Zn^{2+} molecules bound to each ribosome. In response to the shortage of cellular Zn^{2+}, DgcZ becomes activated and strongly induces PGA production via c-di-GMP. Though persuasive, these two hypotheses have not been tested, and the physiological conditions which promote Zn^{2+} regulation of DgcZ activity remain unclear.

4.2 DgcZ and PgaD localization are not responsible for polar PGA production

Production of the exopolysaccharide PGA occurs in response to high c-di-GMP levels and plays a critical role in the initial adhesion of *Escherichia coli*, *Pseudomonas aeruginosa* and *Pseudomonas fluorescens* on abiotic surfaces (Steiner *et al.*, 2013; Agladze *et al.*, 2005; Wang *et al.*, 2005). In *E. coli,* PGA is produced ubiquitously at the cell surface during static

growth conditions and at the bacterial cell poles under shaking conditions (Itoh *et al.*, 2008). While studying the initial adhesion of *E. coli*, Agladze *et al.* (2005) showed the importance of the bacterial cell pole for the process. This, together with the observation that the *csrA::Tn5* strain presents a distinct PGA-dependent permanent polar attachment, indicates the importance of polar PGA production in surface adhesion (Agladze *et al.*, 2005). Another report, states that cellulose production also occurs at the bacterial cell poles in *E. coli* (Le Quéré and Ghigo, 2009). Polysaccharides involved in bacterial adhesion are also produced at the cell poles in other bacterial species, including *Agrobacterium tumefaciens* (Xu *et al.*, 2013) and *Rhizobium leguminosarum* (Laus *et al.*, 2006).

Currently, the regulation of polar production of PGA is unknown. To understand this process and test if spatial confinement of the PgaABCD machinery generated this phenotype, I conducted an analysis of PgaD-gfp localization. The PgaD-gfp protein was delocalized in bacteria grown in permissive conditions for PGA polar production, which suggests that localization of the protein does not determine whether PGA will be produced at the poles or throughout the bacterium.

An alternative hypothesis proposes that the polarly localized DgcZ, the primary DGC in PGA regulation, determines the polar production of PGA. This study shows that although DgcZ-mVENUS localized at one bacterial cell pole in bacteria suspended in an alkaline (8.7) medium without carbon sources, under conditions similar to those employed by Itoh *et al.* (2008) the protein was evenly distributed in the cytoplasm. This observation suggests the confinement of PGA production at the bacterial cell pole is not determined by DgcZ-derived polar c-di-GMP. Additionally, under conditions where DgcZ was localized at the bacterial cell pole, c-di-GMP levels in the cell were under the detection limit of 22 nM.

The data collected and presented in this work demonstrates that PgaD and DgcZ localization is not responsible for the polar production of PGA. An analysis of the extant literature does not provide any explanations to identify how this phenomenon is regulated.

4.3 Hypotheses for DgcZ polar localization in response to external alkaline pH and carbon deprivation

4.3.1 What promotes DgcZ polar localization?

Localization analysis of the diguanylate cyclase DgcZ was conducted during growth in LB medium. A change in location, from cytoplasmic to unipolar, was observed in late stationary phase. A thorough analysis revealed DgcZ polar localization occurred in response to a combination of carbon starvation and exposure to an alkaline pH, which are characteristic of spent LB media (Sezonov *et al.*, 2007). While DgcZ localized evenly in the cytoplasm at a lower pH (6.7) and during exponential growth, the protein moved to the bacterial cell poles in an alkaline medium (pH 8.7) depleted of carbon sources, similar to conditions fostered in LB spent media, or MMA 1X without carbon sources. No DgcZ polar localization was observed in bacteria deprived of carbon in a medium at pH 6.7, or in bacteria grown in an alkaline medium (pH 8.7). This observation indicates that both conditions are required to generate this phenotype.

The polar localization of DgcZ was not influenced by protein concentration or activity. This observation is confirmed by the fact that the inactive DgcZ(H79L,H83L,E208Q)-mVENUS protein, which cannot produce c-di-GMP, and the hyperactive DgcZ(H79L,H83L)-mVENUS, both localized at the bacterial cell pole under permissive conditions.

Microfluidic experiments demonstrated DgcZ polar localization occurred in LB spent medium, depleted of carbon sources, in growth-arrested cells. Most cells underwent unipolar DgcZ localization, and infrequently, some cells displayed bipolar localization.

Because polar localization occurred in growth-arrested cells, and the images obtained using microfluidics chamber microscopy had a sub-optimal resolution, it was not possible to discriminate whether DgcZ localized at the old, or new bacterial cell pole.

E. coli grown on LB medium formed aggregates containing different proteins in stationary phase (Kwiatkowska *et al.*, 2008). In these multicomponent aggregates, 18 distinct proteins involved in separate cellular processes including translation, metabolism, cell architecture and stress responses were identified (Kwiatkowska *et al.*, 2008). As reported by Leszczynska *et al.* (2013), the aggregation of endogenous proteins in stationary phase is associated with the formation of "persister" cells. DgcZ was not identified among the proteins in these aggregates.

Localization at one or two cell poles has been shown for the *H. pylori* protein TlpD, containing a CZB domain homologous to that of DgcZ (Behrens *et al.*, 2016; Collins *et al.*, 2016). TlpD is functional at the cell poles, where it recruits chemotaxis proteins (Collins *et al.*, 2016). TlpD itself is recruited at the poles by the chemotaxis protein CheAY2, as shown by localization experiments in a strain carrying a deletion of the *cheAY2* gene (Behrens *et al.*, 2016). Unlike the case of TlpD, at present, proteins regulating DgcZ localization have not been identified.

4.3.2 Implications of DgcZ degradation upon the resumption of growth

DgcZ polar foci, present in stationary phase bacteria, disappeared after transferring the bacteria into nutrient rich media and the resumption of cell growth. A concomitant analysis of protein concentrations and DgcZ localization revealed that once transferred into nutrient rich medium (LB), the protein was degraded regardless of its localization at the cell pole (pH 8.7) or the cytoplasm (pH 6.7). DgcZ localization, therefore, does not play a role in protein degradation.

That DgcZ foci were disassembled upon growth restart may indicate that DgcZ is not needed in this growth phase. This hypothesis is supported by the observation that at the beginning of exponential growth DgcZ levels were low.

Experiments with the Δ9 strain, carrying deletions of nine major PDE-encoding genes, showed detectable PgaD levels in the late stationary phase. This finding does not exclude the possibility that the polarly localized DgcZ could still be active and stimulate PGA production. Taking all evidence into account, it is tempting to theorize that DgcZ degradation during the bacterial regrowth may serve to "remove" the protein from the growth phase where it is not required.

4.3.3 Role of polarly localized DgcZ

The cell poles of rod-shaped bacteria are the sites where important processes including cell cycle progression, cellular differentiation, and virulence are regulated (Laloux and Jacobs-Wagner, 2014). Some proteins exhibit constant polar localization while others change their localization due to variations in physiological or environmental conditions. The IcsA

protein of the *Shigella flexneri* species, which is involved in bacterial movement, shows constitutive unipolar localization (Goldberg *et al.*, 1993). Conversely, the cell cycle master regulator CtrA in *Caulobacter crescentus* oscillates between the cytoplasm and the cell pole during the cell cycle (McGrath *et al.*, 2006).

Like CtrA, many other proteins including DgcZ change their localizations in response to cell cycle stages, growth phases, or variation in environmental conditions.

Although some factors triggering DgcZ polar localization are identified and characterized, clear evidence of the physiological relevance of this localization pattern is scarce. The fact that DgcZ foci do not disassemble until growth resumed may suggest that the polar-localized protein is "stored" so long as the environmental conditions are constant. This would allow bacteria to rapidly react to new conditions where the presence of DgcZ becomes necessary or beneficial.

The polarly localized DgcZ may also have an "active" function, and might not be simply "stored" in response to stable environmental conditions. In stationary phase, *Escherichia coli* continues to produce proteins at a constant rate over several days (Gefen *et al.*, 2014) and the Clp proteases (ClpXP and ClpAP) remain active (Weichart *et al.*, 2003). In *E. coli* K-12 cells subjected to carbon, nitrogen, or inorganic nutrients starvation, protein degradation rates doubled compared to the values measured in non-starving bacteria (Reeve *et al.*, 1984). Moreover, Reeve *et al.* (1984) found that protein degradation is important for the survival of carbon-starved *E. coli* cells. The increased turnover of proteins during carbon deprivation facilitates the *de novo* synthesis of proteins in the absence of exogenous carbon (Shaikh *et al.*, 2010).

Considering the well-documented role of proteases in carbon starved stationary phase bacteria, one would expect a disadvantageous, or unnecessary protein to be degraded during this growth phase. Since the protease (or proteases) responsible for DgcZ degradation is not known, it is not currently possible to ascertain whether it is active during stationary phase, as has been shown for the Clp proteases (Weichart *et al.*, 2003). The fact that DgcZ is not degraded during stationary phase, despite being in the presence of active proteases, may suggest a role for the DgcZ localization pattern.

Supporting an "active" role of the polarly localized protein is the observation that polar localization occurred in an alkaline pH, a condition which promotes increased *dgcZ* expression (Maurer *et al.*, 2005). In accordance with this previous observation, increased DgcZ-mVENUS was detected in bacteria grown at an alkaline pH (8.7). Alkaline pH has also been shown to activate the Cpx two component system (Maurer *et al.*, 2005), which

stimulates *dgcZ* transcription (Yamamoto and Ishihama, 2006; Price and Raivio, 2009; Raivio *et al.*, 2013). The presence of protein polar localization in the same conditions where expression of *dgcZ* is increased may hint to a physiological relevance of this phenomenon, but may also represent just a casual correlation.

At present, it is not possible to determine whether these hypotheses are correct and whether the polarly localized DgcZ has a functional role or is simply stored there.

4.4 Control of c-di-GMP levels in the *csrA::Tn5* background

In the *crsA::Tn5* strain background c-di-GMP concentrations correlate with PgaD protein levels (Boehm *et al.*, 2009; Steiner *et al.*, 2013). Analysis of the PgaD protein levels presented the opportunity to examine how c-di-GMP concentrations fluctuate during the growth of *crsA::Tn5* strains.

After an initial increase during early exponential phase, PgaD concentrations (and c-di-GMP) decreased and were not detectable in stationary phase. The decrease in the c-di-GMP concentrations recorded in the pre-stationary phase was primarily caused by PDEs. The deletion of the PDE-encoding gene *pdeI* and/or *pdeB* had an effect on PgaD concentrations only when other PDEs were not present. This suggests a cumulative effect of multiple PDEs on the c-di-GMP cellular levels.

A similar decrease in c-di-GMP levels was also observed in the *E. coli* K-12 MG1655 strain, where after reaching a maximum concentration at an OD_{600} of 1.34 in TB medium (corresponding to post-exponential phase), the second messenger levels decreased by ≈50% over the following 3 hours (Spangler *et al.*, 2010). In the MG1655 strain, the c-di-GMP levels influencing cell motility are regulated by the PDE PdeH, though a minor role for PdeI has been shown (Boehm *et al.*, 2010).

Based on the data obtained from the *csrA::Tn5* strain, it is tempting to conjecture that under conditions where CsrA activity is inhibited, at the beginning of stationary phase for instance (Jonas and Melefors, 2009; Liu *et al.*, 1997; Thomason *et al.*, 2012; Jørgensen *et al.*, 2013), the DGC DgcZ and multiple PDEs including PdeI may have a role in the regulation of c-di-GMP related mechanisms, such as motility and surface attachment.

4.5 Role of upstream processes controlling DgcZ production and activity during surface attachment

The regulation of *dgcZ* expression is complex and involves the transcriptional factor CpxR (Yamamoto and Ishihama, 2006; Price and Raivio, 2009; Raivio *et al.*, 2013) and the RNA-binding protein CsrA (Jonas *et al.*, 2008). These regulators control transcription and translation of various targets and are regulated at many levels themselves. It is therefore difficult to decipher which physiological conditions manifest their influence on DgcZ. Despite these inherent complexities and difficulties, an understanding of the highly coordinated regulation of DgcZ is a prerequisite to fully comprehend the physiological role of this protein.

Together with the control of carbohydrate metabolism (Romeo *et al.*, 1993; Sabnis *et al.*, 1995), CsrA regulates several targets involved in biofilm formation (Jonas *et al.*, 2008; Wang *et al.*, 2005; Pannuri *et al.*, 2012). This protein not only represses *dgcZ* mRNA translation, but also that of the *dgcT* mRNA, encoding another DGC (Jonas *et al.*, 2008), and of the *pgaABCD* mRNA, encoding the machinery involved in PGA biosynthesis (Wang *et al.*, 2005; Itoh *et al.*, 2008).

While the effect of CsrA on *dgcZ* has been studied widely (Jonas *et al.*, 2008; Boehm *et al.*, 2009), the effect of CpxR on *dgcZ* is far less documented. The CpxR-mediated transcriptional activation of *dgcZ* has been documented (Yamamoto and Ishihama, 2006; Price and Raivio, 2009; Raivio *et al.*, 2013), however, the downstream effects of this activation were not studied. This work shows that DgcZ and its regulator CpxR contribute to the surface attachment of the *csrA*(wt) strain MG1655 grown at 30 °C. In the same assay, the adhesion of a Δ*cpxR*/Δ*dgcZ* strain was found to be comparable to the attachment of the *dgcZ* deletion strain. Assuming that DgcZ and CpxR act independently, one might expect the effect of a double mutation in these genes to be additive. Since this is not the case, the results suggest that CpxR and DgcZ act through the same pathway.

Agladze *et al.* (2005) reported that deletion of *cpxR* did not affect surface adhesion at 26 °C. The different temperature used in the experiments described by Aglaze *et al.* (2005) and in the assays performed in this work could be one reason for the observed discrepancy. This dissimilar result might also be due to the use of different 96-well plates, since the manufacturer and other characteristics of the plates used by Agladze *et al.* (2005) were not explicitly stated in the work. The conflicting results described here with those reported by

Agladze *et al.* (2005) may be explained by one or a combination of both factors introduced above.

Another piece of evidence supporting the role of CpxR-mediated transcriptional activation of *dgcZ* in surface adhesion was obtained by overproducing the lipoprotein NlpE, a known activator of the Cpx complex during surface sensing. *NlpE* overexpression increased surface attachment by three fold in a DgcZ-dependent fashion in the *csrA::Tn5* strain background.

Thus, the data presented in this study strongly suggest that the effect provoked by CpxR on bacterial attachment, already described by Otto and Silhavy (2002), is, at least in part, mediated by DgcZ.

4.5.1 Carbon starvation co-regulates both Cpx and Csr systems

The Cpx and Csr systems control the transcription and translation of many genes and mRNA respectively, and both influence the transition from motile to sessile lifestyles (Otto and Silhavy, 2002; Jonas *et al.*, 2008).

One of the signals for this transition is nutrients starvation, which is sensed by both Cpx (De Wulf *et al.*, 1999; Otto and Silhavy, 2002) and Csr systems (Jonas and Melefors, 2009; Liu *et al.*, 1997; Thomason *et al.*, 2012; Jørgensen *et al.*, 2013). CpxR is activated for the most part during the post-exponential phase, when nutrients are less abundant (De Wulf *et al.*, 1999).

Otto and Silhavy (2002) observed a similar effect. These researchers described increased surface adhesion in bacteria growing in LB medium in stationary phase until reaching an OD_{600} of 2.0. Under these growth conditions, an OD_{600} of 2.0 for *E. coli* MG1655 corresponds to the post-exponential phase (Fig. 9). In this phase, growth slows down because of reduced carbon availability (Sezonov *et al.*, 2007).

In the post-exponential / pre-stationary phase the concentration of free cytoplasmic CsrA also decreases, due to its titration-regulation by the McaS and CsrB-C sRNAs (Jonas and Melefors, 2009; Liu *et al.*, 1997; Thomason *et al.*, 2012; Jørgensen *et al.*, 2013).

The bacteria in the post-exponential and pre-stationary phase have also increased activity of CpxR, which is a transcriptional activator of *dgcZ*. So, under these conditions, *dgcZ* transcription and translation occur efficiently.

CpxR and CsrA also regulate cell motility. Once phosphorylated, CpxR inhibits motility by repressing the transcription of the *motAB-cheAW* operon (De Wulf *et al.*, 1999). CsrA, on the other hand, stabilizes the *flhCD* mRNA (Wei *et al.*, 2001), which promotes motility. The antagonistic effect of CpxR and CsrA on DgcZ and motility influences the events occurring during bacterial surface adhesion, when motility is inhibited and DgcZ production is increased.

4.6 Effects of DgcZ on flagella abundance and motility

DgcZ overproduction in the *E. coli* MG1655 strain inhibited motility and reduced the amount of flagella in surface-attached bacteria (Jonas *et al.*, 2008). This effect was specific to DgcZ, since the overproduction of DgcT, another diguanylate cyclase, inhibited motility but did not influence the amount of flagella (Jonas *et al.*, 2008). In this study, *dgcZ* overexpression and its effect on motility were validated, and whether the protein had influence on the amount of flagella in non-attached bacteria was tested.

In contrast to surface-attached bacteria, free-living bacteria did not display reduced quantities of flagella in response to DgcZ overproduction. This difference may indicate that DgcZ overproduction only leads to the reduction of flagella in surface-attached bacteria. Since DgcZ controls PGA-mediated surface adhesion via c-di-GMP (Boehm *et al.*, 2009; Steiner *et al.*, 2013), it is plausible that this effect on flagella may occur during surface attachment or immediately afterward. Whether this reduction of flagella is involved in biofilm formation is not clear, since it was observed upon protein overproduction. Further experiments employing physiological conditions are required to thoroughly test this hypothesis.

4.7 Role of DgcZ in connecting surface sensing and adhesion

Over the last decade, several works have explored PGA-mediated biofilm formation (Agladze *et al.*, 2005; Wang *et al.*, 2005; Itoh *et al.*, 2008) and the role of DgcZ in the regulation of this mechanism in the *csrA::Tn5* strain (Boehm *et al.*, 2009; Steiner *et al.*, 2013).

The results from this study suggest that DgcZ has a physiological role in surface adhesion also in the *csrA*(wt) strain MG1655. Moreover, a linking role of DgcZ between surface sensing and attachment to abiotic surfaces is suggested by the following evidence: i) CpxR transcriptionally activates DgcZ (Yamamoto and Ishihama, 2006; Raivio *et al.*, 2013; Raivio, 2014), (ii) *cpxR* deletion reduces attachment in the *csrA*(wt) strain (Otto and Silhavy 2002; this work), and (iii) attachment of the *csrA*::Tn*5* mutant is upregulated upon NlpE overproduction in a DgcZ-dependent way (this work).

It is tempting to speculate that upon surface contact under permissive conditions, for instance during the pre-stationary phase, DgcZ is produced and interferes with flagellar activity via YcgR in a c-di-GMP dependent fashion. DgcZ interference on flagellar activity may impede the escape of bacteria from the surface and PGA production may then stabilize adhesion. In this model, CpxR and CsrA, through the regulation of DgcZ, motility, and PGA production, play an important role in determining, after initial contact with the surface, if bacteria attach or not.

4.8 Comparison with the surface attachment mechanism in *Pseudomonas aeruginosa*

The regulatory network controlling DgcZ production has two main components: CpxR and CsrA. DgcZ activity is then controlled by Zn^{2+}, though the physiological conditions in which this regulation occurs are unclear. When DgcZ is present and active, c-di-GMP is produced and that, in turn, stimulates PGA synthesis (Boehm *et al.*, 2009), which is vital to the bacterial attachment process (Agladze *et al.*, 2005).

Cyclic di-GMP also has a general role in the transition between motile and sessile lifestyles in *E. coli* and in several other bacterial species (Pesavento *et al.*, 2008; Kim and McCarter, 2007; Jonas *et al.*, 2010; Purcell *et al.*, 2012). Recent works by Moscoso *et al.* (2014), and Luo *et al.* (2015) provided insight into the surface adhesion mechanism of *Pseudomonas aeruginosa.* This system is similar to *E. coli* surface adhesion system in many ways (Fig. 27).

In *Pseudomonas*, a CsrA homologue (RsmA) inhibits translation of *sadC* mRNA, coding for a diguanylate cyclase (Moscoso *et al.*, 2014). Interestingly, SadC, like DgcZ in *E. coli*, is involved in surface attachment and becomes active in response to surface sensing (Luo *et al.*, 2015). Though surface sensing is achieved differently in these two systems, the bacterial response involves a diguanylate cyclase and the Csr / Rsm system in both species

(Fig. 27).

Also in *Salmonella typhimurium* the switch between a motile and sessile lifestyle is regulated by the Csr system, along with the DGC STM1987 and the PDE STM3611 (Jonas *et al.*, 2010).

The results presented by this study and from previous research on *P. aeruginosa* and *S. typhimurium* confirm that c-di-GMP plays a vital role in the transition between motile and sessile lifestyle in response to environmental cues, such as nutrient starvation, sensed by the Csr/ Rsm system.
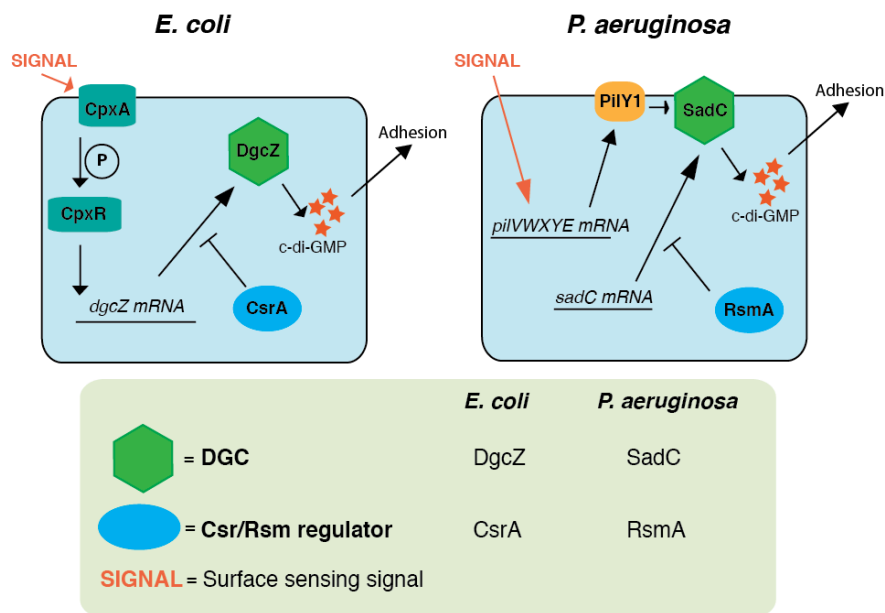

Figure 27. Similarities between adhesion mechanisms in *E. coli* and *P. aeruginosa*. The illustration depicts the adhesion mechanisms in *E. coli* and in *P. aeruginosa*, both sharing the DGC DgcZ or SadC, respectively (Boehm *et al.*, 2009; Luo *et al.*, 2015), and the Csr / Rsm regulator (Wang *et al.*, 2005; Moscoso *et al.*, 2014). Although surface sensing appears to differ between the two species, the second messenger c-di-GMP regulates adhesion in both systems. DGCs are indicated with a green diamond and the CsrA / RsmA regulators are represented with a blue oval.

4.9 Functional implication of DgcZ-FRD interaction

A part of this work describes the interaction of DgcZ with the FrdB subunit of the fumarate reductase complex (FRD), mediated by the CZB domain in DgcZ.

Besides its role in anaerobic respiration, the FRD complex regulates flagellar assembly and activity (Cohen-Ben-Lulu *et al.*, 2008). An *E. coli frd* deletion mutant displays fewer flagella than the wild-type and rarely switches the direction of flagellar rotation (Cohen-Ben-

Lulu *et al.*, 2008). Controlling the direction of flagellar rotation is crucial during surface adhesion, because bacteria with flagellar rotation in a single direction attach to surfaces less efficiently than the wild-type (McClaine and Ford, 2002).

As previously discussed in Section 4.6, DgcZ overproduction resulted in a drastic reduction of flagella in surface-attached bacteria (Jonas *et al.*, 2008), but did not affect the flagella in non-attached bacteria. Since DgcZ and the FRD complex affect the amount and activity of flagella, one might hypothesize that the DgcZ-FrdB interaction may impact flagellar rotation during surface attachment. At present, there is no direct evidence to support such a regulatory link.

The FRD complex associates with FliG (Cohen-Ben-Lulu *et al.*, 2008). Upon surface contact, FRD may sense impediments to flagellar rotation through its interaction with FliG. The FRD complex may alternatively sense surface contact by perceiving changes in bacterial respiration due to this surface contact (Geng *et al.*, 2014). In *E. coli*, in fact, a decrease in respiration was detected by Geng *et al.* (2014) within the first 15 minutes of cell-surface and cell-cell contacts. Since FRD is involved in anaerobic respiration, it may be possible that FRD senses these changes in respiration. Whether the FRD complex is able to "sense" impediments to flagellar rotation or changes in respiration occurring upon surface contact requires additional verification.

4.9.1 Functional implications of superoxide-mediated, increased DgcZ-dependent biofilm formation

Previous research demonstrated that FRD produces superoxide (O_2^-) in *E. coli* (Imlay, 1995). This work showed that upon paraquat-induced superoxide production, DgcZ and the FRD complex are both prerequisites in the observed increase in biofilm.

The role of superoxide and the FRD complex in DgcZ-mediated biofilm formation is not well understood. One hypothesis suggests that under certain conditions which are permissive for PGA production, the FRD complex produces superoxide (Imlay, 1995), which activates DgcZ (Fig. 28). The superoxide may oxidize cysteine 52 in the CZB domain of DgcZ, one of the amino acids involved in zinc coordination (Zähringer *et al.*, 2013). This oxidized cysteine may have a reduced affinity for zinc ions, resulting in DgcZ activation. *In vitro*, the DgcZ(C52A) showed higher activity than the wild-type DgcZ (Zähringer *et al.*, 2013), although no *in vivo* differences were observed.

In this context, the physical interaction between DgcZ and FrdB could limit the diffusion of the highly reactive superoxide and thereby, reduce damage to other macromolecules (Farr *et al.*, 1986). An alternative hypothesis suggest that DgcZ may sense the damage of the iron-sulfur cluster of FrdB induced by superoxide. Reactive oxygen species as superoxide and hydrogen peroxide can in fact damage iron-sulfur clusters (Flint *et al.*, 1993; Djaman *et al.*, 2004).

It is tempting to speculate that during surface sensing, FrdB would interact with DgcZ and increase its enzymatic activity. The c-di-GMP produced by DgcZ would inhibit flagellar rotation via YgcR, impeding the escape of the bacterial cells from the surface. This would increase DgcZ production (via CpxR) and activation (via FRD) resulting in a further increase in c-di-GMP production, leading to PGA-mediated surface adhesion (Fig. 28).

Alternatively, superoxide may affect DgcZ- and FRD-mediated biofilm formation through other unknown mechanisms. Independent evidence for the role of superoxide in biofilms is provided by the increased production of the superoxide dismutase SodC, implicated in the detoxification of superoxide (O_2^-) to O_2 or hydrogen peroxide (H_2O_2), in the biofilms of the *E. coli* O157:H7 strain (Kim *et al.*, 2006). In this strain, the deletion of *sodC* decreased biofilm formation (Kim *et al.*, 2006). These evidences suggest a role for superoxide in this process. Significant changes in the expression of genes encoding proteins that protect against oxidative damage, including the *sodA* gene coding for a superoxide dismutase, were also observed during biofilm development in *Staphylococcus aureus* (Resch *et al.*, 2005).

This work provides evidence for a novel function of superoxide which, together with the FRD complex, increased DgcZ-mediated biofilm formation. Although, the exact mechanism behind this process remains elusive.
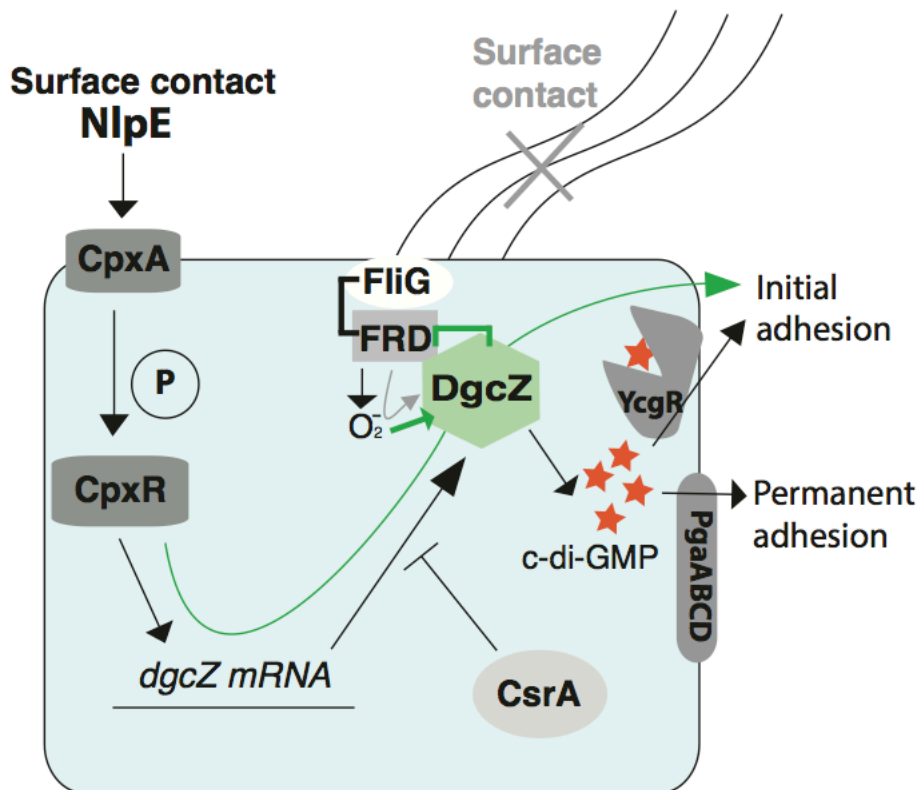
Figure 28. Model of the role of DgcZ in initial and permanent adhesion to abiotic surfaces. Upon surface sensing, NlpE activates the Cpx complex (Snyder *et al.*, 1995; Otto and Silhavy, 2002), resulting in phosphorylation of CpxR (Raivio and Silhavy, 1997) and transcription of the *dgcZ* mRNA (Yamamoto and Ishihama, 2006; Price and Raivio, 2009). Under permissive conditions, e.g. stationary phase, the McaS and CrsB-C mRNA bind CsrA (Jonas and Melefors, 2009; Liu *et al.*, 1997; Thomason *et al.*, 2012; Jørgensen *et al.*, 2013) causing release of the inhibitory effects of CsrA on the *dgcZ* mRNA and allowing translation. The superoxide (O_2^-) produced by the FRD complex (Imlay, 1995) may result in increased production c-di-GMP by DgcZ. This second messenger affects flagellar activity (via YcgR) and PGA production (Boehm *et al.*, 2009), stimulating permanent attachment. Brackets indicate protein interactions. Black indicates events previous known, while green denotes new findings. The grey arrow and the cross indicate hypotheses.

4.10 The CZB domain of TlpD and a hypothetical interaction with FrdB in *Helicobacter pylori*

The interaction shown between the CZB domain of DgcZ and FrdB may also be conserved between diverse bacterial species. Indeed, CZB domain-encoding sequences and *frdB* are present in many bacterial genomes. The CZB domain of the chemosensory protein TlpD from *Helicobacter pylori* was the first of these domains characterized (Draper *et al.*, 2011). This domain is involved in sensing suboptimal energetic conditions and inhibition of the electron transport (Schweinitzer *et al.*, 2008). Considering the role of the FRD complex in respiration

102

and the newly described interaction between a subunit of this complex and the CZB domain of DgcZ in *Escherichia coli*, it is conceivable that a similar interaction occurs in *Helicobacter pylori*. TlpD has been recently shown to interact with the protein AcnB, which, similarly to FrdB, carries an iron-sulfur cluster and is involved in the TCA (tricarboxylic acid cycle) pathway (Behrens *et al.*, 2016). These observations motivated Behrens *et al.* (2016) to hypothesize that the FRD complex may influence the sensory activity of TlpD under oxidative or metabolic stress.

An indirect evidence supporting the interaction of the CZB domain of TlpD with FrdB is a functional overlap between the FRD complex and TlpD (Behrens *et al.*, 2013; Ge *et al.*, 2000). The FRD complex and TlpD are both involved in intestinal colonization in mice and gerbil, respectively (Ge *et al.*, 2000; Behrens *et al.*, 2013).

Although this is an intriguing hypothesis, further research efforts are required to determine whether the CZB-FrdB interaction is conserved in *H. pylori* and other bacteria.

4.11 Analysis of potential DgcZ interaction partners obtained by CoIp

Co-immunoprecipitations were performed to gain insights into the regulation and function of DgcZ polar localization. From exponential and stationary phase, both CoIP attempts identified 11 putative DgcZ interaction partners. These candidates were not present in the negative controls and exhibited a significant score. Among them were FrdA and FrdB, which are discussed above. Another intriguing candidate identified by CoIP was the predicted oxidoreductase YgfK.

Like FrdB, YgfK is an iron-sulfur (Fe-S) protein (Sevcenco *et al.*, 2011). YgfK was identified from exponentially growing bacteria, and this protein had the highest CoIP score. In both exponential and stationary growth phases, DgcZ may interact with the Fe-S protein YgfK and FrdB respectively.

Iron-sulfur proteins are essential in conserved cellular processes, such as respiration, regulation of gene expression, DNA repair, and others (Roche *et al.*, 2013). Iron-sulfur centers are vulnerable to oxidation by superoxide and hydrogen peroxide, which cause the degradation of the clusters (Flint *et al.*, 1993; Djaman *et al.*, 2004). Under anaerobic conditions, the oxidized clusters can be repaired (Djaman *et al.*, 2004).

DgcZ may detect the damage of Fe-S clusters caused by superoxide and respond to it. This hypothesis may explain why DgcZ-dependent biofilm formation was dependent on FRD

after paraquat was added. However, the interactions between DgcZ and these iron-sulfur proteins may have other physiological roles.

Nine other proteins with a significant score were identified but do not show an apparent correlation with DgcZ, or biofilm formation. Notably, CoIP identified three different pyruvate formate lyases (PflB, TdcE and GrcA) in the stationary phase.

Many questions regarding DgcZ, its function and regulation remain unanswered. Characterizing the DgcZ interaction partners represents an approach to answering these questions.

4.12 Conclusion and future perspectives

Surface adhesion is the first step in biofilm formation. This work expands our knowledge of the diguanylate cyclase DgcZ in the attachment of *E. coli* strains to anaerobic surfaces. DgcZ emerges as a major regulator of this process. The protein occupies a central position in the bacterial adhesion network, being regulated by the CpxR and CsrA systems, and controlling PGA production and flagellar activity through c-di-GMP. CpxR and CsrA "inform" the bacterium of environmental conditions by strongly activating DgcZ when nutrients are scarce.

The role of c-di-GMP in signal transduction is well described. DgcZ is an example par excellence, highlighting this signal transduction cascade because it transduces the nutrient starvation signal in bacterial adhesion, via c-di-GMP.

The integral role of DgcZ in surface adhesion poses many intriguing questions. First of these regards the physiological role of zinc in DgcZ regulation. The effect of this ion in the control of the protein activity is clear, however, the internal or external cues that influence zinc availability are unknown.

Another open question concerns the role of superoxide and the FRD complex in DgcZ-mediated biofilm formation. The mechanisms involved in this process and the physiological conditions stimulating superoxide production need to be addressed.

Another challenge and probable "goldmine" is presented by the potential uncharacterized DgcZ interaction partners. Future study of these proteins will foster a greater understanding of DgcZ regulation and the adhesion process.

5. Contributions of Collaborators

Microfluidic experiments were performed by Colette Bigosch, Eawag Dübendorf, Switzerland. I contributed to the design of the experiment.

Mass Spectrometry-based identification of Co-immunoprecipitated preteins was performed by the SYNMIKRO mass spectrometric Core Facility.

Cyclic di-GMP quantification was performed at the Research Core Unit Metabolomics, located at the Institute of Pharmacology in the Hannover Medical School.

6. References

Adler J. 1966. Chemotaxis in bacteria. Science **153:**708-716.

Agladze K, Wang X, Romeo T. 2005. Spatial periodicity of Escherichia coli K-12 biofilm microstructure initiates during a reversible, polar attachment phase of development and requires the polysaccharide adhesin PGA. J Bacteriol **187:**8237-8246.

Amikam D, Galperin MY. 2006. PilZ domain is part of the bacterial c-di-GMP binding protein. Bioinformatics **22:**3-6.

Anantharaman V, Aravind L. 2001. The CHASE domain: a predicted ligand-binding module in plant cytokinin receptors and other eukaryotic and bacterial receptors. Trends Biochem Sci **26:**579-582.

Anderson GG, Goller CC, Justice S, Hultgren SJ, Seed PC. 2010. Polysaccharide capsule and sialic acid-mediated regulation promote biofilm-like intracellular bacterial communities during cystitis. Infect Immun **78:**963-975.

Andersson EK, Bengtsson C, Evans ML, Chorell E, Sellstedt M, Lindgren AE, Hufnagel DA, Bhattacharya M, Tessier PM, Wittung-Stafshede P, Almqvist F, Chapman MR. 2013. Modulation of curli assembly and pellicle biofilm formation by chemical and protein chaperones. Chem Biol **20:**1245-1254.

Arnoldini M, Vizcarra IA, Peña-Miller R, Stocker N, Diard M, Vogel V, Beardmore RE, Hardt WD, Ackermann M. 2014. Bistable expression of virulence genes in salmonella leads to the formation of an antibiotic-tolerant subpopulation. PLoS Biol **12:**e1001928.

Baba T, Ara T, Hasegawa M, Takai Y, Okumura Y, Baba M, Datsenko KA, Tomita M, Wanner BL, Mori H. 2006. Construction of Escherichia coli K-12 in-frame, single-gene knockout mutants: the Keio collection. Mol Syst Biol **2:**2006.0008.

Battesti A, Bouveret E. 2012. The bacterial two-hybrid system based on adenylate cyclase reconstitution in Escherichia coli. Methods **58:**325-334.

Behrens W, Schweinitzer T, Bal J, Dorsch M, Bleich A, Kops F, Brenneke B, Didelot X, Suerbaum S, Josenhans C. 2013. Role of energy sensor TlpD of Helicobacter pylori in gerbil colonization and genome analyses after adaptation in the gerbil. Infect Immun **81:**3534-3551.

Behrens W, Schweinitzer T, McMurry JL, Loewen PC, Buettner FF, Menz S, Josenhans C. 2016. Localisation and protein-protein interactions of the Helicobacter pylori taxis sensor TlpD and their connection to metabolic functions. Sci Rep **6:**23582.

Belas R. 2014. Biofilms, flagella, and mechanosensing of surfaces by bacteria. Trends Microbiol **22:**517-527.

Bellini D, Caly DL, McCarthy Y, Bumann M, An SQ, Dow JM, Ryan RP, Walsh MA. 2014. Crystal structure of an HD-GYP domain cyclic-di-GMP phosphodiesterase reveals an enzyme with a novel trinuclear catalytic iron centre. Mol Microbiol **91:**26-38.

Beloin C, Roux A, Ghigo JM. 2008. Escherichia coli biofilms. Curr Top Microbiol Immunol **322:**249-289.

Bibikov SI, Biran R, Rudd KE, Parkinson JS. 1997. A signal transducer for aerotaxis in Escherichia coli. J Bacteriol **179:**4075-4079.

Bjarnsholt T. 2013. The role of bacterial biofilms in chronic infections. APMIS Suppl**:**1-51.

Blattner FR, Plunkett G, Bloch CA, Perna NT, Burland V, Riley M, Collado-Vides J, Glasner JD, Rode CK, Mayhew GF, Gregor J, Davis NW, Kirkpatrick HA, Goeden MA, Rose DJ, Mau B, Shao Y. 1997. The complete genome sequence of Escherichia coli K-12. Science **277:**1453-1462.

Blount ZD. 2015. The unexhausted potential of E. coli. Elife **4**.

Boehm A, Kaiser M, Li H, Spangler C, Kasper CA, Ackermann M, Kaever V, Sourjik V, Roth V, Jenal U. 2010. Second messenger-mediated adjustment of bacterial swimming velocity. Cell **141:**107-116.

Boehm A, Steiner S, Zaehringer F, Casanova A, Hamburger F, Ritz D, Keck W, Ackermann M, Schirmer T, Jenal U. 2009. Second messenger signalling governs Escherichia coli biofilm induction upon ribosomal stress. Mol Microbiol **72:**1500-1516.

Boyd CD, O'Toole GA. 2012. Second messenger regulation of biofilm formation: breakthroughs in understanding c-di-GMP effector systems. Annu Rev Cell Dev Biol **28:**439-462.

Burhenne H, Kaever V. 2013. Quantification of cyclic dinucleotides by reversed-phase LC-MS/MS. Methods Mol Biol **1016:**27-37.

Cerca N, Jefferson KK. 2008. Effect of growth conditions on poly-N-acetylglucosamine expression and biofilm formation in Escherichia coli. FEMS Microbiol Lett **283:**36-41.

Charoenpanich P, Soto MJ, Becker A, McIntosh M. 2015. Quorum sensing restrains growth and is rapidly inactivated during domestication of Sinorhizobium meliloti. Environ Microbiol Rep **7:**373-382.

Cherepanov PP, Wackernagel W. 1995. Gene disruption in Escherichia coli: TcR and KmR cassettes with the option of Flp-catalyzed excision of the antibiotic-resistance

determinant. Gene **158:**9-14.

Christen B, Christen M, Paul R, Schmid F, Folcher M, Jenoe P, Meuwly M, Jenal U. 2006. Allosteric control of cyclic di-GMP signaling. J Biol Chem **281:**32015-32024.

Chung CT, Niemela SL, Miller RH. 1989. One-step preparation of competent Escherichia coli: transformation and storage of bacterial cells in the same solution. Proc Natl Acad Sci U S A **86:**2172-2175.

Ciofu O, Tolker-Nielsen T, Jensen P, Wang H, Høiby N. 2015. Antimicrobial resistance, respiratory tract infections and role of biofilms in lung infections in cystic fibrosis patients. Adv Drug Deliv Rev **85:**7-23.

Clark WA. 1976. A simplified Leifson flagella stain. J Clin Microbiol **3:**632-634.

Cohen-Ben-Lulu GN, Francis NR, Shimoni E, Noy D, Davidov Y, Prasad K, Sagi Y, Cecchini G, Johnstone RM, Eisenbach M. 2008. The bacterial flagellar switch complex is getting more complex. EMBO J **27:**1134-1144.

Collins KD, Andermann TM, Draper J, Sanders L, Williams SM, Araghi C, Ottemann KM. 2016. The Helicobacter pylori CZB cytoplasmic chemoreceptor TlpD forms an autonomous polar chemotaxis signaling complex that mediates a tactic response to oxidative stress. J Bacteriol.

Danese PN, Pratt LA, Kolter R. 2000. Exopolysaccharide production is required for development of Escherichia coli K-12 biofilm architecture. J Bacteriol **182:**3593-3596.

Danese PN, Silhavy TJ. 1998. CpxP, a stress-combative member of the Cpx regulon. J Bacteriol **180:**831-839.

Datsenko KA, Wanner BL. 2000. One-step inactivation of chromosomal genes in Escherichia coli K-12 using PCR products. Proc Natl Acad Sci U S A **97:**6640-6645.

De Wulf P, Kwon O, Lin EC. 1999. The CpxRA signal transduction system of Escherichia coli: growth-related autoactivation and control of unanticipated target operons. J Bacteriol **181:**6772-6778.

DePas WH, Syed AK, Sifuentes M, Lee JS, Warshaw D, Saggar V, Csankovszki G, Boles BR, Chapman MR. 2014. Biofilm formation protects Escherichia coli against killing by Caenorhabditis elegans and Myxococcus xanthus. Appl Environ Microbiol **80:**7079-7087.

Djaman O, Outten FW, Imlay JA. 2004. Repair of oxidized iron-sulfur clusters in Escherichia coli. J Biol Chem **279:**44590-44599.

Domka J, Lee J, Bansal T, Wood TK. 2007. Temporal gene-expression in Escherichia coli K-12 biofilms. Environ Microbiol **9:**332-346.

Dorel C, Lejeune P, Rodrigue A. 2006. The Cpx system of Escherichia coli, a strategic signaling pathway for confronting adverse conditions and for settling biofilm communities? Res Microbiol **157:**306-314.

Dower WJ, Miller JF, Ragsdale CW. 1988. High efficiency transformation of E. coli by high voltage electroporation. Nucleic Acids Res **16:**6127-6145.

Draper J, Karplus K, Ottemann KM. 2011. Identification of a chemoreceptor zinc-binding domain common to cytoplasmic bacterial chemoreceptors. J Bacteriol **193:**4338-4345.

Duerig A, Abel S, Folcher M, Nicollier M, Schwede T, Amiot N, Giese B, Jenal U. 2009. Second messenger-mediated spatiotemporal control of protein degradation regulates bacterial cell cycle progression. Genes Dev **23:**93-104.

El Andari J, Altegoer F, Bange G, Graumann PL. 2015. Bacillus subtilis Bactofilins Are Essential for Flagellar Hook- and Filament Assembly and Dynamically Localize into Structures of Less than 100 nm Diameter underneath the Cell Membrane. PLoS One **10:**e0141546.

Fang X, Ahmad I, Blanka A, Schottkowski M, Cimdins A, Galperin MY, Römling U, Gomelsky M. 2014. GIL, a new c-di-GMP-binding protein domain involved in regulation of cellulose synthesis in enterobacteria. Mol Microbiol **93:**439-452.

Farr SB, D'Ari R, Touati D. 1986. Oxygen-dependent mutagenesis in Escherichia coli lacking superoxide dismutase. Proc Natl Acad Sci U S A **83:**8268-8272.

Figueroa-Bossi N, Schwartz A, Guillemardet B, D'Heygère F, Bossi L, Boudvillain M. 2014. RNA remodeling by bacterial global regulator CsrA promotes Rho-dependent transcription termination. Genes Dev **28:**1239-1251.

Finney LA, O'Halloran TV. 2003. Transition metal speciation in the cell: insights from the chemistry of metal ion receptors. Science **300:**931-936.

Flint DH, Tuminello JF, Emptage MH. 1993. The inactivation of Fe-S cluster containing hydro-lyases by superoxide. J Biol Chem **268:**22369-22376.

Friedlander RS, Vlamakis H, Kim P, Khan M, Kolter R, Aizenberg J. 2013. Bacterial flagella explore microscale hummocks and hollows to increase adhesion. Proc Natl Acad Sci U S A **110:**5624-5629.

Friedlander RS, Vogel N, Aizenberg J. 2015. Role of Flagella in Adhesion of Escherichia coli to Abiotic Surfaces. Langmuir **31:**6137-6144.

Fux CA, Costerton JW, Stewart PS, Stoodley P. 2005. Survival strategies of infectious biofilms. Trends Microbiol **13:**34-40.

Galperin MY. 2005. A census of membrane-bound and intracellular signal transduction

proteins in bacteria: bacterial IQ, extroverts and introverts. BMC Microbiol **5:**35.

Galperin MY. 2006. Structural classification of bacterial response regulators: diversity of output domains and domain combinations. J Bacteriol **188:**4169-4182.

Galperin MY, Nikolskaya AN, Koonin EV. 2001. Novel domains of the prokaryotic two-component signal transduction systems. FEMS Microbiol Lett **203:**11-21.

Ge Z, Feng Y, Dangler CA, Xu S, Taylor NS, Fox JG. 2000. Fumarate reductase is essential for Helicobacter pylori colonization of the mouse stomach. Microb Pathog **29:**279-287.

Gefen O, Fridman O, Ronin I, Balaban NQ. 2014. Direct observation of single stationary-phase bacteria reveals a surprisingly long period of constant protein production activity. Proc Natl Acad Sci U S A **111:**556-561.

Geng J, Beloin C, Ghigo JM, Henry N. 2014. Bacteria hold their breath upon surface contact as shown in a strain of Escherichia coli, using dispersed surfaces and flow cytometry analysis. PLoS One **9:**e102049.

Goldberg MB, Bârzu O, Parsot C, Sansonetti PJ. 1993. Unipolar localization and ATPase activity of IcsA, a Shigella flexneri protein involved in intracellular movement. J Bacteriol **175:**2189-2196.

Guzman LM, Belin D, Carson MJ, Beckwith J. 1995. Tight regulation, modulation, and high-level expression by vectors containing the arabinose PBAD promoter. J Bacteriol **177:**4121-4130.

Hantke K. 2005. Bacterial zinc uptake and regulators. Curr Opin Microbiol **8:**196-202.

Hassan HM, Fridovich I. 1978. Superoxide radical and the oxygen enhancement of the toxicity of paraquat in Escherichia coli. J Biol Chem **253:**8143-8148.

Hengge R. 2009. Principles of c-di-GMP signalling in bacteria. Nat Rev Microbiol **7:**263-273.

Hengge R, Galperin MY, Ghigo JM, Gomelsky M, Green J, Hughes KT, Jenal U, Landini P. 2016. Systematic Nomenclature for GGDEF and EAL Domain-Containing Cyclic Di-GMP Turnover Proteins of Escherichia coli. J Bacteriol **198:**7-11.

Hensley MP, Gunasekera TS, Easton JA, Sigdel TK, Sugarbaker SA, Klingbeil L, Breece RM, Tierney DL, Crowder MW. 2012. Characterization of Zn(II)-responsive ribosomal proteins YkgM and L31 in E. coli. J Inorg Biochem **111:**164-172.

Hensley MP, Tierney DL, Crowder MW. 2011. Zn(II) binding to Escherichia coli 70S ribosomes. Biochemistry **50:**9937-9939.

Hirano Y, Hossain MM, Takeda K, Tokuda H, Miki K. 2007. Structural studies of the Cpx

pathway activator NlpE on the outer membrane of Escherichia coli. Structure **15:**963-976.

Hobley L, Harkins C, MacPhee CE, Stanley-Wall NR. 2015. Giving structure to the biofilm matrix: an overview of individual strategies and emerging common themes. FEMS Microbiol Rev **39:**649-669.

Imlay JA. 1995. A metabolic enzyme that rapidly produces superoxide, fumarate reductase of Escherichia coli. J Biol Chem **270:**19767-19777.

Itoh Y, Rice JD, Goller C, Pannuri A, Taylor J, Meisner J, Beveridge TJ, Preston JF, Romeo T. 2008. Roles of pgaABCD genes in synthesis, modification, and export of the Escherichia coli biofilm adhesin poly-beta-1,6-N-acetyl-D-glucosamine. J Bacteriol **190:**3670-3680.

Iverson TM, Luna-Chavez C, Cecchini G, Rees DC. 1999. Structure of the Escherichia coli fumarate reductase respiratory complex. Science **284:**1961-1966.

Janjaroen D, Ling FQ, Ling F, Monroy G, Derlon N, Morgenroth E, Mogenroth E, Boppart SA, Liu WT, Nguyen TH. 2013. Roles of ionic strength and biofilm roughness on adhesion kinetics of Escherichia coli onto groundwater biofilm grown on PVC surfaces. Water Res **47:**2531-2542.

Jonas K, Edwards AN, Ahmad I, Romeo T, Römling U, Melefors O. 2010. Complex regulatory network encompassing the Csr, c-di-GMP and motility systems of Salmonella Typhimurium. Environ Microbiol **12:**524-540.

Jonas K, Edwards AN, Simm R, Romeo T, Römling U, Melefors O. 2008. The RNA binding protein CsrA controls cyclic di-GMP metabolism by directly regulating the expression of GGDEF proteins. Mol Microbiol **70:**236-257.

Jonas K, Melefors O. 2009. The Escherichia coli CsrB and CsrC small RNAs are strongly induced during growth in nutrient-poor medium. FEMS Microbiol Lett **297:**80-86.

Jørgensen MG, Thomason MK, Havelund J, Valentin-Hansen P, Storz G. 2013. Dual function of the McaS small RNA in controlling biofilm formation. Genes Dev **27:**1132-1145.

Kaper JB, Nataro JP, Mobley HL. 2004. Pathogenic Escherichia coli. Nat Rev Microbiol **2:**123-140.

Kaplan JB. 2010. Biofilm dispersal: mechanisms, clinical implications, and potential therapeutic uses. J Dent Res **89:**205-218.

Khan S, Spudich JL, McCray JA, Trentham DR. 1995. Chemotactic signal integration in bacteria. Proc Natl Acad Sci U S A **92:**9757-9761.

Kim YH, Lee Y, Kim S, Yeom J, Yeom S, Seok Kim B, Oh S, Park S, Jeon CO, Park W. 2006. The role of periplasmic antioxidant enzymes (superoxide dismutase and thiol peroxidase) of the Shiga toxin-producing Escherichia coli O157:H7 in the formation of biofilms. Proteomics **6:**6181-6193.

Kim YK, McCarter LL. 2007. ScrG, a GGDEF-EAL protein, participates in regulating swarming and sticking in Vibrio parahaemolyticus. J Bacteriol **189:**4094-4107.

Kjaergaard K, Schembri MA, Hasman H, Klemm P. 2000. Antigen 43 from Escherichia coli induces inter- and intraspecies cell aggregation and changes in colony morphology of Pseudomonas fluorescens. J Bacteriol **182:**4789-4796.

Kwiatkowska J, Matuszewska E, Kuczyńska-Wiśnik D, Laskowska E. 2008. Aggregation of Escherichia coli proteins during stationary phase depends on glucose and oxygen availability. Res Microbiol **159:**651-657.

Lacanna E, Bigosch C, Kaever V, Boehm A, Becker A. Evidence for *Escherichia coli* diguanylate cyclase DgcZ interlinking surface sensing and adhesion via multiple regulatory routes. J Bacteriol (resubmitted in April 2016).

Laloux G, Jacobs-Wagner C. 2014. How do bacteria localize proteins to the cell pole? J Cell Sci **127:**11-19.

Laus MC, Logman TJ, Lamers GE, Van Brussel AA, Carlson RW, Kijne JW. 2006. A novel polar surface polysaccharide from Rhizobium leguminosarum binds host plant lectin. Mol Microbiol **59:**1704-1713.

Le Quéré B, Ghigo JM. 2009. BcsQ is an essential component of the Escherichia coli cellulose biosynthesis apparatus that localizes at the bacterial cell pole. Mol Microbiol **72:**724-740.

Leszczynska D, Matuszewska E, Kuczynska-Wisnik D, Furmanek-Blaszk B, Laskowska E. 2013. The formation of persister cells in stationary-phase cultures of Escherichia coli is associated with the aggregation of endogenous proteins. PLoS One **8:**e54737.

Li G, Brown PJ, Tang JX, Xu J, Quardokus EM, Fuqua C, Brun YV. 2012. Surface contact stimulates the just-in-time deployment of bacterial adhesins. Mol Microbiol **83:**41-51.

Li G, Young KD. 2012. Isolation and identification of new inner membrane-associated proteins that localize to cell poles in Escherichia coli. Mol Microbiol **84:**276-295.

Lindenberg S, Klauck G, Pesavento C, Klauck E, Hengge R. 2013. The EAL domain protein YciR acts as a trigger enzyme in a c-di-GMP signalling cascade in E. coli biofilm control. EMBO J **32:**2001-2014.

Liu MY, Gui G, Wei B, Preston JF, Oakford L, Yüksel U, Giedroc DP, Romeo T. 1997. The RNA molecule CsrB binds to the global regulatory protein CsrA and antagonizes its activity in Escherichia coli. J Biol Chem **272:**17502-17510.

Lori C, Ozaki S, Steiner S, Böhm R, Abel S, Dubey BN, Schirmer T, Hiller S, Jenal U. 2015. Cyclic di-GMP acts as a cell cycle oscillator to drive chromosome replication. Nature **523:**236-239.

Lovering AL, Capeness MJ, Lambert C, Hobley L, Sockett RE. 2011. The structure of an unconventional HD-GYP protein from Bdellovibrio reveals the roles of conserved residues in this class of cyclic-di-GMP phosphodiesterases. MBio **2**.

Luo Y, Zhao K, Baker AE, Kuchma SL, Coggan KA, Wolfgang MC, Wong GC, O'Toole GA. 2015. A hierarchical cascade of second messengers regulates Pseudomonas aeruginosa surface behaviors. MBio **6**.

Maurer LM, Yohannes E, Bondurant SS, Radmacher M, Slonczewski JL. 2005. pH regulates genes for flagellar motility, catabolism, and oxidative stress in Escherichia coli K-12. J Bacteriol **187:**304-319.

McClaine JW, Ford RM. 2002. Reversal of flagellar rotation is important in initial attachment of Escherichia coli to glass in a dynamic system with high- and low-ionic-strength buffers. Appl Environ Microbiol **68:**1280-1289.

McGrath PT, Iniesta AA, Ryan KR, Shapiro L, McAdams HH. 2006. A dynamically localized protease complex and a polar specificity factor control a cell cycle master regulator. Cell **124:**535-547.

Mercante J, Suzuki K, Cheng X, Babitzke P, Romeo T. 2006. Comprehensive alanine-scanning mutagenesis of Escherichia coli CsrA defines two subdomains of critical functional importance. J Biol Chem **281:**31832-31842.

Miller JH. 1972. Experiments in Molecular Genetics. Cold Spring Harbor, NY: Cold Spring Harbor Laboratory Press.

Miller JH. 1992. A short course in bacterial genetics (Cold Spring Harbor, NY: Cold Spring Harbor Laboratory Press).

Monroe D. 2007. Looking for chinks in the armor of bacterial biofilms. PLoS Biol **5:**e307.

Moscoso JA, Jaeger T, Valentini M, Hui K, Jenal U, Filloux A. 2014. The diguanylate cyclase SadC is a central player in Gac/Rsm-mediated biofilm formation in Pseudomonas aeruginosa. J Bacteriol **196:**4081-4088.

Mougel C, Zhulin IB. 2001. CHASE: an extracellular sensing domain common to transmembrane receptors from prokaryotes, lower eukaryotes and plants. Trends

Biochem Sci **26:**582-584.

Nagai T, Ibata K, Park ES, Kubota M, Mikoshiba K, Miyawaki A. 2002. A variant of yellow fluorescent protein with fast and efficient maturation for cell-biological applications. Nat Biotechnol **20:**87-90.

Navarro MV, De N, Bae N, Wang Q, Sondermann H. 2009. Structural analysis of the GGDEF-EAL domain-containing c-di-GMP receptor FimX. Structure **17:**1104-1116.

O'Toole GA, Pratt LA, Watnick PI, Newman DK, Weaver VB, Kolter R. 1999. Genetic approaches to study of biofilms. Methods Enzymol **310:**91-109.

Otto K, Silhavy TJ. 2002. Surface sensing and adhesion of Escherichia coli controlled by the Cpx-signaling pathway. Proc Natl Acad Sci U S A **99:**2287-2292.

Outten CE, O'Halloran TV. 2001. Femtomolar sensitivity of metalloregulatory proteins controlling zinc homeostasis. Science **292:**2488-2492.

Pannuri A, Yakhnin H, Vakulskas CA, Edwards AN, Babitzke P, Romeo T. 2012. Translational repression of NhaR, a novel pathway for multi-tier regulation of biofilm circuitry by CsrA. J Bacteriol **194:**79-89.

Patzer SI, Hantke K. 1998. The ZnuABC high-affinity zinc uptake system and its regulator Zur in Escherichia coli. Mol Microbiol **28:**1199-1210.

Paul K, Nieto V, Carlquist WC, Blair DF, Harshey RM. 2010. The c-di-GMP binding protein YcgR controls flagellar motor direction and speed to affect chemotaxis by a "backstop brake" mechanism. Mol Cell **38:**128-139.

Pesavento C, Becker G, Sommerfeldt N, Possling A, Tschowri N, Mehlis A, Hengge R. 2008. Inverse regulatory coordination of motility and curli-mediated adhesion in Escherichia coli. Genes Dev **22:**2434-2446.

Povolotsky TL, Hengge R. 2012. 'Life-style' control networks in Escherichia coli: signaling by the second messenger c-di-GMP. J Biotechnol **160:**10-16.

Povolotsky TL, Hengge R. 2016. Genome-Based Comparison of Cyclic Di-GMP Signaling in Pathogenic and Commensal Escherichia coli Strains. J Bacteriol **198:**111-126.

Price NL, Raivio TL. 2009. Characterization of the Cpx regulon in Escherichia coli strain MC4100. J Bacteriol **191:**1798-1815.

Purcell EB, McKee RW, McBride SM, Waters CM, Tamayo R. 2012. Cyclic diguanylate inversely regulates motility and aggregation in Clostridium difficile. J Bacteriol **194:**3307-3316.

Raivio TL. 2014. Everything old is new again: an update on current research on the Cpx envelope stress response. Biochim Biophys Acta **1843:**1529-1541.

Raivio TL, Leblanc SK, Price NL. 2013. The Escherichia coli Cpx envelope stress response regulates genes of diverse function that impact antibiotic resistance and membrane integrity. J Bacteriol **195:**2755-2767.

Raivio TL, Leblanc SK, Price NL. 2013. The Escherichia coli Cpx envelope stress response regulates genes of diverse function that impact antibiotic resistance and membrane integrity. J Bacteriol **195:**2755-2767.

Raivio TL, Silhavy TJ. 1997. Transduction of envelope stress in Escherichia coli by the Cpx two-component system. J Bacteriol **179:**7724-7733.

Reeve CA, Bockman AT, Matin A. 1984. Role of protein degradation in the survival of carbon-starved Escherichia coli and Salmonella typhimurium. J Bacteriol **157:**758-763.

Reinders A, Hee CS, Ozaki S, Mazur A, Boehm A, Schirmer T, Jenal U. 2015. Expression and Genetic Activation of c-di-GMP specific Phosphodiesterases in Escherichia coli. J Bacteriol.

Resch A, Rosenstein R, Nerz C, Götz F. 2005. Differential gene expression profiling of Staphylococcus aureus cultivated under biofilm and planktonic conditions. Appl Environ Microbiol **71:**2663-2676.

Rinaldo S, Paiardini A, Stelitano V, Brunotti P, Cervoni L, Fernicola S, Protano C, Vitali M, Cutruzzolà F, Giardina G. 2015. Structural basis of functional diversification of the HD-GYP domain revealed by the Pseudomonas aeruginosa PA4781 protein, which displays an unselective bimetallic binding site. J Bacteriol **197:**1525-1535.

Roche B, Aussel L, Ezraty B, Mandin P, Py B, Barras F. 2013. Iron/sulfur proteins biogenesis in prokaryotes: formation, regulation and diversity. Biochim Biophys Acta **1827:**455-469.

Romeo T, Gong M, Liu MY, Brun-Zinkernagel AM. 1993. Identification and molecular characterization of csrA, a pleiotropic gene from Escherichia coli that affects glycogen biosynthesis, gluconeogenesis, cell size, and surface properties. J Bacteriol **175:**4744-4755.

Ross P, Weinhouse H, Aloni Y, Michaeli D, Weinberger-Ohana P, Mayer R, Braun S, de Vroom E, van der Marel GA, van Boom JH, Benziman M. 1987. Regulation of cellulose synthesis in Acetobacter xylinum by cyclic diguanylic acid. Nature **325:**279-281.

Roux A, Beloin C, Ghigo JM. 2005. Combined inactivation and expression strategy to study gene function under physiological conditions: application to identification of new

Escherichia coli adhesins. J Bacteriol **187:**1001-1013.

Ryan RP, Fouhy Y, Lucey JF, Crossman LC, Spiro S, He YW, Zhang LH, Heeb S, Cámara M, Williams P, Dow JM. 2006. Cell-cell signaling in Xanthomonas campestris involves an HD-GYP domain protein that functions in cyclic di-GMP turnover. Proc Natl Acad Sci U S A **103:**6712-6717.

Sabnis NA, Yang H, Romeo T. 1995. Pleiotropic regulation of central carbohydrate metabolism in Escherichia coli via the gene csrA. J Biol Chem **270:**29096-29104.

Saiki RK, Bugawan TL, Horn GT, Mullis KB, Erlich HA. 1986. Analysis of enzymatically amplified beta-globin and HLA-DQ alpha DNA with allele-specific oligonucleotide probes. Nature **324:**163-166.

Schirmer T, Jenal U. 2009. Structural and mechanistic determinants of c-di-GMP signalling. Nat Rev Microbiol **7:**724-735.

Serra DO, Richter AM, Klauck G, Mika F, Hengge R. 2013. Microanatomy at cellular resolution and spatial order of physiological differentiation in a bacterial biofilm. MBio **4:**e00103-00113.

Serra DO, Richter AM, Hengge R. 2013b. Cellulose as an architectural element in spatially structured Escherichia coli biofilms. J Bacteriol **195:**5540-5554.

Sevcenco AM, Pinkse MW, Wolterbeek HT, Verhaert PD, Hagen WR, Hagedoorn PL. 2011. Exploring the microbial metalloproteome using MIRAGE. Metallomics **3:**1324-1330.

Sezonov G, Joseleau-Petit D, D'Ari R. 2007. Escherichia coli physiology in Luria-Bertani broth. J Bacteriol **189:**8746-8749.

Shaikh AS, Tang YJ, Mukhopadhyay A, Martín HG, Gin J, Benke PI, Keasling JD. 2010. Study of stationary phase metabolism via isotopomer analysis of amino acids from an isolated protein. Biotechnol Prog **26:**52-56.

Shu CJ, Ulrich LE, Zhulin IB. 2003. The NIT domain: a predicted nitrate-responsive module in bacterial sensory receptors. Trends Biochem Sci **28:**121-124.

Simm R, Morr M, Kader A, Nimtz M, Römling U. 2004. GGDEF and EAL domains inversely regulate cyclic di-GMP levels and transition from sessility to motility. Mol Microbiol **53:**1123-1134.

Snyder WB, Davis LJ, Danese PN, Cosma CL, Silhavy TJ. 1995. Overproduction of NlpE, a new outer membrane lipoprotein, suppresses the toxicity of periplasmic LacZ by activation of the Cpx signal transduction pathway. J Bacteriol **177:**4216-4223.

Sommerfeldt N, Possling A, Becker G, Pesavento C, Tschowri N, Hengge R. 2009. Gene

expression patterns and differential input into curli fimbriae regulation of all GGDEF/EAL domain proteins in Escherichia coli. Microbiology **155:**1318-1331.

Spangler C, Böhm A, Jenal U, Seifert R, Kaever V. 2010. A liquid chromatography-coupled tandem mass spectrometry method for quantitation of cyclic di-guanosine monophosphate. J Microbiol Methods **81:**226-231.

Spencer ME, Guest JR. 1973. Isolation and properties of fumarate reductase mutants of Escherichia coli. J Bacteriol **114:**563-570.

Steiner S, Lori C, Boehm A, Jenal U. 2013. Allosteric activation of exopolysaccharide synthesis through cyclic di-GMP-stimulated protein-protein interaction. EMBO J **32:**354-368.

Sudarsan N, Lee ER, Weinberg Z, Moy RH, Kim JN, Link KH, Breaker RR. 2008. Riboswitches in eubacteria sense the second messenger cyclic di-GMP. Science **321:**411-413.

Tal R, Wong HC, Calhoon R, Gelfand D, Fear AL, Volman G, Mayer R, Ross P, Amikam D, Weinhouse H, Cohen A, Sapir S, Ohana P, Benziman M. 1998. Three cdg operons control cellular turnover of cyclic di-GMP in Acetobacter xylinum: genetic organization and occurrence of conserved domains in isoenzymes. J Bacteriol **180:**4416-4425.

Taylor BL, Zhulin IB. 1999. PAS domains: internal sensors of oxygen, redox potential, and light. Microbiol Mol Biol Rev **63:**479-506.

Thomason MK, Fontaine F, De Lay N, Storz G. 2012. A small RNA that regulates motility and biofilm formation in response to changes in nutrient availability in Escherichia coli. Mol Microbiol **84:**17-35.

Timmermans J, Van Melderen L. 2010. Post-transcriptional global regulation by CsrA in bacteria. Cell Mol Life Sci **67:**2897-2908.

Tischler AD, Camilli A. 2005. Cyclic diguanylate regulates Vibrio cholerae virulence gene expression. Infect Immun **73:**5873-5882.

Tschowri N, Schumacher MA, Schlimpert S, Chinnam NB, Findlay KC, Brennan RG, Buttner MJ. 2014. Tetrameric c-di-GMP mediates effective transcription factor dimerization to control Streptomyces development. Cell **158:**1136-1147.

Tuckerman JR, Gonzalez G, Gilles-Gonzalez MA. 2011. Cyclic di-GMP activation of polynucleotide phosphorylase signal-dependent RNA processing. J Mol Biol **407:**633-639.

Vallee BL, Falchuk KH. 1993. The biochemical basis of zinc physiology. Physiol Rev

73:79-118.

Wang H, Sodagari M, Ju LK, Zhang Newby BM. 2013. Effects of shear on initial bacterial attachment in slow flowing systems. Colloids Surf B Biointerfaces **109:**32-39.

Wang P, Robert L, Pelletier J, Dang WL, Taddei F, Wright A, Jun S. 2010. Robust growth of Escherichia coli. Curr Biol **20:**1099-1103.

Wang X, Dubey AK, Suzuki K, Baker CS, Babitzke P, Romeo T. 2005. CsrA post-transcriptionally represses pgaABCD, responsible for synthesis of a biofilm polysaccharide adhesin of Escherichia coli. Mol Microbiol **56:**1648-1663.

Wang X, Preston JF, Romeo T. 2004. The pgaABCD locus of Escherichia coli promotes the synthesis of a polysaccharide adhesin required for biofilm formation. J Bacteriol **186:**2724-2734.

Watnick PI, Lauriano CM, Klose KE, Croal L, Kolter R. 2001. The absence of a flagellum leads to altered colony morphology, biofilm development and virulence in Vibrio cholerae O139. Mol Microbiol **39:**223-235.

Wei BL, Brun-Zinkernagel AM, Simecka JW, Prüss BM, Babitzke P, Romeo T. 2001. Positive regulation of motility and flhDC expression by the RNA-binding protein CsrA of Escherichia coli. Mol Microbiol **40:**245-256.

Weichart D, Querfurth N, Dreger M, Hengge-Aronis R. 2003. Global role for ClpP-containing proteases in stationary-phase adaptation of Escherichia coli. J Bacteriol **185:**115-125.

Weilbacher T, Suzuki K, Dubey AK, Wang X, Gudapaty S, Morozov I, Baker CS, Georgellis D, Babitzke P, Romeo T. 2003. A novel sRNA component of the carbon storage regulatory system of Escherichia coli. Mol Microbiol **48:**657-670.

Weiss B. 2007. The deoxycytidine pathway for thymidylate synthesis in Escherichia coli. J Bacteriol **189:**7922-7926.

White AP, Gibson DL, Kim W, Kay WW, Surette MG. 2006. Thin aggregative fimbriae and cellulose enhance long-term survival and persistence of Salmonella. J Bacteriol **188:**3219-3227.

Xu J, Kim J, Koestler BJ, Choi JH, Waters CM, Fuqua C. 2013. Genetic analysis of Agrobacterium tumefaciens unipolar polysaccharide production reveals complex integrated control of the motile-to-sessile switch. Mol Microbiol **89:**929-948.

Yakhnin H, Baker CS, Berezin I, Evangelista MA, Rassin A, Romeo T, Babitzke P. 2011. CsrA represses translation of sdiA, which encodes the N-acylhomoserine-L-lactone receptor of Escherichia coli, by binding exclusively within the coding region of

sdiA mRNA. J Bacteriol **193:**6162-6170.

Yamamoto K, Ishihama A. 2005. Transcriptional response of Escherichia coli to external copper. Mol Microbiol **56:**215-227.

Yamamoto K, Ishihama A. 2005. Transcriptional response of Escherichia coli to external zinc. J Bacteriol **187:**6333-6340.

Yamamoto K, Ishihama A. 2006. Characterization of copper-inducible promoters regulated by CpxA/CpxR in Escherichia coli. Biosci Biotechnol Biochem **70:**1688-1695.

Yoshihara A, Nobuhira N, Narahara H, Toyoda S, Tokumoto H, Konishi Y, Nomura T. 2015. Estimation of the adhesive force distribution for the flagellar adhesion of Escherichia coli on a glass surface. Colloids Surf B Biointerfaces **131:**67-72.

Zacharias DA, Violin JD, Newton AC, Tsien RY. 2002. Partitioning of lipid-modified monomeric GFPs into membrane microdomains of live cells. Science **296:**913-916.

Zähringer F, Lacanna E, Jenal U, Schirmer T, Boehm A. 2013. Structure and signaling mechanism of a zinc-sensory diguanylate cyclase. Structure **21:**1149-1157.

7. Appendix

7.1 MS-based protein identification

Mass spectrometry-based identification of co-immunoprecipitated proteins was performed by employees of the SYNMIKRO Mass Spectrometric Core Facility, Marburg.

Samples were digested in gel by the addition of Sequencing Grade Modified Trypsin (Promega) and incubation at 37 °C overnight, according to the manufacturers protocols. Peptides were eluted by using 200 μL MeCN for 30 minutes in a sonic-bath. Subsequently, the supernatant was transferred to a fresh tube and after evaporation of the solvent in a vacuum concentrator dry samples were dissolved in 25 μL 10% acetonitrile/0.1% TFA.

The mass spectrometric analysis of the samples was performed using an Orbitrap Velos Pro mass spectrometer (ThermoScientific). An Ultimate nanoRSLC-HPLC system (ThermoScientific), equipped with a home-made nano 1.8 μm C18 RP column was connected online to the mass spectrometer through a nanospray ion source. Depending on sample concentration, 1-15 μL of the tryptic digest were usually injected onto a C18 pre-concentration column. Automated trapping and desalting of the sample was performed at a flowrate of 6 μL/min using water/ 0.05% formic acid as solvent.

Separation of the tryptic peptides was achieved with the following gradient of water/ 0.045% formic acid (solvent A) and 80% acetonitrile/ 0.05% formic acid (solvent B) at a flow rate of 300 nL/min: holding 4% B for 5 minutes, followed by a linear gradient to 45% B within 30 minutes and linear increase to 95% solvent B in additional 5 minutes. The column was connected to a stainless steel nanoemitter (ThermoScientific) and the eluent sprayed directly towards the heated capillary of the mass spectrometer using a potential of 2,300 V. A survey scan with a resolution of 60,000 within the Orbitrap mass analyzer was combined with at least three data- dependent MS/MS scans with dynamic exclusion for 30 s either using CID with the linear ion-trap or using HCD and orbitrap detection at a resolution of 7,500.

Data analysis was performed using Proteome Discoverer (ThermoScientific) with SEQUEST and MASCOT (version 2.2; Matrix science) search engines using a user defined database containing the sequence of the protein of interest.

Table S1. List of putative DgcZ-3xFLAG protein interaction partners identified by Co-immunoprecipitation (CoIP) in exponential phase.

Accession	Name	Description	Σ# Unique Peptides	Σ# Peptides
16130780	YgfK	predicted oxidoreductase, Fe-S subunit	27	29
16129494	DgcZ	dyguanylate cyclase	9	10
24051622	PspD	phge shock protein, inner membrane protein	2	4
15803409	YgeY	hypothetical protein Z4211	7	7
24053584	TdcB	threonine dehydratase	2	4
16128870	PflB	pyruvate formate lyase I	7	10
49176316	TdcE	pyruvate formate-lyase 4/2-ketobutyrate formate-lyase	2	3
16130504	GrcA	pyruvate formate lyase subunit	2	3
16130604		alanyl-tRNA synthetase	1	3
16129658		phosphoenolpyruvate synthase	1	2
16130302	EvgS	hybrid sensory histidine kinase in two-component regulatory system with EvgA	1	2
16131060		translation initiation factor IF-2	1	6
3025076	YciW	Hypothetical protein yciW	1	1
56383624		sn-glycerol-3-phosphate dehydrogenase (anaerobic), large subunit	1	2
16129674		translation initiation factor IF-3	1	1
49176276	YgeW	hypothetical protein b2870	1	1
16129974	Wbbl	hypothetical protein b2034	1	1
15801208		3-oxoacyl-(acyl carrier protein) synthase	1	1
16130177		anaerobic glycerol-3-phosphate dehydrogenase subunit B	1	1
16131066		phosphoglucosamine mutase	1	2
16128644		isopentenyl-adenosine A37 tRNA methylthiolase	1	3
24054511		heat shock protein HslVU, proteasome-related peptidase subunit	1	2
24052952	MipA-YeaF	orf, conserved hypothetical protein	1	1
1172545	PNPase	Polyribonucleotide nucleotidyltransferase (Polynucleotide phosphorylase) (PNPase)	1	1

Accession	Name	Description		
16128839		pyruvate dehydrogenase	1	1
24054511		heat shock protein HslVU, proteasome-related peptidase subunit	1	1
56383523	UspE	orf, conserved hypothetical protein	1	1
56383171		(3R)-hydroxymyristol acyl carrier protein dehydratase	1	1
16130021		predicted peptidase	1	1

With green shading are indicated the proteins identified at least by two unique peptides and three peptides.

Table S2. List of putative DgcZ-3xFLAG protein interaction partners identified by Co-immunoprecipitation (CoIP) in stationary phase.

Accession	Name	Description	Σ# Unique Peptides	Σ# Peptides
16129494	DgcZ	dyguanylate cyclase	4	4
56384131	FrdB	fumarate reductase, anaerobic, iron-sulfur protein subunit	2	4
16130604	AlaS	alanyl-tRNA synthetase	2	8
16131979	FrdA	fumarate reductase	2	3
16130575	GabD	succinate-semialdehyde dehydrogenase I, NADP-dependent	2	4
24051999	SlyB	putative outer membrane protein	1	3
24052035	YdhY	putative oxidoreductase, Fe-S subunit [	1	4
16130581	YgaV	predicted DNA-binding transcriptional regulator	1	4
16128319		2-methylcitrate dehydratase	1	5
90111285	YdeM	hypothetical protein b1497	1	5
16132199		thymidine phosphorylase	1	2
546067		FanF	1	4
15800816	OmpA	outer membrane protein 3a (II*;G;d)	1	6
16129799		hypothetical protein b1846	1	3
24054858		protease specific for phage lambda cII repressor	1	3
16130648		RNA polymerase sigma factor	1	5

90111373		imidazole glycerol-phosphate dehydratase/histidinol phosphatase	1	2
16130599		S-ribosylhomocysteinase	1	4
15803767		hypothetical protein Z4592	1	3
24052910		orf, conserved hypothetical protein	1	4
24050786		galactose-1-epimerase (mutarotase)	1	2
15802972		ethanolamine ammonia-lyase, heavy chain	1	2
24054394		regulator for metE and metH	1	3
77734009		TraC2 primase [IncP-1beta multiresistance plasmid pB8]	1	4
90111211		Maf-like protein	1	1
16129718		selenophosphate synthetase	1	1
16130226	YfbR	hypothetical protein b2291	1	1
16128117		glucose dehydrogenase	1	3
24051293		trp repressor binding protein	1	2
90111355		D-cysteine desulfhydrase	1	2
16132171	HsdR	endonuclease R	1	5
16131060	InfB	translation initiation factor IF-2	1	1
24051235	FabA	beta-hydroxydecanoyl thioester dehydrase, trans-2-decenoyl-ACP isomerase	1	2
24054508		2-demethylmenaquinone 2-C-methyltransferase	1	1
16130302	EvgS	hybrid sensory histidine kinase in two-component regulatory system with EvgA	1	4
16128351	TauB	taurine transporter subunit	1	2
16129987	WcaJ	predicted UDP-glucose lipid carrier transferase	1	1
16131389	GadA	glutamate decarboxylase A, PLP-dependent	1	3

With green shading are indicated the proteins identified at least by two unique peptides and three peptides.

CoIP dataset (accompanying Excel file in attached CD-ROM). Putative DgcZ-3xFLAG protein interaction partners identified by Co-immunoprecipitation (CoIP). The file contains two sheets listing results from CoIPs in stationary and exponential phase. Each sheet contains two lists: i) candidates identified at least by two unique peptides and three peptides and ii) candidates identified by less unique peptides / peptides. The lists are sorted according to the parameter "Area" which gives a measure of the relative abundances of the proteins in the sample. None of the candidates was identified in any of the negative control CoIPs.

VIDEO S1 (in attached CD-ROM) Time-lapse microscopy for localization of DgcZ-mVENUS protein in bacteria grown in microfluidic chambers. The video shows the DgcZ localization in the dgcZ-mVENUS/ibpA-mCHERRY/csrA::Tn5 strain. Each frame shows a merged image (phase contrast and mVENUS channel). Images were taken every 12 minutes. Bacteria were flushed into the microfluidic chamber and LB medium was applied for 2 hours (not shown here). A gradient from fresh to nutrient-depleted (spent) medium was applied (3 hours, frame 0 - 15), followed by 16 hours of growth in spent medium (frame 16 - 95), 1 hour of gradient from spent to fresh medium (frame 95 - 100) and 20 hours of fresh medium (frame 101 - 200).

7.2 List of Figures

7.3 List of Tables

7.4 Abbreviations

A	alanine
Ag43	Antigen 43
Amp	ampicillin
A-site	active site
BSA	bovine serum albumin
$CaCl_2$	calcium chloride
cat	chloramphenicol
CHASE	**C**yclases/**H**istidine kinases **A**ssociated **S**ensory **E**xtracellular
$CHCl_3$	chloroform
CoIP	co-immunoprecipitation
Cys (C)	cysteine
CZB	chemoreceptor zinc-binding

c-di-GMP	bis-(3'-5')-cyclic dimeric guanosine monophosphate
DGC	diguanylate cyclase
DIC	differential interference contrast
DMSO	dimethyl sulfoxide
dNTPs	nucleoside triphosphates
dsDNA	**d**ouble **s**trand DNA
E	glutamic acid
EAL	characteristic domain of PDEs
eDNA	**e**xtracellular DNA
EDTA	**E**thylene**d**iamine**t**etraacetic **a**cid
EtOH	ethanol
Fe-S	iron-sulfur (proteins)
FRD	fumarate reductase
g	gram(s)
GAF	domain found in c**G**MP-specific phosphodiesterases, **a**denylyl cyclases and **F**hlA.
GGDEF	characteristic domain of DGCs
GIL	**G**GDEF **I**-site **l**ike (domain)
GlcNAc	N-Acetylglucosamine
GMP	guanosine monophosphate
GTP	guanosine triphosphate
h	hour(s)
His (H)	histidine
HD-GYP	characteristic domain of PDEs
HCl	hydrochloric acid
IPTG	Isopropyl β-D-1-thiogalactopyranoside
I-site	**i**nhibitory **s**ite
K	lysine
kan	kanamycin
KCl	potassium chloride
K_i	zinc inhibition constant for DgcZ
K_2HPO_4	dipotassium phosphate
KH_2PO_4	monopotassium phosphate
kV	kilovolts
L	leucine
L	liter(s)
LB	**l**ysogeny **b**roth
MCPs	**m**ethyl-accepting **c**hemotaxis **p**roteins
Mg^{2+}	magnesium
$MgSO_4$	magnesium sulphate
mL	milliliter
μL	microliter
mM	millimolar
μM	micromolar

MMA	**m**inimal **m**edium **A**
Mn^{2+}	manganese
mRNA	**m**essenger RNA
ms	millisecond
NaCl	sodium chloride
NaOH	sodium hydroxide
ng	nanogram
NIT	**nit**rate- and nitrite sensing domain
nM	nanomolar
ONPG	*ortho*-**N**itro**p**henyl-β-**g**alactoside
PAS	protein domain named after the proteins **P**er/**A**rnt/**S**im
PBS	phosphate-buffered saline
PDE	(c-di-GMP-specific) phosphodiesterase
PEG	polyethylene glycol
PES	polyethersulfone
pGpG	5′-phosphoguanylyl-(3′-5′)-guanosine
PilZ	protein domain
PMSF	**p**henyl**m**ethyl**s**ulfonyl **f**luoride
PNPase	**P**olynucleotide **P**hosphorylase
poly-GlcNAc (PGA)	poly-N-Acetylglucosamine
ppGpp	guanosine tetraphosphate
Q	glutamine
rpm	**r**evolutions **p**er **m**inute
SDS	**s**odium **d**odecyl **s**ulfate
SEM	**s**tandard **e**rror of the **m**ean
SNP	**s**ingle **n**ucleotide **p**olymorphism
sRNA	**s**mall RNA
Str	streptomycin
TIRF	**T**otal **i**nternal **r**eflection **f**luorescence
TSS	**t**ransformation and **s**torage **s**olution
UDP- GlcNAc	Uridine diphosphate *N*-acetylglucosamine
UTR	**u**ntranslated **r**egion
wt	**w**ild-**t**ype
X-Gal	5-bromo-4-chloro-3-indolyl-β-D-galactopyranoside
$ZnSO_4$	zinc sulfate
Zn^{2+}	zinc

8. Acknowledgements

9. Statutory Declaration

I herewith formally declare that I have written the submitted dissertation independently. I did not use any outside support except for the quoted literature and other sources mentioned in the paper.

I clearly marked and separately listed all of the literature and all of the other sources which I employed when producing this academic work, either literally or in content.

This dissertation has not been submitted in its present or similar form to any other domestic or foreign university in connection with a doctoral application or for other examination purposes.

I am aware that the violation of this regulation will lead to failure of the thesis.

_____

(Egidio Lacanna)

_____

(Place, Date)